Optical Regeneration and Noise in Semiconductor Devices

Öhman, Filip; Mørk, Jesper

Publication date:
2005

Document Version
Publisher's PDF, also known as Version of record

Optical Regeneration and Noise in Semiconductor Devices

Filip Öhman

Research Center COM
Technical University of Denmark

February 16, 2005

Acknowledgements

First and foremost I would like to thank my supervisors Jesper Mørk, Bjarne Tromborg and Svend Bischoff, for taking great interest in my, and our common, work and for numerous hours of support and help. Bjarne gets special recognition for never letting me take the easy way, and Jesper for showing me that I could do it in the not so easy way. Obviously, I could never have done it without you.

Of all the great people and colleagues at COM, who have made it a pleasure to work there, one have had more insight into my work and my mind than the rest. Thank you Jens for all the help, discussions on topics large and small and for all the good laughs. Also, to Lotte Jin Christiansen, thank you for showing that our ideas worked.

My warm gratitude also goes to Lone Bjørnstjerne for making all administrative affairs at COM a breeze, and for getting me there and back again, wherever it might have been.

The people at ACREO AB in Kista, Andreas Aurelius, Anders Djupsjöbacka and Anders Berntson, get many thanks for lending me their time and lab during a few short, but intense, visits.

Last but not least, a lot of love to my family, and to Maria for always being there.

Kgs. Lyngby 30/11/2004
Filip Öhman

Abstract

In this report all-optical 2R-regeneration in optical communication systems is investigated. A simple regenerator device based on concatenated semiconductor optical amplifiers (SOAs) and electro absorbers (EAs) is introduced and examined. Experiments show that the monolithic SOA-EA 2R-regenerator has a sharp step-like transfer function with a threshold that is easily adjusted by simply changing the bias voltage over the electro absorbers. Measurements on a modulated signal show that the device can improve the extinction ratio of a degraded signal with more than 5 dB, and improve the receiver sensitivity with more than 8 dB compared to the back-to-back case, using a degraded signal. The noise properties and cascadability of the proposed device are examined through modeling. Furthermore the influence of the saturation properties of the EA on the regeneration performance is investigated. Calculations show that it is possible to increase the nonlinearity of the transfer function and improve the regenerating properties by lowering the saturation power of the EA and concatenating several SOA-EA pairs, although this also adds more noise to the signal.

In order to analyze the influence of the regenerator properties on the bit error rate in a cascade of regenerators, a general model for a 2R-regenerator, neglecting timing jitter, is developed. The model conceptually divides the regenerator into a linear amplifying part and a nonlinear reshaping part. The amplifier adds noise in the form of amplified spontaneous emission and the nonlinear transfer function redistributes the noise and improve the extinction ratio of the signal. The model show that the best choice of decision threshold is made by considering the properties of the cascaded regenerators rather than the signal going into the cascade. Furthermore the interplay between different regenerator properties like noise figure, nonlinearity and extinction ratio is examined. The results show that an increase in nonlinearity can compensate for a higher amplifier noise figure or increase the reach of a transmission link. This kind of investigations make it possible to compare different kinds of regenerators and guide the optimization of regenerators.

Theoretical modeling and direct measurement of the probability density function (PDF) of a continuous wave (cw) signal after an SOA show the nonlinear noise redistribution due to gain saturation and carrier dynamics. The redistribution give both a reduction in the width and change in the overall shape of the PDF, compared to a linear amplification. The redistribution of noise, as described by the changes in the PDF, is central to the understanding of regeneration. The

changes of the noise in an SOA is examined closer by use of a small-signal model, including first and second order noise terms, and a large-signal time-domain simulation. The calculations show the noise spectra and the bandwidth dependence of the noise redistribution in the device. Both pass-through amplification and wavelength conversion through cross-gain modulation is investigated and compared.

Resumé (in Danish)

I denne rapport undersøges optisk 2R-regeneration i optiske kommunikationssystemer. En simpel regenerator baseret på sammensatte optiske halvlederforstærkere (SOA) og elektroabsorbere (EA) præsenteres og undersøges. Eksperimenter viser at den monolitiske SOA-EA 2R-regerator har en skarp ulineær overføringsfunktion med en tærskel, der er nemt justerbar blot ved at ændre spændingsfaldet over elektroabsorberen. Endvidere viser målinger på et moduleret signal at komponenten kan forbedre udslukningsgraden af et forringet signal med mere end 5dB og forbedre modtagerfølsomheden med mere end 8 dB sammenlignet med et forringet signal sendt 'back-to-back'. Støjegenskaberne og kaskadekoblingsegenskaber af komponenten modelleres teoretisk. Desuden undersøges indflydelsen af elektroabsorberens mætningsegenskaber på regenerationsegenskaberne. Udregninger viser at det er muligt at øge overførelsesfunktionens ulinearitet og forbedre regenerationsegenskaberne ved at formindske EA'ens mætningseffekt og sammensætte flere SOA-EA-par, selvom dette også addere mere støj til signalet.

For at analysere regeneratoregenskabernes indflydelse på fejlraten (BER) i en række af regeneratorer, udvikles en generel 2R-regerationsmodel, der dog negligerer tidslig jitter. Modellen opdeler regeneratoren i en lineær forstærkerdel og ulineær del. Forstærkeren adderer støj i form af forstærket spontan emission (ASE) og den ulineære overførselsfunktion omfordeler støjen og forbedre signalets udslukningsgraden. Modellen viser at det bedste valg af beslutningstærskel sker ved at se på egenskaberne af rækken af regeneratore frem for at se på det signal, der går ind i rækken. Samspillet mellem forskellige regneratoregenskaber såsom støjtal, ulinearitet og udslukningsgraden undersøges. Resultatet viser at større ulinearitet kan kompensere for et højere støjtal i forstærkeren eller forøge rækkevidden af transmissionen. Denne type undersøgelse gør det muligt at sammenligne forskellige slags regeneratore og guide optimeringen af regeneratore.

Teoretisk modellering og direkte målinger af sandsynlighedstæthedsfunktionen (PDF) af et 'continuous wave' (CW) signal efter en SOA viser at den ulineære omfordeling af støj både reducerer bredden af og ændrer formen af PDF'en sammenlignet med lineær forstærkning. Omfordelingen af støj, beskrevet som ændringer i PDF'en, er central for at forstå regeneration. Ændringerne i støjen i en SOA undersøges yderligere ved hjælp af teoretiske udregninger. De to anvendte modeller er en små-signal model med både første og anden ordens støj og en stor-signal tidsdomaine simulering. Beregningerne viser støjspektret samt båndbredteafhængigheden af omfordeling af støj i komponenten. Både bølge-

længdekonvertering via krydsgain modulation og transitforstærkning undersøges og sammenlignes.

Contents

Chapter 1

Introduction

Modern communication technology is to a large extent based on the huge information carrying capacity of a light signal in a glass fiber. The large bandwidth and low attenuation of the silica glass, used in optical fibers, makes it possible to send a large amount of information over long distances. In order to use this capacity as efficiently as possible a lot of complementing technologies have been developed over the years. The use of many wavelength channels in the same fiber, so called wavelength division multiplexing (WDM), greatly increase the efficiency of the optical link, and make it possible to increase the capacity of already installed fibers. Another route to increased capacity is to increase the line rate of a single channel, from for example 10 Gb/s to 40 Gb/s. On a subsystem level, this development have been made possible mainly by the development of the erbium doped fiber amplifier (EDFA), which allows for the simultaneous amplification of many wavelength channels, and high speed electronic and optoelectronic devices for sending, receiving and switching the signals in the network. As the line rate and channel count goes up, so does the demands on the subsystems and devices. Today most systems terminate the optical signal at each node by detecting it and transferring it to the electrical domain. The electrical signal is regenerated, and all signal processing is made in the electrical domain. The signal is then transfered back into the optical domain. Since the optical-electrical-optical conversion, and any intermediate processing, requires power hungry and bulky hardware it is believed that substantial benefits would be gained by letting the optical signals that are not to be processed pass the node completely in the optical domain. By doing this the restoring of the signal quality by electrical regeneration is also lost and the degradation of the optical signal will eventually set a limit to transmission distance. To remedy this all-optical regeneration is needed.

This report is based on the assumption that all-optical signal regeneration will be needed in an optical communication system, although the validity of this assumption is discussed and questioned by many. The electronics that would be replaced is getting faster and cheaper as the technology develops and there are still some fundamental issues regarding the new all-optical technologies that needs to be investigated and understood. This report tackles some of the issues regarding

all-optical regeneration by first, in chapter 2, describe the basics of signal quality and all-optical regeneration. Furthermore some basic concepts needed later in the report and some common devices used for all-optical signal processing, most importantly the semiconductor optical amplifier (SOA), are introduced. In chapter 3 noise measurements and models for describing the noise in an SOA are presented and discussed. A general model for describing a cascade of regenerators, which can be used for comparing different regenerators and investigating the impact of regenerator parameters on the cascadability, is presented in chapter 4. The model is used to investigate the interplay between different regenerator parameters such as noise figure, nonlinearity and extinction ratio. In chapter 5 a concrete suggestion for a simple regenerator components based on concatenated sections of saturable gain and absorption is introduced. The theoretical models are used to investigate and optimize the regenerator and some experimental investigations are presented. Finally, in chapter 6 the report is summarized and concluded.

Chapter 2

Background

One of the most basic components that is needed in any communication system is a repeater. Whether the repeater is a child playing a whispering game or a watchman with a signaling fire on top of a mountain the idea is the same; receive the signal and resend it in a way that makes it possible to increase the total distance that the signal travels, preferably without introducing any errors.

In a simple optical communication system the signal is sent by a transmitter consisting mainly of a source of optical power, usually a laser diode, which is modulated by an electrical signal. The optical signal is sent through a glass fiber and is detected in the other end by a receiver, which converts the signal back to the electrical domain. A repeater in such a system is a receiver and transmitter coupled together. The optical signal is detected and transfered from the optical to the electrical domain and is then transfered back to an optical signal and resent using the transmitter part of the repeater. Such a repeater is usually referred to as an OEO-repeater or optoelectronic repeater. Any signal-restoring operation, or regeneration, in an OEO-repeater is done in the electrical domain. The costs associated with the conversion between the two domains, the high power consumption and the relatively slow electronics are some of the arguments for finding alternatives to the OEO-repeater. In the all-optical approach to an optical communication system the conversion to the electrical domain is avoided by regenerating the signal in the optical domain using an all-optical regenerator.

In an optical network using multiple wavelengths a change of wavelength might be needed in network nodes, for example in order to avoid contention or as a base for future wavelength routing techniques. A wavelength converter basically performs the same function as a repeater with the addition of the possibility to change the wavelength of the output light. Although the regeneration functionality is not necessarily included in wavelength conversion, it is quite common that wavelength converters also regenerates the signal. Just as for repeaters, wavelength converters can be optoelectronic or all-optical. In this work the focus will be on all-optical regeneration and some basic differences between whether wavelength conversion is made or not, in a specific component, will be investigated. Other properties of wavelength converters, however, will not be discussed. Whenever regeneration

or wavelength conversion is mentioned the all-optical version is assumed, unless specifically stated otherwise.

Both the regenerator and wavelength converter have been heavily researched and developed during the last decade or so and a lot of different approaches and devices have been suggested for providing the functionalities.

2.1 Basics of regeneration

In an optical communication system there are several sources of signal degradation. The most basic one is loss. Although modern optical fibers have very low loss, it is there, and splices, couplers etc. do not make things better. Furthermore there are chromatic dispersion, fiber non-linearities and other processes that degrades the signal as it travels in a system. In order to be able to send the signal long distances, compensation for these degradations is required.

The degradations mentioned so far are all, in principle, deterministic in their character. This means that the impact of them is known, or can be calculated, in advance. It also means that they could be compensated for or avoided. Just as the sources of degradation are plentiful so are the solutions. Some approaches try to improve the robustness of the signal by clever modulation formats [1–3] that are influenced less by certain sources of signal degradation. Fiber dispersion can be compensated by discrete compensation in for example fiber bragg gratings [4] or by tailoring the links in such a way that the dispersion in different parts of the fiber cancel each other [5]. In a similar way loss can be compensated for by amplification in discrete amplifiers, like the erbium doped fiber amplifiers that revolutionized optical communication [5], or distributed in the fiber link through raman amplification [5]. Fiber non-linearities can be avoided by designing the systems in a way that avoid high optical intensities in the fibers. These deterministic degradations in themself would not be a problem if the corresponding compensations techniques were ideal. However the compensations are seldom ideal and even in principle some of the degradations cannot be compensated in a straight forward way.

As soon as there is some random contribution to the signal degradation the approach with pre-determined compensation schemes fail. Random processes that impairs the signal includes for example amplifier noise and crosstalk between channels, but can also be random effects, like environmental influences, on the in principle deterministic degradations. This means that the signal in an all-optical system sooner or later has to be regenerated. This is even more important once the all-optical approach is used in switches and routers, since the signal then can travel a long way without ever being electrically regenerated.

Before we get deeper into this investigation, some discussion about the basic concepts of information and errors that will be important in the following presentation has to be discussed.

2.1.1 BER and signal quality

The basic function of a communication system is to send information from one place to another. Information can take many forms and can be sent in different formats. In order to make this presentation clear it is important to define some basic concepts.

A signal can be sent in analog or digital form. An analog signal is a continuously varying signal in time, for example the electrical signal from the pick-up of a record player. A digital signal, however, only takes a few, in a binary case only two, discrete values. These two values represent the two logical symbols of the binary system, normally called zero and one. This work will only discuss digital, binary signals.

In an optical communication system the logical symbols are encoded on the optical signal by modulation. There are three different properties of the optical carrier wave that can be modulated, the amplitude, the phase and the frequency. In advanced modulation formats different combinations of modulation of these basic properties are used. This work, however, will only consider the most simple of all modulations, which is when the light intensity is turned on and off and is called on-off-keying, OOK. Furthermore there are two basic forms of modulation format, non return-to-zero, NRZ, and return-to-zero, RZ. In NRZ the pulses representing the one-symbol has a duration of the complete bit-slot and the intensity is not returned to zero between consecutive one-bits. In RZ the pulses have a fixed width in time smaller than the bit-slot.

One important measure of the quality of a communication system is how many errors that are introduced in the sent information. This measure for the amount of errors is usually referred to as bit error rate, or BER for short. BER is just the number of errors per sent bit or, in a probability picture, the probability of making an erroneous identification of a bit. The concept of this is shown schematically in Fig. 2.1. The signal, in this case NRZ, with random fluctuations are described

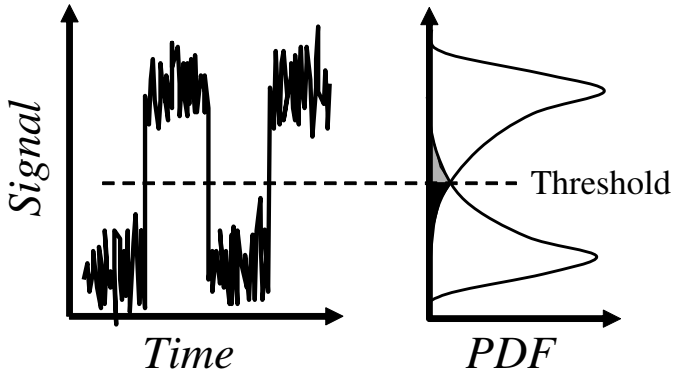

Figure 2.1: The concept of PDFs and BER.

with two probability density function (PDF), one for each logical symbol, giving the probability density for detecting a certain signal level. When the information encoded in the signal is to be read a decision has to be made for each bit regarding if it is a one or a zero. The most straight forward way of doing this is by introducing a threshold, or decision, level. If the signal is below this level it is considered to be a zero and if above it is a one bit. The probability of deciding on one although the bit was a zero is the area under the PDF of the zero-bits above the threshold, gray area in Fig. 2.1, and the probability of deciding on zero for a one-bit is the area of the PDF of the one-bits below the threshold, black area in Fig. 2.1. The total probability for an error, that is the BER, is then the sum of the error probability for the ones and the zeros divided by two, assuming equal probability for the bit being a one or zero. The threshold should obviously be chosen in order to give a BER as small as possible.

The PDFs of the signal can, as described, be used to calculate the BER of the signal. The problem is that the complete PDFs of the signal are often cumbersome to find, and usually approximations are used instead. The basic idea is to measure or calculate the mean value and standard deviation of the noise and then assume the PDF-shape. One common approximation is to assume a Gaussian distribution [5], which is a good approximation when thermal and shot noise in the detector dominates the signal. For noise from optical amplifier a non-central χ^2-distribution is often a good approximation [6].

Another measure of the signal quality is the so called Q-factor, which is defined as [5]

$$Q = \frac{\bar{P}_1 - \bar{P}_0}{\sigma_1 + \sigma_0} \tag{2.1}$$

where $\bar{P}_{1,0}$ and $\sigma_{1,0}$ are the mean values and standard deviation of the one and zero level, respectively. When a Gaussian approximation is used a direct relationship between the BER and Q-factor can be established [5]

$$\mathrm{BER} = \frac{1}{2}\mathrm{erfc}\left(\frac{Q}{\sqrt{2}}\right) \approx \frac{\exp(-Q^2/2)}{Q\sqrt{2\pi}} \tag{2.2}$$

where the erfc-function is the complementary error function. It is important to notice that the direct relationship between BER and Q-factor is valid only for Gaussian PDFs. If, as in the general case, the complete distribution is not uniquely defined by the mean and standard deviation it is quite possible to have a process that decrease the standard deviation, and hence increase Q, but at the same time increase the overlap between the PDFs, and hence the BER. For some processes it is therefore important to use the complete PDFs to properly describe the signal quality. As we will see later in this report, regeneration is such a process.

In the Q-factor the difference between the signal levels of the one- and zero-level is included. Another measure of the separation of the signal levels, but without the variance, is the extinction ratio, ER. This ratio is defined by

$$\mathrm{ER} = \frac{\bar{P}_1}{\bar{P}_0}. \tag{2.3}$$

Another simple measure of signal quality is the signal-to-noise ratio, SNR. When discussing SNR it is important to be clear about what is meant since there are a few different definitions. In the PDF picture introduced above the SNR is often defined as the ratio between the square of the mean power and the variance of the one-level

$$\mathrm{SNR} = \frac{\bar{P}_1^2}{\sigma_1^2}. \tag{2.4}$$

This definition makes sense if one considers an ideal noise-less detector with a responsivity equal to one, since the optical power is then identical to the electrical current from the detector. Noting that the electrical power varies as the square of the current this definition is equivalent to defining the SNR as the ratio between electrical average signal power and noise power, or in other words the electrical signal-to-noise ratio.

The optical signal-to-noise ratio, OSNR, on the other hand, is defined as the ratio between optical signal power and optical noise power, as measured within a specific bandwidth by for example an optical spectrum analyzer.

As the way of studying the signal in this work will mainly be that of the PDF-picture the electrical SNR will be used, and implied by the use of the abbreviation, SNR, unless explicitly stated otherwise.

The effect of any signal impairments on this picture is to increase the overlap between the PDFs by making them wider or by moving them closer together, and hence increase the BER. The job of the regenerator is thus to counteract this and keep the BER low, which brings us to the next section.

2.1.2 1, 2 and 3R regeneration

It is common to divide regeneration into three functionalities [7], re-amplification, re-shaping and re-timing, see Fig. 2.2. Re-amplification is the use of optical ampli-

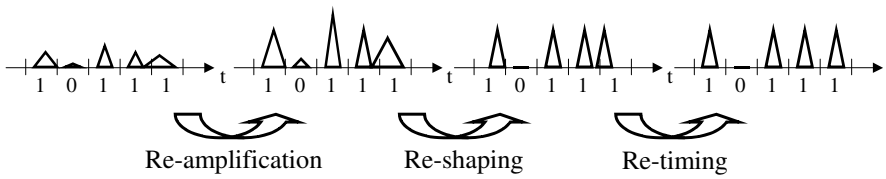

Figure 2.2: The concept of re-amplification, re-shaping and re-timing, i.e 3R-regeneration.

fication to increase the signal power in order to compensate for fiber attenuation and coupling losses. Re-shaping implies the improvement of the signal quality by, for example, extinction ratio improvement, noise redistribution and, in the case of pulsed systems, pulse compression. Re-timing is used for reducing timing

jitter, i.e. a random disturbance of the timing of the signal-pulses, and can for example be accomplished by extracting the clock frequency from the signal and transferring the data to a new low jitter pulse train locked to the extracted clock. The three functionalities (re-amplification, re-shaping and re-timing) together are usually referred to as 3R-regeneration, while in 2R-regeneration the re-timing is omitted and 1R being only amplification. Now, let us have a closer look at the three Rs.

1R

Re-amplification is just normal in-line amplification, which for many years have been performed by rare-earth element doped fiber amplifiers, and most commonly erbium doped fiber amplifiers, EDFAs. Other types of amplifiers include raman amplifiers and semiconductor optical amplifiers. In the PDF-picture from section 2.1.1 amplification is, at least in the ideal case, a linear process, that is the gain does not depend on the input signal power. This gives an output power that is a linear function of the input power with a slope equal to the gain. Because of this the only change induced by an ideal noise-less amplifier is to scale the PDFs to higher signal power by an amount given by the gain of the amplifier. If noise is included in the consideration the PDFs are also broadened and the BER increased, see Fig. 2.3. If the noise added by the amplifier is considered to be independent

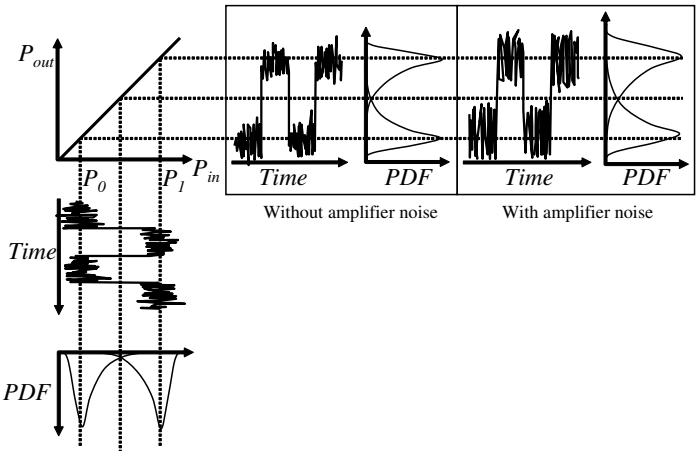

Figure 2.3: The influence of linear amplification, without and with amplifier noise, on the signal and the PDFs.

from the noise of the input signal, the variance at the output is just the sum of the variances of the input and amplifier noise. One important figure of merit for linear amplifiers is therefore the noise figure, defined as the ratio between the input and output signal to noise ratio [8]. The noise figure is a measure of how much noise, and hence potential errors, the amplifier adds to the signal.

2R

Re-shaping is achieved by a component with a non-linear intensity transfer function as shown in Fig. 2.4. The non-linearity allows for two main improvements of the signal. The steep middle part, in combination with the low output intensity at the zero level, increases the ratio between the intensity for the logical ones and zeros, i.e. the extinction ratio (ER). The small slopes at low and high intensities ensure that large amplitude variations at the input is transferred to smaller variations at the output, that is the variance of the amplitude fluctuations is decreased leading to narrower PDFs and increased signal to noise ratio. This process will be referred to as noise redistribution. The limiting case of a step function is equivalent to making a decision between a logical one and zero, as done in for example optoelectronic repeaters. It is important to note that the increase in extinction

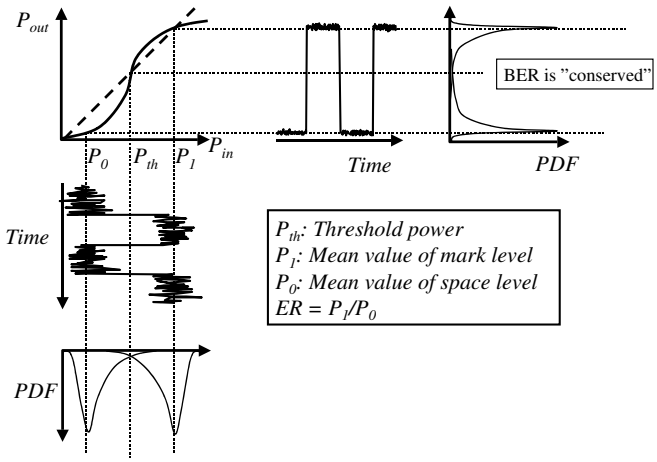

Figure 2.4: The concept of re-shaping of a NRZ intensity modulated signal using a non-linear intensity transfer function.

ration and compression of the PDFs shown in Fig. 2.4 does not imply an improved bit error rate (BER) after the regenerator. Obviously a simple decision cannot remove errors and the best result an ideal regenerator can achieve is to have the same BER at the output as at the input. What a regenerator does is to collect all the accumulated errors at that point in the system and conditions the signal for further transmission in a way that decreases the rate of error accumulation later in the transmission line. One indicator on how well the regenerator does this is given by the intensity transfer function. Shown in Fig. 2.5 is a simple calculation of BER as function of number of cascaded regenerators for different transfer functions, using a model based on the static non-linear transfer function [9]. As seen in the insert the amount of non-linearity of the transfer function strongly affects the evolution of the BER in the cascade, with the limit of a step

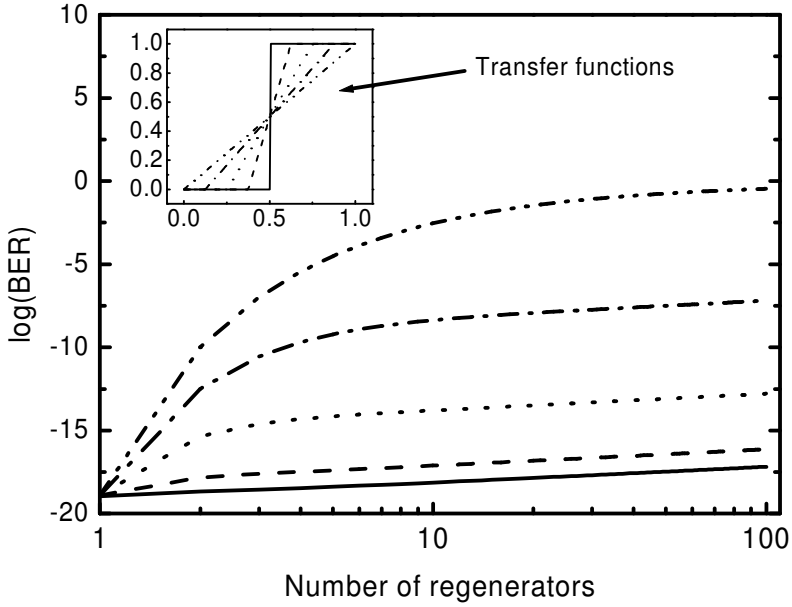

Figure 2.5: Calculated BER as function of number of regenerators for different degrees of non-linearity. The corresponding nonlinear transfer functions are shown in the inset.

function acting as an ideal decision giving a linear increase in errors. However, after one regenerator the BER is the same for all transfer functions, clearly showing that a regenerator cannot change the BER. The fact that all different non-linearities give the same BER after one regenerator, indicates the importance of considering the BER evolution in a cascade of regenerators when evaluating the performance. Experimentally this can be done in for example a recirculating loop. However, it has been shown [10] that by making sure that a suitable noise source is placed between the regenerator under investigation and the decision circuit of the receiver evaluating the BER, it is possible to get an idea of the performance of a single regenerator. This set-up is in fact just a cascade of two 'regenerators', one non-linear and one linear, and although it does not give as much information as a loop set-up, it is far easier to implement.

Even though we can experimentally evaluate the performance of a regenerator it is hard to define a figure of merit similar to the noise figure of linear amplifiers. A regenerator will always add noise, either through an active component like an SOA or by the fact that it introduces additional losses, which have to be compensated

for by an optical amplifier. Just like for a linear amplifier the amount of noise, and hence additional errors, that is added by the regenerator is important for the performance. This can be seen in Fig. 2.5 as the slope of the curves at a large number of regenerators. A lot of noise gives a faster increase in BER with number of regenerators. However, since the non-linear regeneration process is designed to improve the signal-to-noise ratio, the standard definition of noise figure does not really describe the amount of noise added, and is somewhat problematic to use for this purpose. The non-linearity of the intensity transfer function gives some indication about the performance, as seen, but it is just a static transfer function. It is a memory-less system, described by the time averaged input to output power relation and as such does not take any dynamics into consideration. As will be shown later in this report, the dynamics of the regenerator plays an important role in the noise re-distribution, which makes the static non-linear transfer function a less than complete way of describing the regenerator.

3R

Re-timing is needed since the pulses representing the one-symbol can drift out of their respective bit-slots in time. The process of compensating for this moves the pulses toward the center of their respective bit-slot, as shown schematically in Fig. 2.2. There are different ways of implementing re-timing but all of them require that the timing information of the incoming signal is recovered, so called clock recovery. All-optical clock recovery can be made using, for example, injection locking of a mode-locked laser [11, 12]. This process results in a clock signal or regular pulse train with a frequency equal to the bit rate of the incoming signal, as seen in Fig. 2.6. The signal is then re-timed either by synchronous modulation of the signal using the recovered clock [13], or by transferring the input signal to the recovered pulse train by use of an optical gate [14].

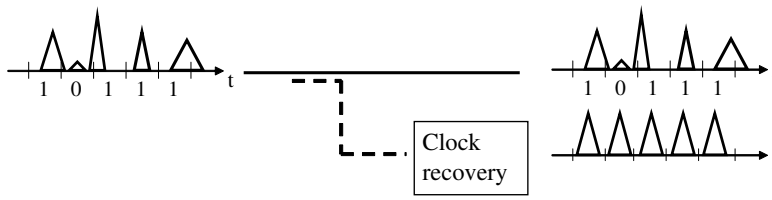

Figure 2.6: The concept of clock recovery.

In 2R-regeneration, that is if the re-timing is not performed, there is a trade-off between amplitude noise and timing jitter, since the non-linear transfer function responsible for the re-shaping also converts amplitude fluctuations to timing jitter [15]. This process is more pronounced for stronger non-linearities, which we have seen improves the amplitude re-shaping. This further complicates the task of finding measures of a good regenerator. Timing jitter and re-timing will, however, not be investigated in this work.

2.2 Basics of wavelength converters

In WDM-systems, which utilize the large bandwidth of optical fibers by sending several channels at different wavelength at the same time, it is sometimes necessary to change the wavelength. Some all-optical wavelength converter works by the principle that the incoming optical signal at the original wavelength opens and closes an all-optical gate, which in turn modulates a probe signal at the new wavelength, Fig. 2.7. Just like in the case of a repeater without wavelength conver-

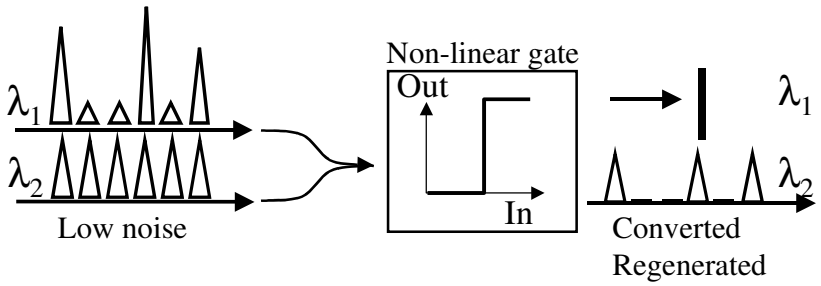

Figure 2.7: The concept of wavelength conversion with 3R-regeneration in nonlinear gate.

sion the gate can operate linearly, without any regeneration, or using a non-linear transfer function, which can make regeneration possible.

As a regenerator the wavelength converter uses a fundamentally different mode of operation than the simple regenerator, without wavelength conversion. In a wavelength converter the signal is transferred from the incoming degraded signal to a locally produced low noise probe. This is true even if the signal is converted to the same wavelength, as long as the original signal is not reused at the output. In this work the two modes of operation will be designated pass-through, for the case where the input signal is reused at the output, and wavelength conversion, for the case when the signal is transferred to a low noise probe. The differences between these two modes regarding noise redistribution, in a specific device, is one of the things that will be investigated.

2.3 The SOA, an introduction

A large part of this thesis is concerned with the semiconductor optical amplifier, SOA for short, or devices incorporating an SOA. However, no detailed investigations of specific device design will be made, and hence a complete picture of the device will not be presented. This section will try to give a short overview of the SOA. For further details the references [5, 16] can be studied.

A semiconductor optical amplifier is as the name implies an amplifier for an optical electromagnetic field made in semiconductor material. Structurally, the

SOA consists of an active gain medium and a waveguide for confinement of the optical field. The device is a traveling wave amplifier, which means that the optical field is injected into one end of the waveguide, is amplified as it travels along the amplifier and leaves the device through the other end of the waveguide. Compared to a laser diode, which has basically the same structure, the SOA have anti-reflection coatings on the facets in order to reduce reflections, since the Fabry-Perot cavity that would result between two reflecting facets would result in a very limited bandwidth [5]. To be able to further reduce the reflection the facets are usually angeled a few degrees in relation to the waveguide so that less of the optical field is reflected back into the waveguide, and thus feedback is decreased.

The optical gain is based on stimulated emission where an incoming photon stimulates the recombination of an electron and a hole, which results in the emission of a new photon with the same energy, phase and direction of propagation as the incoming photon. In order to have gain in the material this process must dominate over the case where an incoming photon stimulates the creation of an electron-hole pair, and is absorbed in the process. The condition under which the stimulated emission dominates over the stimulated absorption is called population inversion. Since the stimulated emission depends on the recombination of electrons and holes, the density of electrons in the conduction band and holes in the valence band must be above a certain level in order to reach population inversion. In intrinsic, i.e. undoped material the density of electrons and holes are the same and is usually referred to as just carrier density.

In order to increase the carrier density in the active region the material has to be pumped, which means that energy is provided to excite the electrons from the valence band to the conduction band and hence increase the carrier density. An SOA is usually pumped electrically, which means that carriers are injected into the active region by an electrical current through contacts connected to the SOA.

The material structure of an SOA is normally a p-i-n doped structure and the active part, i.e. where the useful stimulated emission takes place, is within the intrinsic region. This region is also designed to have a lower energy band gap and higher refractive index in order to confine both carriers and photons in the same region and increase the stimulated emission.

2.4 Regenerator and wavelength converters, a few examples

There are many different suggestions for specific implementations of regenerators in the literature. In most cases they are based on fiber or semiconductor components [7, 17–29]. The strengths of regenerators based on nonlinearities in optical fibers are mainly the very fast response time and low insertion loss. However the long fibers needed to achieve adequate nonlinearity make the devices bulky and sensitive to fluctuating environmental conditions, such as temperature [7]. Shorter fibers can be used but at the trade-off against the use of high input power. Semiconductor components on the other hand are small and can be integrated with other components, making them potentially compact and cheap. One difficulty is

that they have quite complicated dynamics on different time scales, some of which are comparable to the bit rate of modern optical communication systems [30]. This means that the response of the component to a specific signal bit depends on the bit-pattern preceding it in time. This effect is called pattern dependence, and might lead to strong signal degradation [31, 32].

The semiconductor devices most commonly used for signal processing in general, and regeneration specifically, are semiconductor optical amplifiers (SOAs) and electro absorbers (EAs). The way the functionality is achieved varies and is subject to substantial innovation. In this section a few examples of different ideas for all-optical repeaters, both regenerators and wavelength converters, will be presented.

2.4.1 SOA gate

A single SOA can be used as an all-optical gate by using the gain saturation, that is the effect that a high intensity in the amplifier reduces the carrier density and hence the optical gain [33]. If two signals is injected in the device a modulation on one of them can be transferred to the other through this effect, called cross gain modulation (XGM). As seen in Fig. 2.8 a high intensity in signal one leads to a low gain in the SOA and a low output intensity of signal two. A low signal level

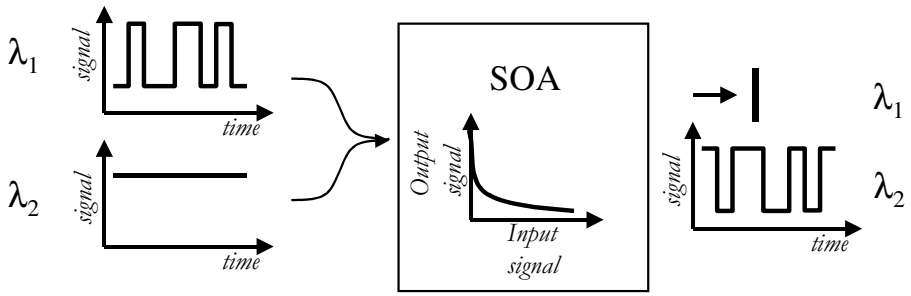

Figure 2.8: The concept of cross gain modulation in an SOA. The schematic transfer function is shown in the middle.

on the first signal does not saturate the gain, resulting in a high output power of the second signal. The signals can be injected co- or counter propagating. In the co-propagation scheme the two signals have to be at different wavelength and an optical filter is needed to remove the original signal at the output. In the counter propagating setup the wavelength conversion can be made to any wavelength without filtering, including the original wavelength.

2.4.2 Saturable absorbers

A very simple regenerator uses a single saturable absorber, for example an electro-absorber (EA), in order to achieve extinction ratio improvement and to a certain extent noise redistribution [19, 34–37]. The device absorbs low intensity noise, for example amplified spontaneous emission, while high intensity pulses are transmitted with low loss, Fig. 2.9. Although this setup improves the PDF at the zero

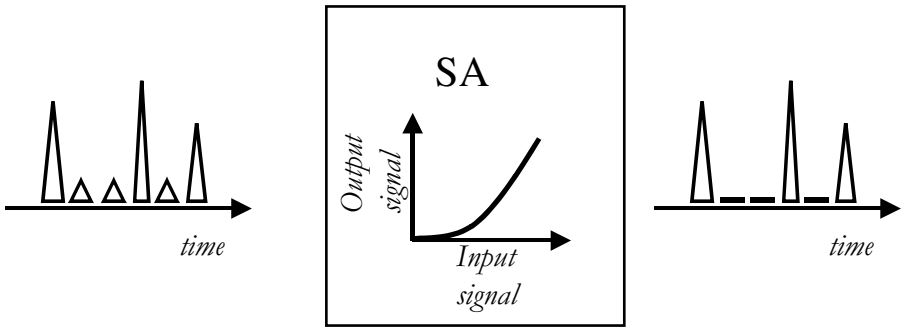

Figure 2.9: Concept of extinction ratio improvement in an saturable absorber.

level, the amplitude fluctuations of the one level is not affected or can even be increased [38]. One way to remedy this is to combine the saturable absorber with a SOA. The gain saturation in the amplifying section then gives a flat intensity transfer function also at high intensities and can thereby regenerate also the one level [39,40]. This device will be further discussed later. Another suggestion for reducing the amplitude variations on the logical one-level is to use a highly nonlinear fiber and an optical bandpass filter [41].

2.4.3 Interferometers

The most common approach for wavelength conversion and regeneration uses cross-phase modulation in an interferometric structure [23, 42]. A schematic example of a Mach-Zehnder (MZI) configuration is shown in Fig. 2.10. The input signal (λ_1) modulates the carrier density in semiconductor devices in the interferometer arms and thereby changes the refractive index. The change in refractive index transfers the intensity modulation of the input channel to a phase modulation of the output channel (λ_2), which is then transferred back to intensity modulation through interference at the output of the interferometer. If the input signal is injected in both interferometer arms but with a slight delay, Δt, such that the phase difference between the two arms is reset by the delayed signal, the time duration that the gate is open, the switching window, is controlled by the delay time. This can substantially increase the speed of the device compared to a setup where the switching window is controlled by the carrier lifetime in the SOAs [43].

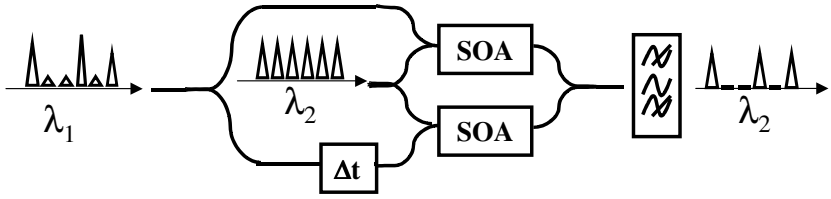

Figure 2.10: Mach-Zehnder interferometer for wavelength conversion and 3R-regeneration, in a delayed scheme.

With proper biasing the interferometer approach can also be used in pass-through mode [22, 24]. Other interferometric structures than an MZI can be used, for example an SOA multi mode interferometer (SOA-MMI) [26]. The perhaps simplest device uses a single SOA and a passive asymmetric interferometer and is called delayed-interferometer signal-wavelength converter (DISC), to achieve a similar functionality as the MZI described above [43].

2.4.4 Polarization rotators

Another approach uses the non-linear birefringence in an SOA. Due to the asymmetry in effective refractive index and confinement factor between the transverse electric (TE) and transverse magnetic (TM) modes in the waveguide, a change in carrier density leads to different phase changes for the two orthogonal polarization states and thus to a polarization rotation. By placing a polarization filter after the SOA and controlling the input polarization the intensity dependent polarization rotation can be used to achieve a non-linear transfer function and, hence, regeneration [25].

2.5 Summary

By using a probability density function picture of an intensity modulated signal the concept of regeneration, and its impact on signal quality, was introduced. The focus was on the reshaping using a non-linear intensity transfer function. The problem of defining a figure of merit for a 2R-regenerator was discussed briefly. Although the regeneration is indeed performed by a discrete component, the complete effect of the regeneration and hence the performance of the regenerator can only be seen as the signal is propagated through the system and a cascade of regenerators. Furthermore, regeneration is a non-linear process in the PDF-perspective, which renders the common measure of added noise, the noise figure, less useful. It also means that the shape of the PDFs are changed. The static non-linear transfer functions, which in principle could calculate the redistribution of the PDF, do

not take the dynamics of the device into consideration, and do therefore not give the complete picture. The questions this discussion leaves us with are the main objective of this work. They will not all be answered, but they will be the reason for almost all of the investigations in the following chapters.

The work horse of many devices for all-optical signal processing, the SOA, was introduced and briefly described. A small part of the multitude of examples of wavelength converters and regenerators employing this device was presented.

Not all of the tools and concepts used later on have been introduced so far, but in order to avoid putting the reader to sleep too early, more details will be presented in the report as they are needed. Now; let us move on to the more nitty-gritty part of this report.

Chapter 3

Noise in SOAs

3.1 The origin of SOA noise

As seen in Sec. 2.4 the SOA is used in many devices for regeneration and wavelength conversion. As any amplifier the SOA, in addition to providing gain, is also a source of noise. In principle there are different sources of noise in an SOA, such as noise from pump sources, carrier noise, and so-called amplified spontaneous emission, ASE. The dominant one [44] is in most cases ASE. This section will deal with the basics of amplified spontaneous emission in order to define some fundamental concepts. Detailed modeling of the influence of ASE noise in a saturated SOA is the topic for Sec. 3.4.

First a few words on other noise sources before starting with ASE. As described in Sec. 2.3 the gain in an SOA is provided by the inversion of carrier populations in the conduction and valence bands. Any random fluctuation in the carrier density will thus translate into a variation in gain and hence in the output optical field, this will be referred to as carrier noise. The carrier density is mainly determined by four processes, pumping, stimulated and spontaneous emission and non-radiative recombinations. The noise due to the pump source obviously depends on what pump source is used and can be included in the carrier noise. The non-radiative recombinations of carriers are all the processes, which decreases the number of excited carriers without producing any photons. The excess energy is instead dissipated as heat in the active material. The processes are combination at recombination centers such as defects, surfaces and interfaces in the material and Auger recombination. Auger recombination is when the energy from a hole-electron recombination is transfered to another carrier as kinetic energy, which is then scattered higher up in the conduction band. A detailed description of carrier noise is given in [45] but since for most cases it is dominated by the ASE it will not be studied in this work.

In any optical amplifier working through stimulated emission there will also be spontaneous emission [16], where photons are emitted from the spontaneous recombination of an electron-hole pair, i.e. without a stimulating photon. In this process the emitted photon has random phase and propagation direction. Some of

these spontaneously emitted photons will propagate along the waveguide, in both directions, be amplified, and exit at the facets. Since the spontaneous emission is random it will be a source of noise. It also means that for each spontaneously emitted photon there is one less electron-hole pair, which means that this process also contributes to the carrier noise. Since the gain spectrum of an SOA normally is fairly wide, the spontaneous emission can take place over a wide range of energies and the ASE is hence a broad-band noise source. In simple linear noise models, [46] for example, the ASE noise is considered to be a broad band noise field with a certain mean power. At the detector the different frequency components of this field beats with the signal field and itself, giving rise to what is called signal-spontaneous and spontaneous-spontaneous beat noise. The signal-spontaneous beat noise dominates at higher signal levels, while the spontaneous-spontaneous beat noise dominates at low signal levels. The ASE power is determined by the gain, the bandwidth and the inversion factor. However, as the ASE travels along the waveguide in an SOA it will interact nonlinearly with the input signal and with itself [44,47–53]. This nonlinear interaction is limited to a narrow bandwidth around the signal and leads to changes in the spectra of the signal field and to changes in the noise statistics. These kind of nonlinear interactions will be studied in this chapter.

3.2 Noise redistribution

As discussed in Sec. 3.1 the non-linear behavior of a saturated SOA is important for the properties of the added ASE. In a cascade of non-linear amplifiers the redistribution of the accumulated noise at the input of the amplifier also has to be considered. Again a more detailed discussion will be made later in this chapter, but already here a simplified and naive discussion based on the static transfer function will be made.

The intensity variations due to noise at the input of the SOA will modulate the carrier density, and hence the gain, through stimulated emission. A high input intensity leads to many electron-hole recombinations, which lowers the carrier density and results in low gain, and a low input intensity in the opposite way leads to high gain. Viewing the input signal as continuous wave, with a specific mean value, and with a small random modulation due to noise, this relation; high input intensity compared to the mean → lower gain and low input intensity → higher gain, give a self gain modulation, which counteracts the input variations, leading to smaller variations, relative to the mean, on the output than on the input, if no added noise is considered.

This process is obviously strongly dependent on the speed of the different carrier dynamics, but it can still be very instructive to view it in a static, memory less case. In this case the intensity transfer characteristics of the SOA is described by a time-averaged power transfer function, which is what would be measured when the output power is measured as a function of the input power with an ordinary power meter. One example of such a function for an SOA is shown in Fig. 3.4 in the next section. Let us assume that the transfer function can be

described mathematically as $y = f(x)$, where x represents the input power and y the output power. The stochastic variables describing the input and output signal including noise is then related through the same function, $Y = f(X)$. In this picture the probability density functions of the signal at the input and output is described by $\mathrm{PDF}_X(x)$ and $\mathrm{PDF}_Y(y)$, respectively. The output PDF is then given as a function of the input PDF by

$$\mathrm{PDF}_Y(y) = \left|\left(f^{-1}\right)'(y)\right| \mathrm{PDF}_X\left(f^{-1}(y)\right);\ y \in I_2, \tag{3.1}$$

assuming that f is real and a bijective mapping of an interval, I_1, of x on an interval, I_2, of y, and that f has a continuous derivative $f'(x) \neq 0$ in I_1. $f^{-1}(y)$ is the inverse function of $f(x)$ [54]. Using this relation a mathematical description or measurement of the transfer function can be used to calculate the output PDF assuming a certain input. It should be noted already now that the use of a static transfer function implies an infinitely fast device with a gain that can instantaneously follow the intensity variations. However, for a long cascade of amplifiers, or regenerators, where the accumulated noise can be large, the consideration of how a non-linear process redistributes the noise at the input has to be considered, and such an assumption might be justified under certain conditions. The examination of this type of redistribution, but including dynamic effects and ASE noise, is the main topic of the rest of this chapter.

3.3 PDF measurements

3.3.1 Measuring technique

In Sec. 2.1.1 the PDF-picture of a noisy signal was introduced in order to describe BER and regeneration. As a theoretical tool it is useful when describing the transformation of noise in a non-linear component, as seen in Sec. 3.2. In this section the PDFs and the redistribution of noise will be measured and shown to be more than just a neat theoretical picture [55–57].

The experimental setup is shown in Fig. 3.1. The first part of it is a light

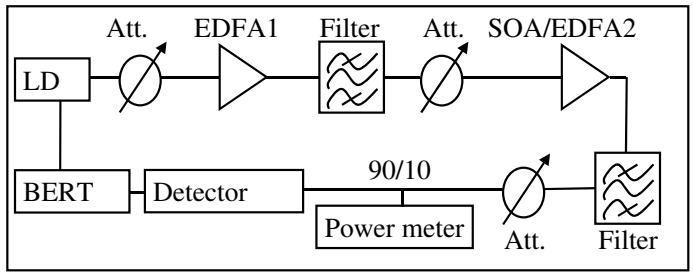

Figure 3.1: Setup for measuring the PDF after an optical amplifier.

source in the form of a continuous wave laser (LD) and a noise source in the form of a variable attenuator and a fiber amplifier (EDFA1). This setup allows for varying the signal-to-noise ratio of the input signal to the SOA by varying the input power to EDFA1 using the attenuator. The examined amplifiers are a commercial bulk InP/InGaAsP SOA and a fiber-based pre-amplifier (SOA/EDFA2), which is used for comparison. The equipment used for examining the output signal was a detector, a power meter and a bit-error rate test-set (BERT).

The probability density functions (PDFs) are derived from measuring the BER as function of decision threshold voltage [48, 58], and the principle is shown in Fig. 3.2. The low power tail (left side) of the PDF is measured assuming that the continuous wave signal is a string of ones. By changing the decision threshold of the BER test-set the BER-dependence on threshold level can be mapped out. As described in Sec. 2.1.1 the BER is derived from the integral of the PDF and hence the PDF can be calculated as the derivative of the BER with respect to threshold voltage.

$$\mathrm{PDF} = \frac{\Delta \mathrm{BER}}{\Delta V_{\mathrm{th}}} \tag{3.2}$$

The high power tail (right side) of the PDF is measured in the same way but where the signal is assumed to consist of a string of zeros. Since the main interest in this investigation is in the optical noise rather than the noise from the detector, the measured voltage can be related to the optical power by making sure that the detector is linear in the measuring range and relating the measured mean values of the PDFs at different power levels to that of the measured optical power at the detector. In all figures the PDFs will be plotted as a function of optical power.

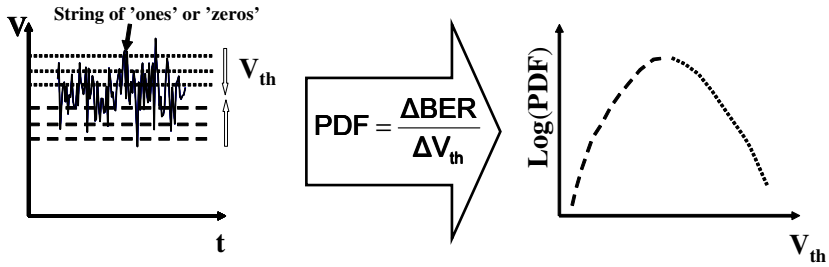

Figure 3.2: PDF measuring technique.

This way of measuring the PDF allows for measuring as far out in the tails as the BER test set can accurately count errors. If the idea is, as in our case, to examine changes in the PDFs far out in the tails where they influence the number of errors relevant in a communication systems perspective, this method will thus per definition give relevant PDF measurements.

To start out let's compare the measured results to that of the concept of non-linear noise redistribution discussed in Sec. 3.2. This is done in Fig. 3.3, Fig. 3.4 and Fig. 3.5. The measured input PDF is shown in the lower part of Fig. 3.3. The

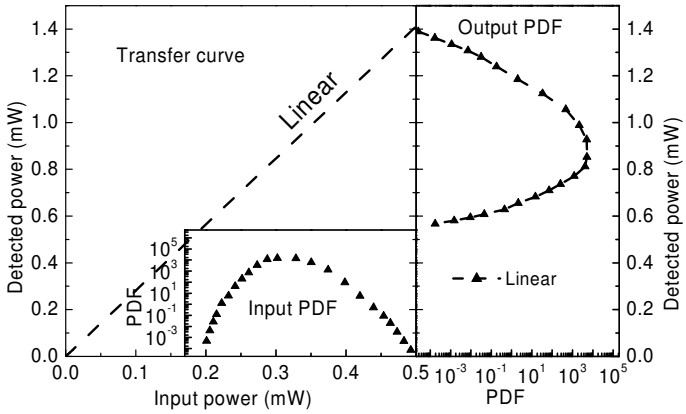

Figure 3.3: Linear transformation of PDF. The input PDF is shown at the bottom, to the left is the transfer function and to the right the transfered PDF.

upper left part shows a linear transfer function, corresponding to the steady state gain of the SOA at the specific input power described by the input PDF. The right part of the figure shows the input PDF transformed with the linear function. The signal to noise ratio of the input signal, as deduced from the PDF, is 22dB.

Fig. 3.4 shows the same input PDF but the transfer function in this figure is the measured nonlinear transfer function, i.e. time-averaged output power versus input power, and the input PDF is transformed using this function, giving the result shown to the right. The two transformations in Fig. 3.3 and Fig. 3.4 follows the procedure outlined in Sec. 3.2 and show the expected results. For the linear case the output PDF differs from the input by a constant factor, which is the gain (or slope) of the transfer function. In the non-linear case the mean value of the output PDF is given by the gain at that specific point of the transfer function, while the over all shape is changed due to the change of slope of the transfer function with input power. Most obvious of the changes in shape is the much more narrow PDF at the output. Now let's see what the measured PDF looks like.

In Fig. 3.5 we compare the measured output PDF (solid circles) to the transformed PDFs of Fig. 3.3 and Fig. 3.4. The measured PDF ends up in between the two previous cases. Since the gain of the SOA is obviously quite strongly saturated, and hence can not be considered to be in a linear regime the linear transformation is not expected to give a good description of the SOA, but why does not the measured transfer function give better agreement? The detailed explanation of this will be made in Sec. 3.6.1, when we also have the theoretical results, but already here a first qualitative explanation can be made.

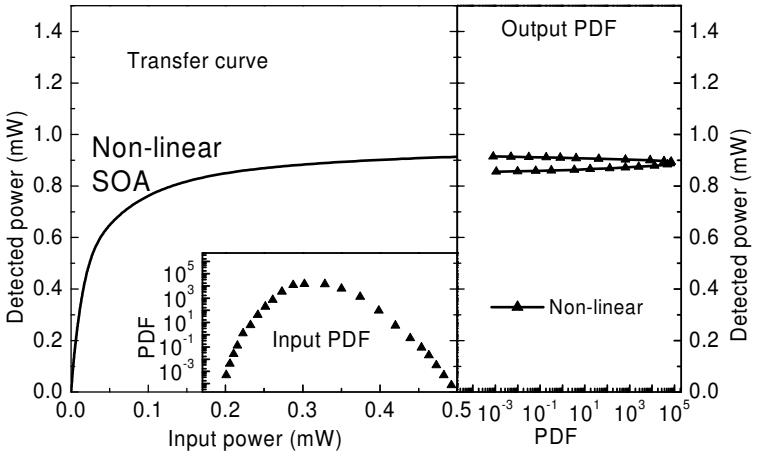

Figure 3.4: Non-linear transformation of PDF using measured static transfer function of an SOA. The input PDF is shown at the bottom, to the left is the transfer function and to the right the transfered PDF.

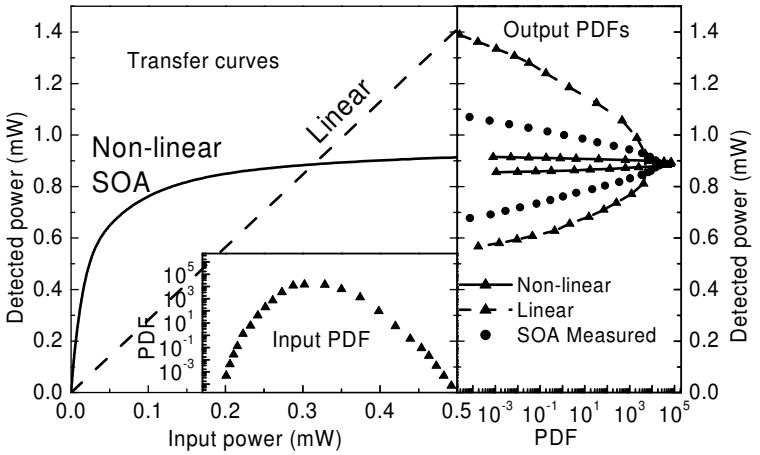

Figure 3.5: Measured PDF compared to the limiting cases of linear and static non-linear transformation of PDF.

The reason for the discrepancy is that the transfer function does not contain any information of the dynamics of the device, as described by its recovery time. The linear case corresponds to a slow device (long recovery time) so that the gain cannot follow the intensity variations of the high bandwidth noise, which then only

experiences the mean gain. The measured static transfer function corresponds to a high speed device (short recovery time) so that the gain modulation follows the intensity variations instantaneously. The bandwidth of the noise is controlled by the optical filter before the SOA and is in the order of one nanometer, or 125 GHz. The recovery time of a typical SOA is on the order of a hundred picoseconds, corresponding to a modulation bandwidth of less than 10 GHz. The limited modulation bandwidth of the SOA compared to the noise bandwidth results in that only the low frequency part of the noise spectrum is redistributed according to the non-linear transfer function, while the high frequency part only experience the linear gain. In the present case, the measurement bandwidth ($B_e \approx 10$ GHz) is of the same order of magnitude as the modulation bandwidth of the SOA. This means that the noise transformation can be described neither by the static (saturation) transfer curve, which implies too strong noise suppression due to the non-linearity, nor by a linear transfer function, which neglects the gain dynamics all-together.

3.3.2 Gain saturation dependency

By measuring the PDF at different input powers the redistribution at different levels of gain saturation can be examined. The gain as a function of input power can be seen in Fig. 3.6, where the measuring points of -5, -12, -20 and -30 dBm are also marked by arrows. These measuring points were chosen to give PDFs from the non-saturated, strongly saturated as well as intermediate regimes. In

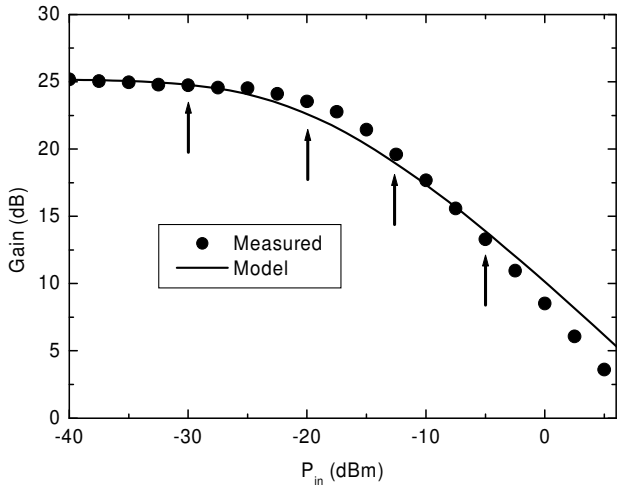

Figure 3.6: Measured gain of the examined SOA as function of input power. The input power levels where the PDFs are measured are marked by arrows.

Fig. 3.7 the PDFs after the SOA are compared to the EDFA in a case without the noise source, i.e. where the input noise originates only from the laser diode

and is very low. In Fig. 3.8 a case with noise source is shown, and the input signal-to-noise ratio is about 22dB, as evaluated from the input PDF. In the low

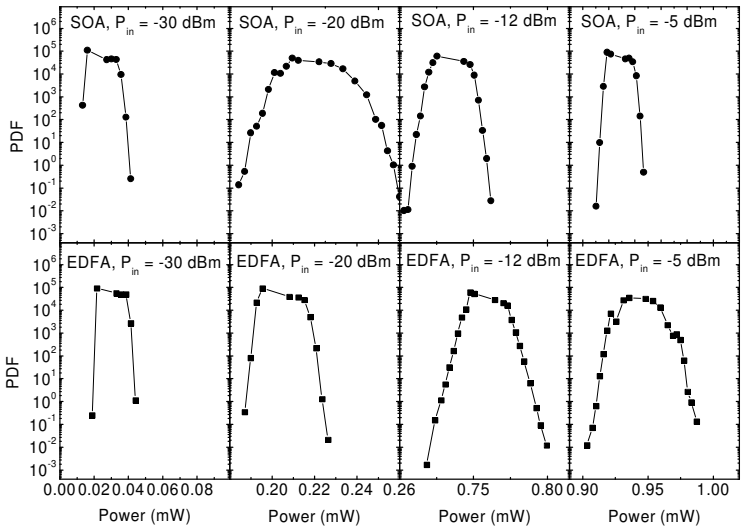

Figure 3.7: Comparison of measured PDFs after an EDFA and an SOA with low input noise.

input noise case in Fig. 3.7 the PDFs are mainly dominated by electrical noise from the receiver set-up, as will be discussed more later in this section. This can be seen by noticing that the most narrow PDFs all look the same, indicating the same noise contributions, regardless of input noise or signal power level. In the case with the noise source, however, the PDFs are dominated by optical noise and the differences between the SOA and the EDFA can be examined. In Fig. 3.8 it is clearly seen how the noise distribution after the SOA narrows, compared to the EDFA, as the mean power increases. This is expected from the decrease of the slope of the SOA power transfer function, Fig. 3.4, going from low to high powers. The slow dynamics of the EDFA compared to the measurement bandwidth renders the EDFA a linear device, in terms of noise transformation, and no narrowing is seen. For the -5 dBm input power case the output PDF of the EDFA is compared to the input PDF transformed using the linear transfer function. Apart from a slight broadening due to the added ASE in the EDFA the PDF shape is the same, again indicating a linear device.

In order to analyze the measured PDFs further the central moments can be extracted by calculating the cumulant generating function [59]. The cumulant generating function is defined as the natural logarithm of the moment generating function, which is the expectation value of e^{-sx} or

$$\mathrm{CGF}(s) = \ln\left(\mathrm{MGF}(s)\right) = \ln\left(\int_{-\infty}^{\infty} \mathrm{PDF}(x) e^{-sx} dx\right). \tag{3.3}$$

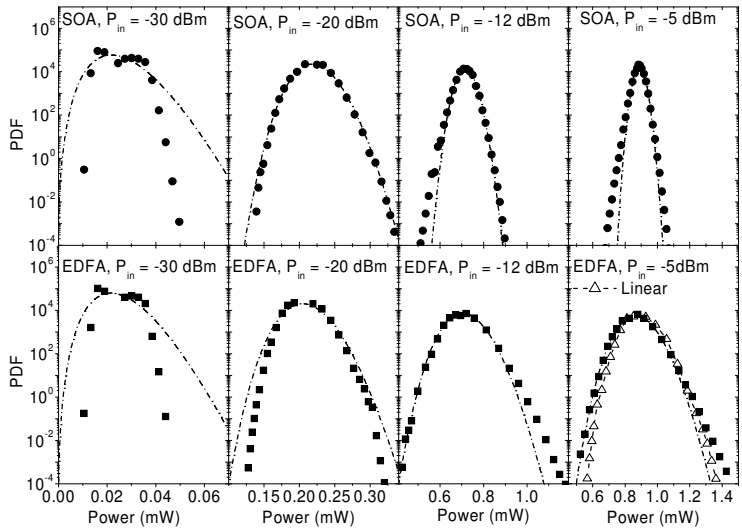

Figure 3.8: Comparison of measured PDFs after an EDFA and an SOA with high input noise. Both cases are also compared to a non-central χ^2-distribution with the same mean and variance (dash-dotted). The EDFA is in the -5 dBm case also compared to the input PDF transformed with the linear gain (open triangles)

From the cumulant generating function the cumulants of order n can be calculated by

$$k_n = (-1)^n \left. \frac{\partial^n \mathrm{CGF(s)}}{\partial s^n} \right|_{s=0}. \tag{3.4}$$

The first order cumulant is identical to the mean value and order two and three are identical to the respective central moments defined by

$$m_n = \int_{-\infty}^{\infty} (x-\mu)^n \mathrm{PDF}(x) dx, \tag{3.5}$$

where μ is the mean value of the distribution. The definition of central moments is more easy to relate to than the cumulant generating function and from Eq. (3.5) it is seen that the second order central moment (or cumulant) is the variance. In practice it is easier to calculate the MGF as the Fourier transform of the PDF, which is the method used in this work.

Fig. 3.8 also includes non-central χ^2 distributions plotted using the mean and variance calculated from the measured PDF. The poor agreement at -30 dBm input power is again due to that the PDFs are dominated by electrical receiver noise rather than the optical noise. At higher input powers the agreement in the SOA case is fairly good with some deviations in the tails, which are attributed to noise redistribution. In the EDFA case the measured output PDF differs from the non-central χ^2 distribution in a similar way as the input PDF. This again indicates

that the EDFA is linear when it comes to noise redistribution, while the SOA is non-linear and redistributes the noise.

In order to see the noise redistribution in the SOA more clearly the skewness and standard deviation of the PDFs, for the high input noise case, are plotted versus their mean values in Fig. 3.9 and Fig. 3.10, respectively. The skewness is

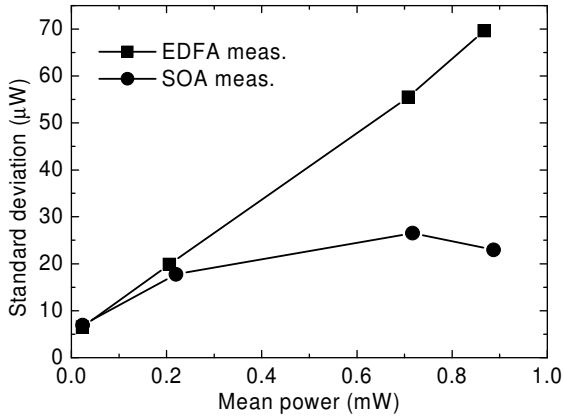

Figure 3.9: Measured standard deviation as a function of mean power for the high input noise case.

the normalized third order central moment

$$\gamma_s = \frac{m_3}{m_2^{3/2}} \tag{3.6}$$

and describes the asymmetry of the PDF [59], with a positive/negative number indicating a long high/low power tail. This property of the skewness can also be seen in Fig. 3.11 and from Eq. (3.5) where the odd order central moments are seen to have different signs for distributions skewed to different sides of their respective mean values.

In Fig. 3.12 the standard deviation of the low noise case is plotted versus the mean value, in order to see the impact of ASE from the two amplifiers.

The non-linear transfer function of the SOA reduces the width of the PDF compared to the linear EDFA. This noise compression is seen both for the case with high input noise, Fig. 3.9, but also when the noise at the input is low, Fig. 3.12. For low input noise, the higher ASE noise of the SOA is seen at low powers, as a larger standard deviation, while at high power the noise suppression due to gain saturation and self-modulation reduces the ASE noise for the SOA. The noise level of the detector can also be deduced from Fig. 3.9 and Fig. 3.12 by noting that in all cases the standard deviation approaches the same finite value for low powers, and low optical noise. This indicates a noise level of about 6 μW, which fits fairly well with the noise equivalent power of the detector, specified to be 3 μW at 10 GHz. For the cases with high input noise the optical noise clearly dominates at

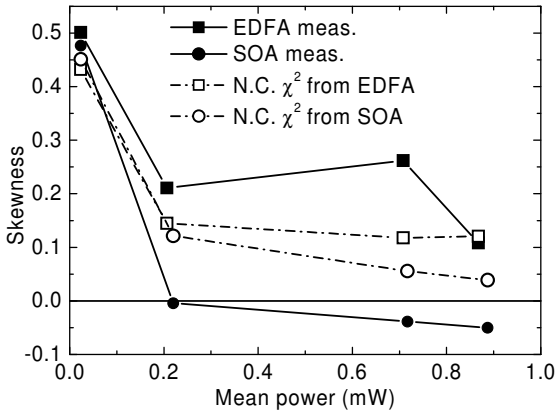

Figure 3.10: Measured skewness as a function of mean power for the high input noise case. The skewness for non-central χ^2-distributions with the same mean and standard deviation is shown (open symbols) for comparison.

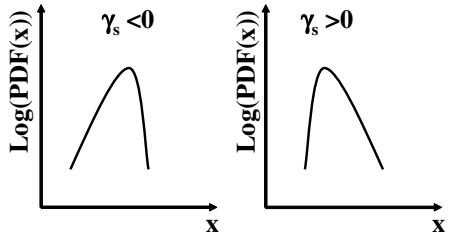

Figure 3.11: Schematic picture of the skewness of a PDF.

higher input powers, while for the low input noise the optical noise is comparable to the detector noise.

Furthermore, it is seen in Fig. 3.10 that the noise redistribution in the SOA gives a shift from positive to negative skewness when the power is increased. This shift toward negative skewness for higher powers indicates that the usual approximation of a non-central χ^2-distribution no longer holds, since this distribution always has positive skewness. The comparison to the non-central χ^2-distribution is shown explicitly in Fig. 3.10, where the skewness of this distribution is calculated using the measured mean and standard deviation. A negative skewness also means a higher probability of errors at the one-level, which to some degree counteracts the suppression of the standard deviation, compared to the linear case, and should be considered when for example all-optical regeneration in SOA-based devices is considered.

In summary the experimental examination of the statistics of a noisy signal at

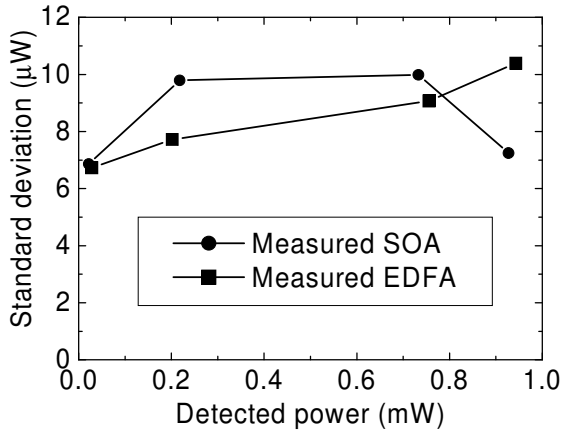

Figure 3.12: Standard deviation as a function of mean power for the low input noise case.

the output of a saturated SOA in the form of PDFs show both a compression of the noise and a change in the overall shape of the PDF. These noise redistributions will be examined further using theoretical modeling and calculations presented in Sec. 3.4. The examinations and comparison to the experimental results presented above will be done in Sec. 3.5. An investigation of the influence of noise suppression, in the form of lower standard deviation, and skewness on the BER will be investigated in Sec. 3.6.4.

3.4 SOA noise models

This section describes the different models we use to investigate the noise in SOAs. The actual results from the models is presented in Sec. 3.5, where the different models are compared to each other and measurements. Some details of the derivations are left out of this section and presented in the appendices.

All the different noise models are based on the same device model; a standard rate equation model for the carrier density in an SOA, and a propagation equation for the electric field, described in [60]. The analysis of noise in the SOA is performed in two different ways, a small-signal analysis and a large-signal simulation. In both cases, the noise model is based on the same basic assumptions. The noise is thus incorporated in the equations by Langevin forces, in accordance with [44] and [61]. The resulting equations for carrier density and optical field are,

$$\frac{\partial N}{\partial t} = \frac{I}{qV} - \frac{N}{\tau_s} - \frac{g(N)}{A\hbar\omega_0}|\tilde{E}|^2 + \tilde{f_N} \tag{3.7}$$

$$\frac{\partial \tilde{E}}{\partial z} = \frac{1}{2}(g(1-i\alpha) - \alpha_{\text{int}})\tilde{E} + \tilde{f_E}. \tag{3.8}$$

In these equations, I is the injected current, q is the elementary charge, V is the active volume, τ_s is the spontaneous carrier lifetime, A is the effective cross-section area of the active region, $\hbar\omega_0$ is the photon energy, α is the linewidth enhancement factor and α_{int} is the waveguide loss and $\tilde{E}(t,z)$ is the complex envelope of the optical field normalised such that $|\tilde{E}|^2$ is the power. The time variable t is a shifted time coordinate, $t = t_{\text{real}} - z/v_g$, where t_{real} is the real time coordinate and v_g is the group velocity. The gain, $g(N)$, is approximated as a linear function of the carrier density and it is assumed that the carrier frequency ω_0 is chosen at the gain peak. The gain is then

$$g(N) = a(N - N_0) \tag{3.9}$$

where a is the differential modal gain and N_0 is the carrier density at transparency. $\tilde{f}_N$ and $\tilde{f}_E$ are the noise terms (Langevin forces) for the carriers and spontaneous emission respectively. The electric field and the noise terms are from now on normalized with the square root of the saturation power, $E = \tilde{E}/\sqrt{P_{\text{sat}}}$, $f_i = \tilde{f}_i/\sqrt{P_{\text{sat}}}$ $(i = E, N)$. The spontaneous emission is considered as a Gaussian noise source with correlation functions

$$\begin{aligned} \langle f_E(z_1,t_1) f_E^*(z_2,t_2)\rangle &= \frac{\hbar\omega_0}{P_{\text{sat}}} g_s n_{\text{sp}} \delta(z_1 - z_2) R(t_1 - t_2) \\ \langle f_E(z_1,t_1) f_E(z_2,t_2)\rangle &= 0 \end{aligned} \tag{3.10}$$

where the saturation power and steady state gain coefficient are

$$P_{\text{sat}} = \frac{A\hbar\omega_0}{a\tau_s}, \tag{3.11}$$

$$g_s = \frac{g_0}{1 + P/P_{\text{sat}}}, \tag{3.12}$$

$n_{\text{sp}} \approx (g_s + aN_0)/g_s$ is the spontaneous emission factor and g_0 is the gain coefficient without any optical input power. The steady state solution of the gain is achieved by setting the time derivative and noise terms in Eq. (3.7) to zero. The carrier noise, described by f_N, can be shown, in many cases, to be small compared to the amplified spontaneous emission noise [44], and will be neglected in the following examinations. The function $R(\tau)$, which controls the correlation in time, can be chosen to represent the physical system under consideration. By noting that the Fourier transform of $R(\tau)$ is the spectrum of the noise, through the Wiener-Khinchin theorem [62], a physical choice of $R(\tau)$ should give the local normalized spontaneous emission spectrum of the amplifier. Commonly a white, i.e. constant, noise spectrum is chosen. This can often be motivated by limiting the investigations to a frequency range within which the spectrum is actually flat. However, this assumption has the drawback that a constant, unlimited noise spectrum means that there is infinite noise power. In this work we will compare different models based on the same basic assumptions, and one of the models is a sampled time-domain simulation. The time step, Δt, which we use for the discrete sampling of our signal, give us a numerical limit to our spectrum through the sampling theorem. By assuming that the signal is a sample-and-hold signal, i.e. the

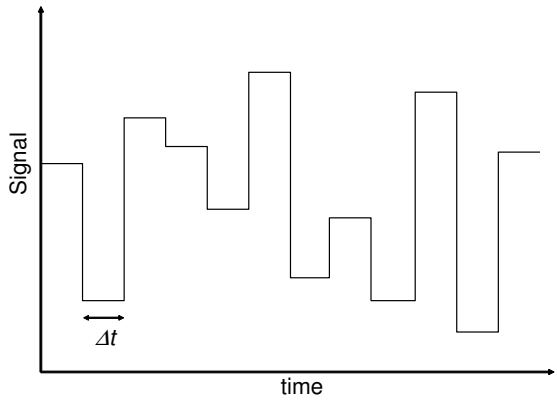

Figure 3.13: Schematic of a sample-and-hold signal

signal is constant between sampling points as shown in Fig. 3.13, the correlation in time becomes

$$R(\tau) = \begin{cases} 0; & |\tau| \geq \Delta t \\ \frac{1}{\Delta t}\left(1 - \frac{|\tau|}{\Delta t}\right); & |\tau| \leq \Delta t. \end{cases} \tag{3.13}$$

This correlation corresponds to a sinc^2-shaped spectrum, which also limits the amount of noise power. As long as the sampling interval is short enough to make the noise spectrum much wider than any filtering in the system this assumption gives results very similar to the white noise assumption.

Now we will move on to describing the models used. The basic equations above will first be analyzed using a small-signal assumption in Sec. 3.4.1 and then using a large-signal, statistical simulation approach in Sec. 3.4.2.

3.4.1 Small signal analysis

The first of the two noise descriptions assumes that the noise is small compared to the signal field and hence can be considered as a small perturbation.

If Eq. (3.8) is written

$$\frac{\partial E}{\partial z} = \frac{1}{2}(g(1 - i\alpha) - \alpha_{\mathrm{int}})E + \lambda f_E. \tag{3.14}$$

the electric field, including any random fluctuations from the noise terms, can be expanded in a Volterra series [63] in the arbitrarily chosen parameter λ

$$E(\lambda) \approx E_{\mathrm{s}} + E_1\lambda + E_2\lambda^2 + ... + E_n\lambda^n \tag{3.15}$$

were E_s is the electric field without noise and

$$E_1 = \frac{1}{1!}\left.\frac{\mathrm{d}E}{\mathrm{d}\lambda}\right|_{\lambda=0}$$
$$E_2 = \frac{1}{2!}\left.\frac{\mathrm{d}^2E}{\mathrm{d}\lambda^2}\right|_{\lambda=0}$$
$$E_n = \frac{1}{n!}\left.\frac{\mathrm{d}^nE}{\mathrm{d}\lambda^n}\right|_{\lambda=0}.$$

By setting the arbitrary chosen λ equal to unity, splitting the electric field in its amplitude and phase

$$E = \rho \mathrm{e}^{i\phi} \tag{3.16}$$

and limit the order of the expansion to 2, Eq. (3.15) can be written as

$$\begin{aligned} E &\simeq (\rho_\mathrm{s} + \rho_1 + \rho_2)e^{i(\phi_\mathrm{s}+\phi_1+\phi_2)} \\ &= \rho_\mathrm{s}e^{i\phi_\mathrm{s}}\left(1 + \frac{\rho_1}{\rho_\mathrm{s}} + \frac{\rho_2}{\rho_\mathrm{s}}\right)e^{i(\phi_1+\phi_2)} \\ &= E_\mathrm{s}E_\mathrm{p}. \end{aligned} \tag{3.17}$$

In Eq. (3.17) ρ_1, ρ_2, ϕ_1 and ϕ_2 can be seen as the perturbations of the steady state field to first and second order due to noise. By series expansion of the exponential E_p can be written as

$$E_\mathrm{p} \simeq 1 + \frac{\rho_1}{\rho_\mathrm{s}} + i\phi_1 + \frac{\rho_2}{\rho_\mathrm{s}} - \frac{\phi_1^2}{2} + i\left(\phi_2 + \frac{\rho_1\phi_1}{\rho_\mathrm{s}}\right) + ... \tag{3.18}$$

The gain coefficient is, in the same manner, written as

$$g = g_\mathrm{s} + g_1 + g_2. \tag{3.19}$$

where g_1 and g_2 are perturbations to the steady state gain g_s.

The small-signal analysis can thus be performed, in principle, to any order in the expansion of the field and gain. The first order expansion has already been done by Shtaif et al. [44], and will, in a short form be presented and used later as a reference. This first order model, however, can only give information about the mean and standard deviation of the noise distribution, as will be seen. Since this investigation of the noise redistribution also includes the change in PDF shape, as described for example by the skewness, a higher order model is needed. A model taking the second order terms into considerations have been developed by the author and his supervisors and will be presented next.

Second order

By inserting Eq. (3.17) into Eq. (3.8) and comparing it to the same equation for E_s, i.e. without noise, an equation for E_p is achieved

$$\frac{\mathrm{d}E_\mathrm{p}}{\mathrm{d}z} = \frac{1}{2}(g - g_\mathrm{s})(1 - i\alpha)E_\mathrm{p} + \frac{f_E}{E_\mathrm{s}}. \tag{3.20}$$

Now Eq. (3.18) is inserted in Eq. (3.20) and the terms of the same order are collected. The first and second order equations become

$$\frac{\partial}{\partial z}\left(\frac{\rho_1}{\rho_s}+i\phi\right)=\frac{1}{2}g_1(1-i\alpha)+\frac{f_E}{E_\mathrm{s}} \tag{3.21}$$

$$\frac{\partial}{\partial z}\left(\frac{\rho_2}{\rho_\mathrm{s}}-\frac{\phi_1^2}{2}+i\left(\phi_2+\frac{\rho_1\phi_1}{\rho_\mathrm{s}}\right)\right)=\frac{1}{2}\left(g_2+\frac{g_1\rho_1}{\rho_\mathrm{s}}+i\phi_1 g_1\right)(1-i\alpha) \tag{3.22}$$

These equations are then split into their real and imaginary parts, the results are for first order:

$$\frac{\partial}{\partial z}\left(\frac{\rho_1}{\rho_\mathrm{s}}\right)=\frac{1}{2}g_1+N_\rho \tag{3.23}$$

$$\frac{\partial}{\partial z}\phi_1=-\frac{\alpha}{2}g_1+N_\phi \tag{3.24}$$

where $N_\rho=\mathrm{Re}(f_E/E_\mathrm{s})$ and $N_\phi=\mathrm{Im}(f_E/E_\mathrm{s})$. The equations for the second order become:

$$\begin{aligned}\frac{\partial}{\partial z}\left(\frac{\rho_2}{\rho_\mathrm{s}}-\frac{\phi_1^2}{2}\right)&=\frac{1}{2}\left(g_2+\frac{g_1\phi_1}{\rho_\mathrm{s}}+\alpha\phi_1 g_1\right)\Rightarrow\\ \Rightarrow\frac{\partial}{\partial z}\left(\frac{\rho_2}{\rho_\mathrm{s}}\right)&=\frac{1}{2}\left(g_2+\frac{g_1\phi_1}{\rho_\mathrm{s}}\right)+\phi_1 N_\phi\end{aligned} \tag{3.25}$$

$$\begin{aligned}\frac{\partial}{\partial z}\left(\phi_2+\frac{\rho_1\phi_1}{\rho_\mathrm{s}}\right)&=-\frac{\alpha}{2}\left(g_2+\frac{g_1\rho_1}{\rho_\mathrm{s}}\right)+\frac{g_1\phi_1}{2}\Rightarrow\\ \Rightarrow\frac{\partial}{\partial z}\phi_2&=-\frac{\alpha}{2}g_2-\phi_1 N_\rho-\frac{\rho_1}{\rho_\mathrm{s}}N_\phi.\end{aligned} \tag{3.26}$$

Using Eq. (3.9) in Eq. (3.7) the differential equation for the gain becomes

$$\frac{\partial g}{\partial t}=\frac{g_0-g}{\tau_\mathrm{s}}-\frac{g}{\tau_\mathrm{s}}|E|^2 \tag{3.27}$$

The first order gain equation is then (using Eq. (3.17), Eq. (3.18) and Eq. (3.19))

$$\tau_\mathrm{s}\frac{\partial g_1}{\partial t}=-g_1-\rho_\mathrm{s}^2 g_1-2g_\mathrm{s}\rho_\mathrm{s}\rho_1 \tag{3.28}$$

and the equation for the second order gain

$$\tau_\mathrm{s}\frac{\partial g_2}{\partial t}=-g_2-\rho_\mathrm{s}^2 g_2-(g_\mathrm{s}\rho_1^2+2\rho_\mathrm{s}g_1\rho_1+2g_\mathrm{s}\rho_\mathrm{s}\rho_2). \tag{3.29}$$

So far the first and second order perturbations have been introduced and the corresponding differential equations for the field and gain have been formulated. Now it is time to solve these equations for ρ_1, ρ_2 and ϕ_1.

Solving Eq. (3.28) and Eq. (3.29) in the frequency domain yields

$$g_1(z,\omega) = \frac{-2g_s\rho_s^2}{1+\rho_s^2+i\omega\tau_s}\frac{\rho_1}{\rho_s} \tag{3.30}$$

$$g_2(z,\omega) = -\frac{g_s\rho_1 \otimes \rho_1 + 2\rho_s g_1 \otimes \rho_1 + 2g_s\rho_s\rho_2}{1+\rho_s^2+i\omega\tau_s}. \tag{3.31}$$

where $\otimes$ means a convolution in the frequency domain. The frequency domain equations for the first and second order amplitude and the first order phase then becomes

$$\frac{\partial}{\partial z}\left(\frac{\rho_1}{\rho_s}\right) = -\frac{g_s\rho_s^2}{1+\rho_s^2+i\omega\tau_s}\frac{\rho_1}{\rho_s} + N_\rho \tag{3.32}$$

$$\frac{\partial}{\partial z}\left(\frac{\rho_2}{\rho_s}\right) = -\frac{g_s\rho_s^2}{1+\rho_s^2+i\omega\tau_s}\frac{\rho_2}{\rho_s} + B(\omega,z) \tag{3.33}$$

$$\frac{\partial}{\partial z}(\phi_1) = \frac{\alpha g_s\rho_s^2}{1+\rho_s^2+i\omega\tau_s}\frac{\rho_1}{\rho_s} + N_\phi \tag{3.34}$$

with solutions, in the frequency domain,

$$\frac{\rho_1(z,\omega)}{\rho_s(z)} = \left(H(0,\omega)\frac{\rho_1(0,\omega)}{\rho_s(0)} + \int_0^z H(z',\omega)N_\rho(z',\omega)dz'\right)H(z,\omega)^{-1} \tag{3.35}$$

$$\frac{\rho_2(z,\omega)}{\rho_s(z)} = \left(H(0,\omega)\frac{\rho_2(0,\omega)}{\rho_s(0)} + \int_0^z H(z',\omega)B(z',\omega)dz'\right)H(z,\omega)^{-1} \tag{3.36}$$

$$\begin{aligned}\phi_1(z,\omega) = \phi_1(0,\omega) &- \alpha\left(\frac{H(0,\omega)}{H(z,\omega)} - 1\right)\frac{\rho_1(0,\omega)}{\rho_s(0)} \\ &+ \int_0^z \left[\alpha\left(1 - \frac{H(z',\omega)}{H(z,\omega)}\right)N_\rho(z',\omega) + N_\phi(z',\omega)\right]dz'\end{aligned} \tag{3.37}$$

where

$$H(z,\omega) = \exp\left(-\int_z^L \frac{g_s\rho_s^2}{1+\rho_s^2+i\omega\tau_s}dz'\right) \tag{3.38}$$

and

$$B(z,\omega) = \frac{1}{2}\frac{g_1 \otimes \rho_1}{\rho_s} - \frac{1}{2}\frac{g_s\rho_1 \otimes \rho_1 + 2\rho_s g_1 \otimes \rho_1}{1+\rho_s^2+i\omega\tau_s} + \phi_1 \otimes N_\phi. \tag{3.39}$$

Assuming that all terms of the second order cancel each other out, for both the real and imaginary part, at the input of the amplifier, the second order amplitude into the amplifier is

$$\frac{\rho_2(0,\omega)}{\rho_s(0)} = \frac{\phi_1(0,\omega)^2}{2}. \tag{3.40}$$

By using Eq. (3.35) - Eq. (3.39) in Eq. (3.17) and Eq. (3.18) the output field from the SOA can be expressed.

The output field from the SOA is now filtered with a real time response function, $F(t)$, corresponding to an optical filter with a bandwidth much smaller than the spontaneous emission spectrum. The real response function means that there

is no frequency to amplitude modulation conversion in the filter. The filtered output field is then, in the time domain,

$$\begin{aligned} E_{\mathrm{F}}(L,t) = E_{\mathrm{s}}(L) \Bigg[& 1 + F * \frac{\rho_1(L,t)}{\rho_{\mathrm{s}}(L)} + iF * \phi_1(L,t) \\ & + F * \frac{\rho_2(L,t)}{\rho_{\mathrm{s}}(L)} - F * \frac{\phi_1(L,t)^2}{2} \\ & + i \left(F * \phi_2(L,t) + F * \frac{\rho_1(L,t)\phi_1(L,t)}{\rho_{\mathrm{s}}(L)} \right) + ... \Bigg] \end{aligned} \tag{3.41}$$

where $*$ means a convolution in the time domain. The filtered and normalised output power is thus

$$\begin{aligned} P(L,t) = |E_{\mathrm{F}}|^2 = P_{\mathrm{s}} \Bigg[& 1 + 2F * \frac{\rho_1}{\rho_{\mathrm{s}}} + \left(F * \frac{\rho_1}{\rho_{\mathrm{s}}} \right)^2 \\ & + 2F * \frac{\rho_2}{\rho_{\mathrm{s}}} + (F * \phi_1)^2 - F * \phi_1^2 + ... \Bigg] \end{aligned} \tag{3.42}$$

By inserting the time domain versions of Eq. (3.35), Eq. (3.36) and Eq. (3.37) in Eq. (3.42) it can be written on the form

$$\begin{aligned} P(t) = P_{\mathrm{s}} \Bigg(& 1 + 2 \int K_\rho(z, t-t') N_\rho(t') dz dt' \\ & + 2 \int K_\rho(z, t-t') \frac{\rho_1(z,t')}{\rho_{\mathrm{s}}(z,t')} \delta(z+) dz dt' \\ & + \sum_{\alpha,\beta} \int N_\alpha(z_1,t_1) O_{\alpha,\beta}(z_1, t-t_1; z_2, t-t_2) N_\beta(z_2,t_2) dz_1 dz_2 dt_1 dt_2 \Bigg) \end{aligned} \tag{3.43}$$

where the sum over α and β means the sum of all pair-vise combinations of N_ρ, N_ϕ, $\rho_1(z)\delta(z+)/\rho_{\mathrm{s}}$ and $\phi_1(z)\delta(z+)$,

$$K_\rho(z,t) = F(t) * H(z,t), \tag{3.44}$$

and $\delta(z+) = \delta(z-\epsilon)$ where ϵ is a positive number, which approaches zero. The operator $O_{\alpha,\beta}$ will be discussed more later. The integrals over z_1, t_1 and z_2, t_2 are split into sums of integrals over M cells of volume $\Delta V = \Delta z \Delta t$. Furthermore a $2M + 2L_t$-dimensional noise vector

$$\vec{n}^T = (n_{\rho 1}, ..., n_{\rho M}, n_{\phi 1}, ..., n_{\phi M}, n_{\rho_0 1}, ..., n_{\rho_0 L_t}, n_{\phi_0 1}, ..., n_{\phi_0 L_t}) \tag{3.45}$$

is introduced, where

$$n_{\rho i} = \int\int_{\text{cell } i} N_\rho(z,t)dzdt \tag{3.46}$$

$$n_{\phi i} = \int\int_{\text{cell } i} N_\phi(z,t)dzdt \tag{3.47}$$

$$n_{\rho_0 i} = \int\int_{\text{cell } i} \frac{\rho_1(z,t)}{\rho_s(z)}\delta(z+)dzdt \tag{3.48}$$

$$n_{\phi_0 i} = \int\int_{\text{cell } i} \phi_1(z,t)\delta(z+)dzdt \tag{3.49}$$

$M = L_z L_t$ and L_z and L_t are the number of cells in the z- and t-direction, respectively. In the noise vector, $\vec{n}$, $n_{\rho i}$ and $n_{\phi i}$ represents the spontaneous emission noise and $n_{\rho_0 i}$ and $n_{\phi_0 i}$ the noise at the input of the SOA. In $\vec{n}$ only those L_t elements of $n_{\rho_0 i}$ and $n_{\phi_0 i}$ where $z = 0$ are included since all other elements of the input noise are zero. K_ρ is similarly expressed as a $2M + 2L_t$-dimensional vector

$$\vec{k}^T = (k_{\rho 1}, ..., k_{\rho M}, 0, ..., 0, k_{\rho_0 1}, ..., k_{\rho_0 L_t}, 0, ..., 0) \tag{3.50}$$

where $k_{\rho i}$ is $K_\rho(z, t-t')$, where (z, t') belongs to the i-th cell and $k_{\rho_0 i}$ is the same but only for the L_t cells where $z = 0$. In a similar way the operator $O_{\alpha,\beta}$ is expressed as a $2M + 2L_t$-dimensional matrix O. For $i \leq M, j \leq M$ the matrix element $O_{i,j}$ is the value of $O_{\rho,\rho}(z_1, t-t_1; z_2, t-t_2)$ where (z_1, t_1) belongs to the i-th cell and (z_2, t_2) belongs to the j-th cell. For $M < i \leq 2M, j \leq M$ the matrix element is $O_{\phi,\rho}(z_1, t-t_1; z_2, t-t_2)$ where (z_1, t_1) belongs to the $(i-M)$-th cell and (z_2, t_2) belongs to the j-th cell, and so on. The matrix is further explained in Appendix A. The power can thus be expressed as

$$P(t) = P_s(1 + 2\vec{k} \cdot \vec{n} + \vec{n} \cdot O\vec{n}). \tag{3.51}$$

The output power of the SOA is now expressed in a compact matrix formulation. What remains is to evaluate the matrix O and find the expression for the PDF at the output.

The PDF of any random variable can be calculated as the inverse Fourier transform of the characteristic function, which is just the moment generating function $\text{MGF}(s)$ with $s = i\omega$ [59]. For the output power of the SOA the PDF is thus given by

$$\text{PDF}(P) = \frac{1}{2\pi}\int \text{MGF}_P(i\omega)\text{e}^{i\omega P}d\omega. \tag{3.52}$$

Since the noise source representing the spontaneous emission is assumed to be Gaussian, and assuming Gaussian noise also at the input of the SOA it is seen from Eq. 3.46 - 3.49 that the components of $\vec{n}$ form a set of jointly Gaussian random variables. The moment generating function is thus [59]

$$\begin{aligned}\text{MGF}_P(s) &= \left\langle e^{-sP} \right\rangle \\ &= \left((2\pi)^{2M+2L_t}\det(D)\right)^{-\frac{1}{2}} \int \exp\left[-sP - \frac{1}{2}\vec{n} \cdot D^{-1}\vec{n}\right] d^{2M+2L_t}n\end{aligned} \tag{3.53}$$

where D is the diffusion matrix

$$D_{ij} = \langle n_i n_j \rangle \,. \tag{3.54}$$

Inserting the output power from Eq. (3.51) in Eq. (3.53) gives

$$\begin{aligned} \mathrm{MGF}_P(s) &= \left((2\pi)^{2M+2L_t} \det D\right)^{-\frac{1}{2}} \exp\left(-sP_\mathrm{s}\right) \\ &\times \int \exp\left[-2sP_\mathrm{s}\vec{k}\cdot\vec{n} - \frac{1}{2}\vec{n}\cdot(D^{-1} + 2sP_\mathrm{s}O)\vec{n}\right] d^{2M+2L_t} n \\ &= \frac{1}{\sqrt{\det\left(1 + 2sP_\mathrm{s} D^{\frac{1}{2}} O D^{\frac{1}{2}}\right)}} \\ &\times \exp\left[-sP_\mathrm{s} + 2(sP_\mathrm{s})^2 \vec{k}\cdot\left(D^{-1} + 2sP_\mathrm{s}O\right)^{-1}\vec{k}\right], \end{aligned} \tag{3.55}$$

which is the moment generating function for the output power in the time domain. Since the PDF can be calculated directly from the moment generating function this is the main result of this model, together with the expression for O_{ij}, which is given later.

In order to calculate the matrix element

$$\vec{k}\cdot\left(D^{-1} + 2sP_\mathrm{s}O\right)^{-1}\vec{k} \tag{3.56}$$

it is convenient to transform it to the frequency domain. The Fourier transformation is a unitary transformation which leaves the matrix element invariant. It just becomes

$$\tilde{k}^*\cdot\left(\tilde{D}^{-1} + 2sP_\mathrm{s}\tilde{O}\right)^{-1}\tilde{k} \tag{3.57}$$

where $\tilde{k}$, $\tilde{D}$ and $\tilde{O}$ are the vector $\vec{k}$ and operators D and O in the frequency domain. The integration over space and frequency is, just as in the time domain, split into a sum over M cells of volume $\Delta z \Delta\omega/2\pi$. The i-th cell is called V_i and the number of cells in the z- and ω-direction is called L_z and L_ω, respectively. For $i \leq M$ the i-th component of the vector $\tilde{k}$ is then

$$\tilde{k}_i = F^*(\omega)H^*(z,\omega) \tag{3.58}$$

where $(z,\omega) \in V_i$. For $M < i \leq 2M$ and $2M + L_\omega < i$ the i-th component of $\tilde{k}$ is zero and for $2M < i \leq 2M + L_\omega$

$$\tilde{k}_i = F^*(\omega)H^*(0,\omega) \tag{3.59}$$

where $(\omega) \in V_{i-2M}$.

The operator $\tilde{D}$ has matrix elements

$$\tilde{D}_{ij} = D_i(z,\omega)\frac{\Delta\omega}{2\pi}\delta_{i,j} \tag{3.60}$$

$$D_i(z,\omega) = \frac{\hbar\omega_0 g_s n_{sp}}{2P_{sat}\rho_s^2}\frac{\sin^2\left(\frac{\omega\Delta t}{2}\right)}{\left(\frac{\omega\Delta t}{2}\right)^2}\Delta z, \begin{cases} i \le M, & (z,\omega)\in V_i \\ M < i \le 2M, & (z,\omega)\in V_{i-M} \end{cases} \tag{3.61}$$

$$D_i(0,\omega) = \frac{\sigma^2\Delta t}{P_s(0)}\frac{\sin^2\left(\frac{\omega\Delta t}{2}\right)}{\left(\frac{\omega\Delta t}{2}\right)^2}, \begin{cases} 2M < i \le 2M+L_\omega, & (0,\omega)\in V_{i-2M} \\ 2M+L_\omega < i, & (0,\omega)\in V_{i-(2M+L_\omega)} \end{cases} \tag{3.62}$$

where σ^2 is the variance of the real and imaginary part of the input noise field. The numbering of the elements in $\tilde{O}$, $\tilde{D}$ and $\tilde{k}$ might seem a bit confusing at first, and a better description is given in Appendix A. The correlation function of the input noise is in Eq. (3.62), just as for the spontaneous emission, assumed to have a sinc^2-shaped spectrum, in order to describe a sample-and-hold signal.

In order to be able to compare the model to the experiments, a simple detector model also has to be included. In this work detection is in all cases considered to be ideal and noiseless direct detection, such that the optical intensity noise is the only noise considered in the detector. Furthermore, the limited detector bandwidth is considered as an additional filtering of the intensity, since the photo current in the detector is directly proportional to it. In the second order model this means that $\tilde{k}_i \to F_e^*(\omega)\tilde{k}_i$, where $F_e(\omega)$ is the filter function of the electrical filter. A similar change is made to the matrix elements of the operator O, which is given in Appendix A.

First order

If only the first order perturbations in Eq. (3.18) and Eq. (3.19) are considered the result for the electrical field and power in the time domain is

$$E_F = E_s\left[1 + F * \frac{\rho_1}{\rho_s} + iF * \phi_1\right]. \tag{3.63}$$

$$P(t) = |E_F|^2 = P_s\left[1 + 2F * \frac{\rho_1}{\rho_s}\right] \tag{3.64}$$

Just like in the second order case the moment generating function can be expressed as

$$\begin{aligned} \mathrm{MGF}_P(s) &= \left((2\pi)^{4M}\det D\right)^{-\frac{1}{2}}\exp\left(-sP_s\right) \\ &\quad\times\int\exp\left(-2sP_s\vec{k}\cdot\vec{n} - \frac{1}{2}\vec{n}\cdot D^{-1}\vec{n}\right)d^{4M}n \\ &= \exp\left(-sP_s + 2(sP_s)^2\tilde{k}\cdot\tilde{D}\tilde{k}\right), \end{aligned} \tag{3.65}$$

since the operator $\tilde{O}$ is zero when no second order terms are included. By taking

the inverse Fourier transform of $\mathrm{MGF}_P(i\omega)$ the PDF can be calculated

$$\mathrm{PDF}(P) = \frac{1}{2\pi}\int \mathrm{MGF}_P(i\omega)\mathrm{e}^{i\omega P}d\omega = \frac{1}{\sqrt{8\pi\tilde{k}^*\cdot\tilde{D}\tilde{k}P_\mathrm{s}^2}}e^{-\frac{(P-P_\mathrm{s})^2}{8\tilde{k}^*\cdot\tilde{D}\tilde{k}P_\mathrm{s}^2}}, \tag{3.66}$$

which is a Gaussian distribution with mean value P_s and variance $4\tilde{k}^*\cdot\tilde{D}\tilde{k}P_\mathrm{s}^2$. If the square of the first order amplitude noise is included in Eq. (3.64)

$$P(t) = |E_\mathrm{F}|^2 = P_\mathrm{s}\left[1 + 2F * \frac{\rho_1}{\rho_\mathrm{s}} + \left(F\otimes\frac{\rho_1}{\rho_\mathrm{s}}\right)^2\right] \tag{3.67}$$

the moment generating function can be expressed by noting that $\tilde{O} = \tilde{k}^\dagger\tilde{k}$. The results is

$$\mathrm{MGF}_P(s) = \frac{1}{\sqrt{1+2sP_\mathrm{s}\tilde{k}^*\cdot\tilde{D}\tilde{k}}}\exp\left(-\frac{sP_\mathrm{s}}{1+2sP_\mathrm{s}\tilde{k}^*\cdot\tilde{D}\tilde{k}}\right). \tag{3.68}$$

The calculation of the corresponding PDF is quite cumbersome, but the MGF can be identified as the MGF of a non-central χ^2-distribution [59], with the mean value $P_\mathrm{s}(1+\tilde{k}^*\cdot\tilde{D}\tilde{k})$ and variance $2P_\mathrm{s}^2(|\tilde{k}^*\cdot\tilde{D}\tilde{k}|^2+2\tilde{k}^*\cdot\tilde{D}\tilde{k})$. In summary this mean that by including only the first order terms a Gaussian distribution is achieved, and by partially including second order terms the result is a non-central χ^2-distribution. However, as seen before, the measured PDFs, at high gain saturation, had a distribution that could not be described either by a Gaussian or a non-central χ^2-distribution, which motivates the use of the second order implementation.

The first order model also give us the possibility to calculate the noise spectra of the SOA. This was done by Shtaif et al. using a semiclassical and quantum mechanical treatment of the correlation functions for f_N and f_E. Their results show that the different treatments differs only by a shot noise term in the expressions for relative intensity noise (RIN) and phase noise spectra [44]. Furthermore they showed the different contributions from input noise, spontaneous emission and carrier noise. In this work only the input and spontaneous emission noise will be considered, as in the second order case. The relative intensity noise (RIN) spectrum is defined as

$$\mathrm{RIN}(z,\omega) = \frac{S_{\delta\rho^2,\delta\rho^2}(z,\omega)}{\rho_\mathrm{s}^4(z)} = 4\frac{S_{\delta\rho,\delta\rho}(z,\omega)}{\rho_\mathrm{s}^2(z)} \tag{3.69}$$

where

$$S_{x,y}(\omega) = \int_{-\infty}^{\infty}\langle x^*(t)y(t+\tau)\rangle e^{i\omega\tau}d\tau \tag{3.70}$$

is the cross correlation power spectrum between the two processes $x(t)$ and $y(t)$.

By using Eq. (3.35) and the correlation function of the noise term the expression for the RIN spectrum can be calculated.

$$\mathrm{RIN} = R_0 + R_\mathrm{sp} \tag{3.71}$$

where the different terms represent the noise contribution from the input signal and spontaneous emission, respectively. The expressions for the noise terms are

$$R_0(\omega) = |H(0,\omega)|^2 \mathrm{RIN}(0,\omega) \tag{3.72}$$

$$R_{\mathrm{sp}}(L,\omega) = \frac{\hbar\omega_0}{P_{\mathrm{sat}}} \int_0^L |H(z,\omega)|^2 \frac{2g_{\mathrm{s}} n_{\mathrm{sp}}}{\rho_{\mathrm{s}}^2} \frac{\sin^2 \frac{\omega\Delta t}{2}}{\left(\frac{\omega\Delta t}{2}\right)^2} dz \tag{3.73}$$

By comparing these noise spectra to the expression for the variance of the Gaussian distribution described above

$$\begin{aligned} 4\tilde{k}^* \cdot \tilde{D}\tilde{k} P_{\mathrm{s}}^2 = \Bigg[& \frac{\hbar\omega_0}{P_{\mathrm{sat}}} \int_0^L |F(\omega)H(z,\omega)|^2 \frac{2g_{\mathrm{s}} n_{\mathrm{sp}}}{\rho_{\mathrm{s}}^2} \frac{\sin^2 \frac{\omega\Delta t}{2}}{\left(\frac{\omega\Delta t}{2}\right)^2} \frac{dz d\omega}{2\pi} \\ & + \int |F(\omega)H(0,\omega)|^2 \frac{\sigma^2 \Delta t}{P_{\mathrm{s}}(0)} \frac{\sin^2 \frac{\omega\Delta t}{2}}{\left(\frac{\omega\Delta t}{2}\right)^2} \frac{d\omega}{2\pi} \Bigg] P_{\mathrm{s}}^2 \end{aligned} \tag{3.74}$$

it can be seen that the signal-to-noise ratio for the Gaussian distribution at the detector, including optical and electrical filtering, is the well known

$$\mathrm{SNR} = \left(\int_{-\infty}^{\infty} |F_e(2\pi f) F(2\pi f)|^2 \, \mathrm{RIN}(2\pi f) df \right)^{-1} \tag{3.75}$$

This definition is identical to the ratio between the mean power squared and the intensity noise variance within the bandwidth of the filters, as described in Sec. 2.1.1.

Eq. (3.70) can also be used to calculate the phase noise spectrum by use of Eq. (3.37) and the correlation functions. The result is

$$S_{\phi_1,\phi_1} = \Phi_0 + \Phi_{\mathrm{sp}}, \tag{3.76}$$

where

$$\begin{aligned} \Phi_0(\omega) = & S_{\phi_1,\phi_1}(\omega,0) + \frac{\alpha^2 \mathrm{RIN}(\omega,0)}{4} |H(0)-1|^2 \\ & - \frac{2\alpha}{\rho_{\mathrm{s}}(0)} \mathrm{Re}\left[(H(0)-1) S_{\phi_1,\rho_1}(\omega,0) \right] \end{aligned} \tag{3.77}$$

$$\Phi_{\mathrm{sp}}(\omega) = \frac{\hbar\omega_0}{4P_{\mathrm{sat}}} \int_0^L \left(\alpha^2 |H-1|^2 + 1 \right) \frac{2g_{\mathrm{s}} n_{\mathrm{sp}}}{\rho_{\mathrm{s}}^2} dz. \tag{3.78}$$

In the same way the cross correlation between the amplitude and phase noise can be calculated. In Eq. (3.77) $S_{\phi_1,\rho_1}(\omega,0)$ is the cross-correlation between amplitude and phase noise at the input, which we can assume to be zero as long as the input noise has not passed through any nonlinear device or filter with intensity to phase or phase to intensity conversion. The phase and cross correlation spectra will in this work only be used in order to compare the simulations and the first order small-signal calculation.

3.4.2 Simulation

The second noise description assumes a sampled signal in the time domain and includes ASE noise in the SOA by adding a noise field with appropriate statistics. This model was developed by Cassioli et al. [61] and we will only present the parts that are relevant to this work.

The SOA is divided into short sections of length Δz. The sections are modeled as ideal SOAs by ignoring the noise terms and the internal losses. Equations (3.7) and (3.8), without noise terms, can then be rewritten as an ordinary differential equation

$$\frac{\partial h}{\partial t} = \frac{h_0 - h}{\tau_\mathrm{s}} - \frac{|E_\mathrm{in,tot}(t)|^2}{\tau_\mathrm{s}}[\exp(h) - 1] \tag{3.79}$$

where h is the integrated gain

$$h(t) = \int_0^{\Delta z} g(z + z_i, t)\,\mathrm{d}z, \tag{3.80}$$

$h_0 = g_0 \Delta z$ and z_i is the z-coordinate of section number i. The output field for the ideal section is thus

$$E_\mathrm{out}(t) = E_\mathrm{in,tot}(t) \exp\left[\frac{1}{2}(1 - i\alpha)h(t)\right] \tag{3.81}$$

The internal losses and noise are modeled by solving the ideal loss-less model for the short sections and then including the losses and noise of the propagating light at the interfaces between the sections. The properties of the noise field are calculated from equations (3.7) and (3.8) and the correlation functions of the noise terms.

By assuming that the spontaneous emission coefficient is independent of saturation, that it is constant, within the short section Δz and that the internal losses are zero, equation Eq. (3.8) can be solved. The solution is

$$\begin{aligned} E(z,t) = E_\mathrm{in} \exp\left(\int_0^z \frac{1}{2} g(z'',t)(1 - i\alpha)dz''\right) + \\ + \int_0^z f_E \exp\left(\int_{z'}^z \frac{1}{2} g(z'',t)(1 - i\alpha)dz''\right) dz'. \end{aligned} \tag{3.82}$$

At $z = \Delta z$ this can be written as

$$E(\Delta z, t) = (E_\mathrm{in}(t) + E_\mathrm{ASE}(\Delta z, t)) \exp\left(\int_0^{\Delta z} \frac{1}{2} g(z',t)(1 - i\alpha)dz'\right) \tag{3.83}$$

where

$$E_\mathrm{ASE}(\Delta z, t) = \int_0^{\Delta z} f_E(z',t) \exp\left(-\int_0^{z'} \frac{1}{2} g(z'',t)(1 - i\alpha)dz''\right) dz' \tag{3.84}$$

E_ASE describes the added ASE noise in the section transformed to the input of the section. In order to find the correct statistical properties the autocorrelation function of E_ASE should be calculated.

The correlation function in time, Eq. (3.13), is a sharply peaked function of τ with a width of the order of the sampling interval. Assuming that the gain does not change during this time period the autocorrelation function becomes

$$\langle E_{\mathrm{ASE}}(\Delta z,t)E^{*}_{\mathrm{ASE}}(\Delta z,t+\tau)\rangle = \frac{\hbar\omega_0 n_{\mathrm{sp}}}{P_{\mathrm{sat}}}\left(1-\exp\left(-h(\Delta z,t)\right)\right)R(\tau) \tag{3.85}$$

The Fourier transform of Eq. (3.85) gives the power spectral density and the noise power is thus

$$P_{\mathrm{ASE}} = \int_{-\infty}^{\infty}\hbar\omega_0 n_{\mathrm{sp}}\left(1-\frac{1}{G}\right)\tilde{R}(\omega)\frac{d\omega}{2\pi} = \hbar\omega_0 n_{\mathrm{sp}}\left(1-\frac{1}{G}\right)\frac{1}{\Delta t} \tag{3.86}$$

where $G=\exp(h\Delta z))$.

The added noise field is written as

$$E_{\mathrm{ASE}} = E_{\mathrm{real}} + iE_{\mathrm{imag}} \tag{3.87}$$

where E_{real} and E_{imag} is the real and imaginary part of the noise field, respectively. They have a Gaussian distribution with zero mean and variance according to

$$\mathrm{Var}[E_{\mathrm{real}}] = \mathrm{Var}[E_{\mathrm{imag}}] = \frac{1}{2}\frac{\hbar\omega_0 n_{\mathrm{sp}}\left(1-\frac{1}{G}\right)}{P_{\mathrm{sat}}}\frac{1}{\Delta t}. \tag{3.88}$$

As discussed before the sampling interval introduces a band-limited Gaussian noise. In reality different effects, for example the gain spectrum of the SOA, limit the ASE bandwidth. Since our model does not include such limiting effects Δt is chosen to be small enough to properly include the modulation bandwidth of the simulated devices. On the other hand, Δt has to be limited such that the ASE power does not contribute significantly to the saturation of the SOA, i.e. Δt cannot be too small. This limitation is due to the uni-directional nature of the model, i.e. ASE traveling backwards in the SOA is not considered. Neglecting this effect will underestimate the noise figure of the SOA since the backward traveling ASE will saturate the gain in the beginning of the amplifier, but the effect is small compared to that of saturation from the signal. Accepting this limitation of the model we choose Δt to properly include the bandwidth of the devices and make sure that the ASE power is very small compared to the mean input power.

In practice E_{real} and E_{imag} are constructed by two pseudo-random sequences with zero mean and unit variance that are multiplied by the square root of the right hand side of Eq. (3.88). The total field including the signal and noise is then used in the model for the ideal sections, i.e.

$$E_{\mathrm{in,tot}} = E_{\mathrm{in}} + E_{\mathrm{ASE}} \tag{3.89}$$

where E_{in} is the input field of the section.

The output field from the model is finally analyzed statistically to find the mean, variance, skewness and a histogram estimating the probability density function. Since the method has the characteristics of a statistical simulation it is hereafter referred to as the 'simulation'.

3.5 Comparison of models and experiments

We now have three theoretical tools to use for examining the noise redistribution seen in the experiments presented in Sec. 3.3; the numerical simulation and the small-signal analysis to first and second order. In this section these tools will be compared to the experiments and to each other.

The parameters used in the calculations are a mixture of known physical parameters of the measurements setup (length of SOA, bias current, input powers and detection bandwidth), reasonable guesses (coupling losses, waveguide losses, linewidth enhancement factor, and carrier life time) and fitted parameters (small-signal gain, saturation power and input signal to noise ratio). The parameter values used, unless specified, are shown in table 3.1. It should also be noted

Parameter	**Value**
Device length, L [μm]	500
Bias current, I [mA]	200
Input SNR at 10 GHz, [dB]	26
Detection bandwidth, B_e [GHz]	10
Optical filter bandwidth, B_o [GHz]	30
Total simulation bandwidth, $1/\Delta t$ [GHz]	62.5
Coupling losses, [dB]	4
Time constant, τ_s [ps]	100
Saturation power, P_{sat} [mW]	6
Internal loss, α_{int} [m^{-1}]	500
Linewidth enhancement factor, α	5
Small signal gain, g_0 [m^{-1}]	15789
Differential modal gain, a [m^2]	$3.77 \cdot 10^{-20}$
Carrier density at transparency, N_0 [m^{-3}]	$1 \cdot 10^{24}$

Table 3.1: Parameter values used in the calculations when comparing to experiments.

that the fitting has only been made by making sure that a reasonable qualitative agreement in the gain curve and standard deviation figure is reached, and no quantitative fitting procedure has been used. All comparisons of the experiments to the calculations should therefore be limited to qualitative statements.

The first, and most straight-forward, comparison is to directly look at the measured and calculated PDFs. These are shown in Fig. 3.14. The top row show the measurements, and are the same as in Fig. 3.8, together with a non-central χ^2-distribution calculated using the mean and standard deviation extracted from the measured PDFs as explained in Sec. 3.3. The bottom row show the results from the three models.

A more detailed comparison by using the central moments will be made later in this section but first there is a more general comment regarding the models that can be made directly from the PDFs. The usefulness of analytical expressions for the PDFs is clearly seen when comparing the tails of the measured and simulated

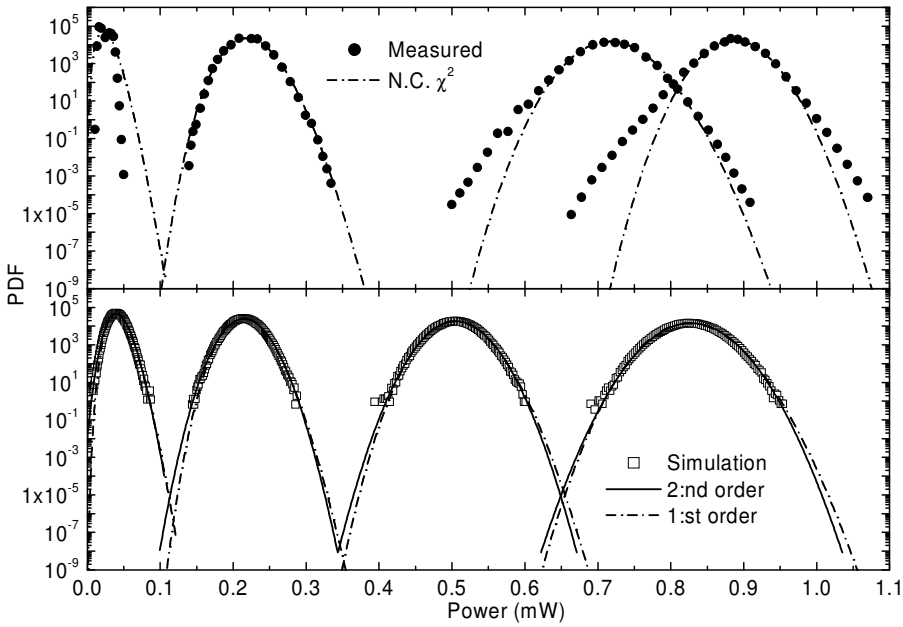

Figure 3.14: Measured and simulated PDFs. The top row show measured PDFs (dots) and non-central χ^2-distributions with the same mean and standard deviation. The bottom row show the results of the three different implementations of the noise model. For the first order case the non-central χ^2-distribution was used

PDFs. Since the measurements use a technique where errors are counted using a bit-error rate test set, the measured PDFs give an indication on how far out in the tails of the distribution information is needed in order to be able to make statements about the influence of the noise redistribution on BER values of the magnitude of that measured by the test set, that is in the order of 10^{-10} to 10^{-9}. In Fig. 3.14 it is seen that the simulations do not reach that far out in the tails. In order to extend the simulations further, within a reasonable simulation time, more advanced simulation techniques, for example importance sampling, has to be used or extrapolations has to be made [64].

Although the PDFs in Fig. 3.14 can be studied directly the differences between the different models are small and it is hard to see. It is easier to compare the results if we again use the central moments, or more specific, the standard deviation and skewness. The standard deviation as function of mean power is shown in Fig. 3.15. The calculated results do not show an equally strong noise suppression as the measurements at high powers. The overall behavior with increasing input power, and hence gain compression, is however very similar. The stronger effect of noise compression in the experiments can to some degree be explained by the sharper saturation characteristics of the experimental gain curve as compared to

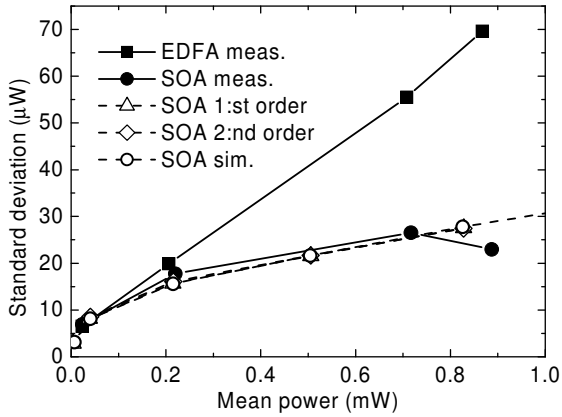

Figure 3.15: Measured and calculated standard deviation as a function of mean power for the high input noise case. All three implementations of the model are plotted (open symbols).

the model as seen in Fig. 3.16. This figure show that the fitted model fairly well describe the gain level within the interesting range. However the model is not very successful in describing the slope with which the gain decreases at high input powers. This slope, as discussed in Sec. 2.1.2 and Sec. 3.3, is the reason for the noise compression, and a higher slope means a stronger noise compression as seen in the experiments.

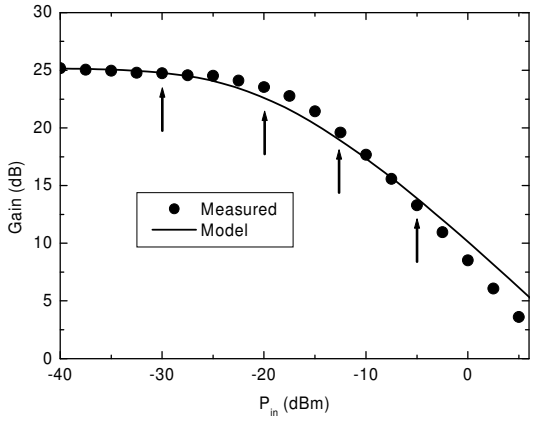

Figure 3.16: Measured gain of the examined SOA as function of input power

Returning to Fig. 3.15, and comparing the different calculations to each other, it is seen that they give very similar results. This is of course expected since

they are all based on the same basic assumptions about the ASE, input noise and saturation characteristics of the SOA.

Moving on, the skewness as function of mean power is shown in Fig. 3.17. Again we see that the measurement show a stronger noise redistribution than the calculations. Comparing the theoretical calculations to each other a clear

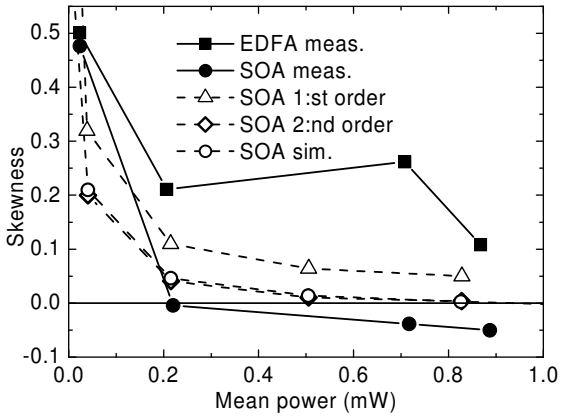

Figure 3.17: Measured and calculated skewness as a function of mean power for the high input noise case. In the first order case the non-central χ^2-distribution is used.

difference is seen, which needs further explanation. The first order calculation does not take the redistribution of the PDF, apart from the suppression of the width, into consideration and the PDF is the standard non-central χ^2-distribution, which always has a positive skewness. The simulation on the other hand does in principle include the complete redistribution of the noise. The simulation does show a shift to negative skewness for high input power, but does not show as strong redistribution as in the experiment, just as for the standard deviation. The second order small-signal calculation give more or less identical results as the simulation, which show that the inclusion of the second order terms in the small-signal expansion does indeed accurately describe the noise compression as well as the redistribution of the noise.

3.5.1 Further comparison of noise models

As seen in Sec. 3.5 there are some differences in the results between the three implementations of the noise model. In this section the differences between the models, and the limitations of the models, will be investigated further. First some of the important limitations of the model and the different implementations need further comments.

As already mentioned the fact that the electric field in the SOA only travels in one direction means that counter propagating ASE is neglected. Therefore

the gain saturation from the ASE power needs to be small compared to that due to the signal power in order for this assumption to hold. The two parameters controlling this is the input power and the total simulated bandwidth, $1/\Delta t$. A high input power obviously means that the relative contribution of the ASE is small. The sampling interval is important since a short interval corresponds to a wide spectrum and hence a larger ASE power. This can be illustrated by looking at the steady state solution of Eq. (3.7) and Eq. (3.8) for the power

$$P(z) = P(0)\exp\left[\int_0^z (g-\alpha_{\rm int})dz'\right] + \int_0^z \exp\left[\int_{z'}^z (g-\alpha_{\rm int})dz''\right] r_{\rm sp}(z',\omega)dz'\frac{d\omega}{2\pi} \tag{3.90}$$

where $r_{\rm sp} = \hbar\omega_0 g n_{\rm sp}\sin^2(\omega\Delta t/2)/(\omega\Delta t/2)^2$ is the rate of spontaneous emission into the guided mode per unit frequency per unit length. The resulting output power related to the steady state output power without ASE is plotted against input power in Fig. 3.18.

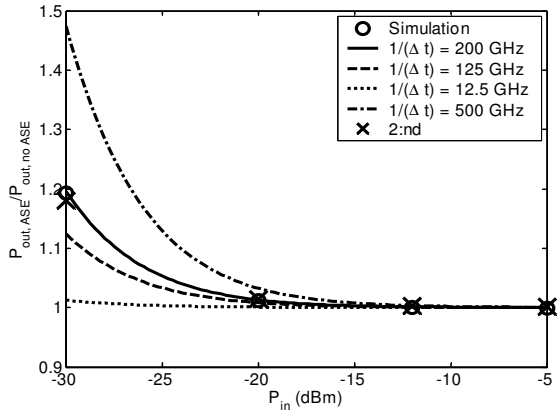

Figure 3.18: Comparison of the output power from the SOA including ASE power and output power not including ASE. The lines correspond to Eq. (3.90) and the markers show the results from the simulation (circles) and second order (crosses).

The lines illustrate the solution to Eq. (3.90) for different simulation bandwidths, $1/\Delta t$. It is clearly seen that an increase in bandwidth results in additional ASE power. In Fig. 3.18 the dependence on input power is also seen, and as expected the relative importance of the ASE contribution is decreased with increasing input powers.

Together with the analytical solution the results from simulation, circles, and the second order case, crosses, at a bandwidth of 200 GHz are also shown. The second order case does not fit as well as the simulations. This might be due to the limited resolution in frequency that can be used for larger bandwidth in the second order case, which will be discussed later in this section.

Another limitation that is also somewhat connected to the level of saturation is the assumption that the carrier noise can be neglected. Shtaif et al. showed that this assumption holds for fairly strong saturation levels, as long as only intensity noise is considered [44]. However, when phase noise is considered the carrier noise plays a more important role, especially at higher saturation levels. As seen in Eq. (3.42), the phase noise also contributes to the intensity fluctuations when higher order terms are included. The maximum input power used in the calculations is, however, small compared to the levels where the carrier noise is important according to Shtaif, but the inclusion of carrier noise should be investigated further. The phase, and hence the carrier noise will also be more important when for example interferometric devices are investigated, since they use cross-phase modulation.

One assumption that is limited to the small-signal investigations is the consideration of the variations in the electrical field due to noise as small perturbations to the steady state solution. This seems to imply that the small-signal implementations would not work for very low signal-to-noise ratios. This is investigated more closely in Fig. 3.19, where the RIN-spectra for different input signal to noise ratios are plotted using both the simulations and the first order small-signal cases. As seen in the figure the small-signal assumption holds nicely down to a SNR of 10 dB at a detection bandwidth of 10 GHz. From this we can conclude that we can safely use the small-signal analysis and expect it to agree well with the simulations for more or less any reasonable amount of input noise.

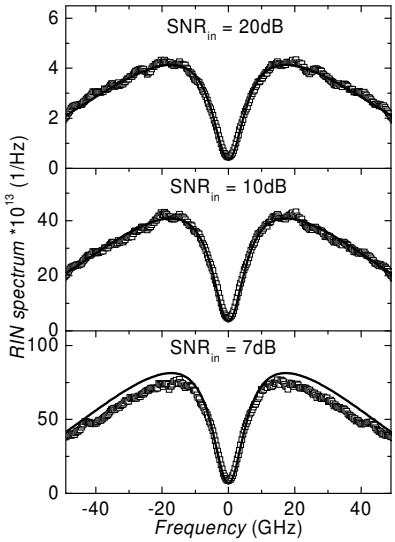

Figure 3.19: RIN after an SOA for different levels of input signal-to-noise ratio, as calculated using the simulations (squares) and the first order small-signal analysis (lines). The input power is -5 dBm.

Finally, when comparing the models, a few words should be written about the numerical implementations and how computationally heavy the models are. The simulation is a direct statistical calculation in the time domain without any additional tricks to speed up the calculation, e.g. importance sampling. This means that in order to be able to see the effects of the noise redistribution on the PDFs, a lot of samples have to be simulated, which in turn leads to long simulation times. The presented simulations typically uses about 500,000 samples and takes several hours to complete on an ordinary PC. The simulation, done in this simple way, is also limited in how far out in the tails of the PDFs one can readily get, even with very long simulation time on several computers. The second order small-signal calculations is a matrix calculation, including calculation of all the matrix elements and then calculating the determinant and inverting the matrix for every point in the moment generating function. The two last operations can be done very fast once the eigenvalues and eigenvectors of the matrix has been calculated, but for large matrices this can take quite some time. The largest problem of the second order calculations is, however, the scaling of the matrix with the discretization in z and ω. The number of matrix elements scales as $(L_z L_\omega)^2$, where L_z and L_ω is the number of discrete points in z and ω, respectively. This quickly leads to problems with limited computer memory as the discretization is made finer. The first order calculation, on the other hand, is a very fast and efficient tool to calculate the noise spectra and signal-to-noise ratio, but does not give any information on the shape change of the PDF.

3.6 Noise suppression in an SOA

Although the previous sections have discussed the noise suppression and redistribution capabilities of the SOA, the SOA as a single component is not a regenerator. The reason for this is simple. The nonlinear transfer function of the SOA has, as we have seen, the ability to suppress noise at a high input power corresponding to the logical one-level of a data signal. However, it does not suppress any noise at the zero-level and the extinction ratio is furthermore severely degraded since the zeros experience much higher gain than the ones. This means that the nonlinear SOA can never be used for regenerating a modulated signal. The noise suppression can, however, be used as soon as the signal is continuous wave, as has been the case in all our experiments and calculations so far. Such applications are sometimes referred to as a noise eater and examples of such applications are in spectrum-sliced WDM systems [65, 66] and in fiber lasers [67]. In this section we will further investigate some aspects of the noise redistribution in an SOA using the presented models.

3.6.1 Dynamics of the noise redistribution

The two most important parameters governing the noise redistribution are the level of gain saturation, as investigated in Sec. 3.5, and the device speed. The result of the limited optical modulation bandwidth of the SOA on the intensity noise spectrum was shown in Fig. 3.19 in the previous section. The dip in the

RIN spectrum is due to the limited speed of the device as dictated by the carrier dynamics. The noise is thus only suppressed for frequencies within the modulation bandwidth of the SOA, while the high frequency noise passes unsuppressed.

In Fig. 3.20 the connection between limited modulation bandwidth and signal-to-noise ratio is shown. The SNR is related to the relative intensity noise spectrum

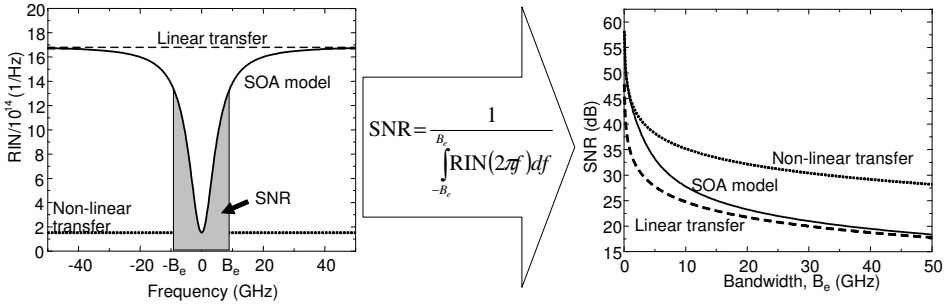

Figure 3.20: The calculated RIN spectrum show that the standard deviation of the noise after the SOA ends up in between the limiting cases of linear and static non-linear transfer functions.

through

$$\mathrm{SNR} = \left(\int_{-\infty}^{\infty} |F_e(2\pi f) F(2\pi f)|^2 \, \mathrm{RIN}(2\pi f) df \right)^{-1}. \tag{3.91}$$

Assuming a square electrical filter, F_e, with much smaller bandwidth than the optical filter, F, thus gives an SNR as shown in Fig. 3.20. This figure clearly show why the measured PDF in Fig. 3.5 ended up in between the limiting cases of the linear and the static transfer functions. The RIN spectrum in the figure is calculated, assuming that the input noise dominates over the added ASE noise, using the first order model and shows how the suppression of the intensity noise approaches the static case for small frequencies, while for large frequencies the input signal just passes through unchanged, as in the linear case. The result is a SNR, or standard deviation if the power is constant, that changes from the static case for small detection bandwidths to the linear case for large bandwidths. In the measurements in Sec. 3.3.1 the detection bandwidth was 10 GHz and as seen in Fig. 3.20 this gives a standard deviation somewhere in between the static and linear cases, as seen in the experiment.

Since the finite speed of the device results in noise redistribution only within a limited bandwidth the dependence on carrier dynamics can be investigated by changing the detection bandwidth. In Fig. 3.21 simulations of the variance (a) and the skewness (b) are plotted as functions of the detection bandwidth for different input powers. Since the standard deviation and hence the skewness depends on the detection bandwidth even without any noise redistribution the curves have been normalized with the linear case. Furthermore, the curves are normalized with their respective values at the maximum simulated bandwidth in order to fa-

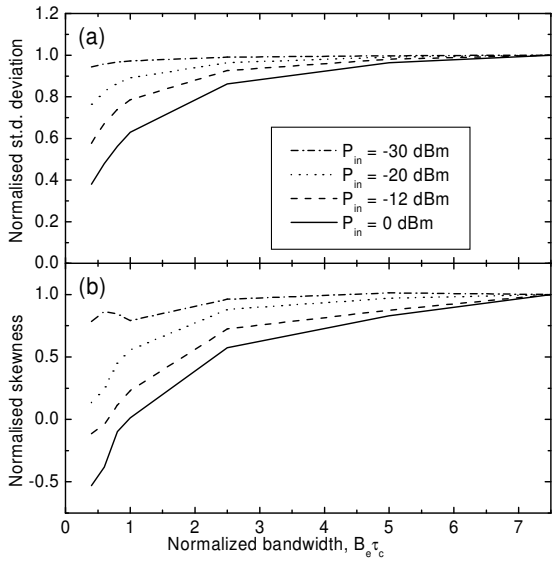

Figure 3.21: Normalised simulated standard deviation and skewness as function of normalised bandwidth.

cilitate comparison between the different input powers. For low input powers, i.e. small saturation, the amplifier is more or less linear, which means that the difference between the static and linear transfer functions is small, and the bandwidth dependence is not dramatic. Hence, both the variance and skewness are fairly constant. However, for high input powers, i.e. in the gain saturation regime, the bandwidth is more important due to the gain/carrier dynamics. Both the variance and skewness show that there is a substantial redistribution of the noise at small bandwidths. For larger measurement bandwidths, the self-modulation due to gain dynamics is relatively slow and the redistribution is smaller. This again shows that the noise redistribution is strongly dependent on the speed of the device as dictated by the carrier dynamics.

3.6.2 Intensity and phase noise

So far in our investigations we have only looked at the intensity noise of the signal. Due to the dependence of refractive index on the carrier density in a semiconductor there is a coupling between intensity and phase modulation. The strength of this coupling is described by the linewidth enhancement factor, α. Fig. 3.22 shows not only the intensity noise spectrum but also the phase noise and cross-correlation spectra.

Just as before a very good agreement between the simulations and the small-signal calculations is seen in all spectra. The reason the agreement is not perfect in the imaginary part of the cross-correlation spectra is the limited simulation

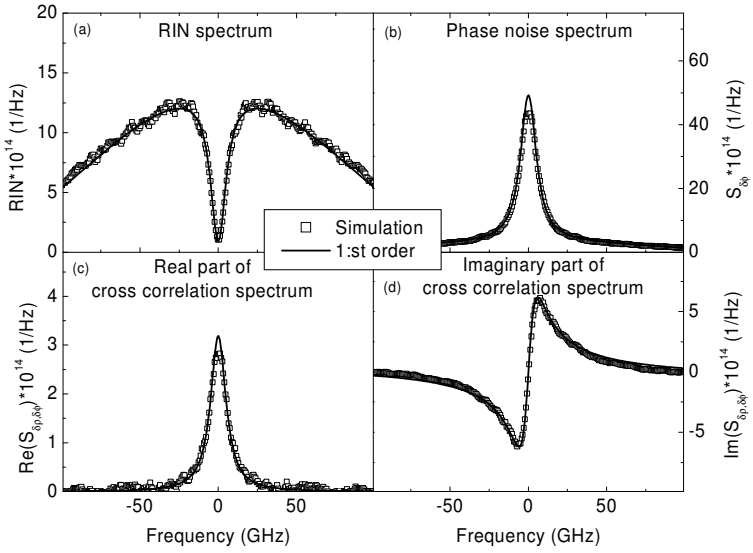

Figure 3.22: RIN spectra (a), phase noise spectra (b), and the spectra of the cross-correlation between amplitude and phase noise (c) and (d), using simulations (open squares) and first order small-signal (solid lines) models. The input power is -5 dBm.

bandwidth and the use of the fast Fourier transform. Due to the discrete sampling in the time domain the spectrum will be periodic. Since the imaginary part of the spectrum changes sign it will go through zero at the maximum simulation frequency, given by the sampling period.

The change in the phase noise spectra due to the SOA is opposite that of the intensity noise. This is because the carrier density fluctuations induced by the noise, which counteract the intensity noise, modulate the phase through the change in refractive index and thus enhance the phase noise. Since it is the same carrier density fluctuations that is responsible for both the suppression of intensity noise and the enhancement for the phase noise, the two spectra have very similar shape [44]. The enhancement is largest for small frequencies where the carriers can follow the intensity fluctuations, while at high frequencies the phase noise remains more or less unchanged.

3.6.3 Pass-through and wavelength conversion

The SOA can be used for many signal processing functionalities and in many different configurations, as briefly described in Sec. 2.4. As a single component it can for example be used for wavelength conversion through cross-gain modulation. Just as in the case of a single input signal the noise at the output of an XGM setup consists of two different contributions; the noise added by the SOA in the form

of ASE and the transfered noise of the input signals. In this section we will compare the noise redistribution in the two cases of pass-through self-modulation and wavelength conversion through XGM [68]. The simulations will be used and is here expanded to include two input signals in accordance with reference [69].

We consider an SOA with two input channels, signal 1 and signal 2, as shown in Fig. 3.23. In the XGM case we assume the input noise in signal 1 to be dominant,

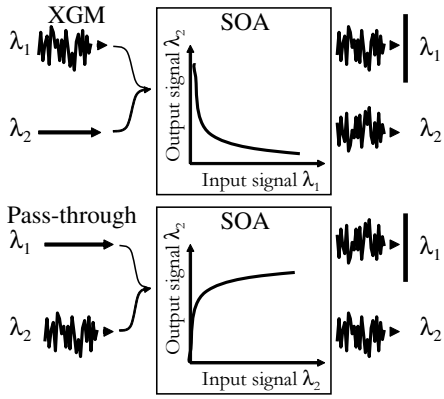

Figure 3.23: Concept of cross-gain modulation and pass-through scheme using an SOA. For XGM the noise is transfered from signal 1 to signal 2 and in the pass-through case the noise is on signal 2 at the input. In both cases signal 2 is studied at the output.

and study how it is transferred to signal 2. In the pass-through case we assume that the dominant input noise is on signal 2. In both cases we examine signal 2 at the output. In the pass-trough case the purpose of signal 1 is only to make sure the operating conditions, like gain saturation and carrier lifetime, are the same as in the XGM case.

All the simulations are performed at a total input power of -5 dBm and an input signal to noise ratio of the noisy signal of 15 dB at a detection bandwidth of 10GHz. While keeping the total input power constant three different relative input powers of the two signals are considered, $P_{1,in}$=$9P_{2,in}$, $P_{1,in}$=$P_{2,in}$ and $P_{2,in}$=$9P_{1,in}$. These operating points are shown in Fig. 3.24 and Fig. 3.25, together with the intensity transfer functions for the two cases (pass-through and XGM). In each case the three transfer curves are for fixed input signals $P_{1,in}$ (pass-through) or $P_{2,in}$ (XGM) given by the operating points.

The noise compression in an SOA due to gain modulation is well understood for both XGM [70, 71] and pass-through [44, 55]. The simple static picture is similar to the single signal case, studied previously in this work. A low slope of the transfer function leads to a narrower noise distribution and a curvature of the function gives a change in the PDF-shape. From these simplified considerations the transfer functions can give an indication of what noise redistribution to expect.

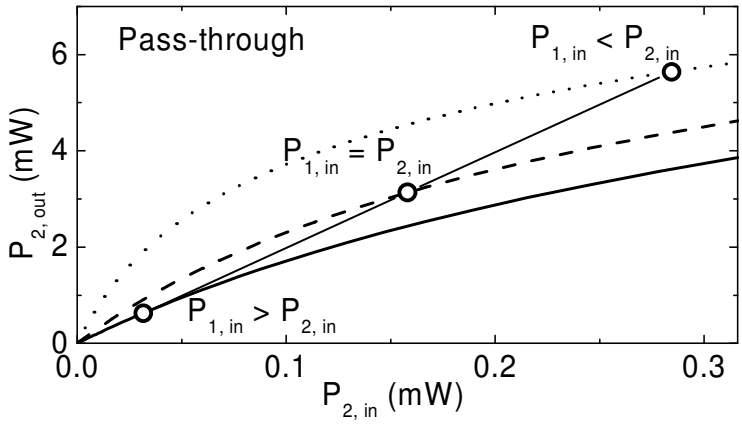

Figure 3.24: Transfer functions of the pass-through case. The three chosen operating points are shown as circles.

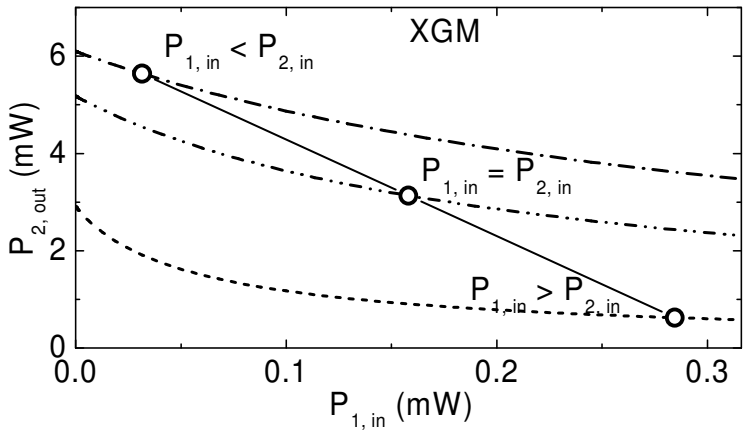

Figure 3.25: Transfer functions of the XGM case. The three chosen operating points are shown as circles.

In the pass-through case a high P_1 means that a change in P_2 does not change the gain by much, and that the transfer curve is fairly linear. On the other hand, when P_1 is small P_2 has a larger impact on the gain and a non-linear transfer function is the result. Similar considerations can be made in the XGM case and as seen in Fig. 3.25 this also leads to one extreme with almost linear transfer characteristics and one with stronger non-linearity.

Now, let us have a look at the results of the simulations. First we look at the intensity noise spectra of the two cases in order to investigate some of the

dynamics involved. The spectra, shown in Fig. 3.26, clearly display the different noise transfer dynamics. The pass-through case show a spectrum similar to what

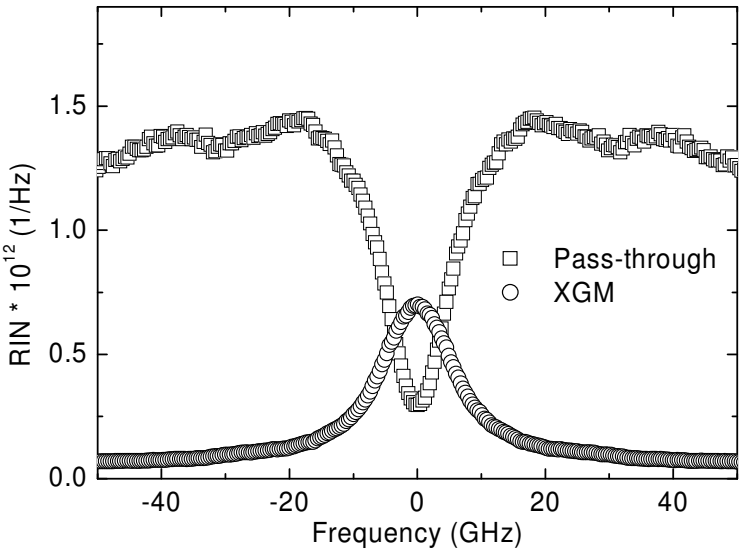

Figure 3.26: Examples of RIN-spectra in pass-through and XGM cases.

we have seen previously for a single input signal, with a high-pass characteristic. This is of course as it should be, since the self-modulation of the intensity through the gain of the SOA is the same. The role of the other input signal in this case is just to keep the saturation at the same level as in the wavelength conversion case.

The XGM case shows a differently shaped spectrum with a low-pass characteristic of the noise and is just the opposite of the pass-through case. The noise at the output of signal 2 originates from the input signal 1 and is transferred by the gain modulation. The limited speed of this modulation means that the intensity fluctuations are only transferred at low frequencies, and hence we get larger noise for small bandwidth in the XGM case.

Fig. 3.27 shows the output standard deviation normalized with the saturated gain and with the standard deviation at the input, for the same detection bandwidth. The noise suppression due to the low slope of the transfer functions, as seen in Fig. 3.24 and Fig. 3.25, is seen for both cases. For the XGM this means that a high P_1 results in larger noise suppression, while for the pass-through case a larger suppression is achieved for large P_2. This seems to agree with the intuitive picture that if the gain saturation is dominated by the signal that is not changed (P_2 in the XGM- and P_1 in the PT-case) a change in the weaker signal does not induce a significant change in the carrier density. Furthermore the different bandwidth dependencies of the two cases, low-pass for XGM and high-pass for pass-through, is seen. The standard deviation relative to that of the input decreases with increasing

detection bandwidth for the XGM and increases in pass-through mode. For the XGM case an interesting interplay between the transferred noise and added ASE is seen when the same simulation but without ASE is plotted (lines with squares in Fig. 3.27). The high-pass characteristic of the ASE from the saturated SOA [44] counteracts the low-pass characteristic of the transferred noise and results in a fairly constant standard deviation with detection bandwidth. The large relative influence of the ASE in the low P_1 case is due to the small input noise resulting from the small input power and the constant signal to noise ratio.

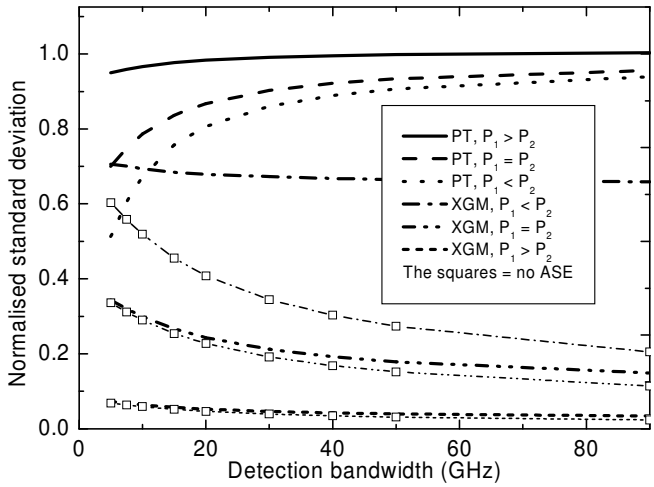

Figure 3.27: Standard deviation normalized with the input standard deviation and the saturated gain of the amplifier, for both pass-through and wavelength conversion. The influence by the ASE is shown by also including calculations where the ASE has not been included (squares).

The skewness of the two cases is shown in Fig. 3.28. For the pass-through case there is a shift toward smaller skewness for all operating points, in accordance with [55, 57] and what is expected from the curvature of the non-linear static transfer function. In the XGM case, however the situation is a bit more complex. The input intensity noise has a non-central χ^2-distribution, in accordance with Gaussian noise in the optical field. This distribution always has a positive skewness and when it is transferred through the XGM the high power side of the input distribution becomes the low power side of the output distribution, and hence the distribution is mirrored and the output skewness becomes negative. This effect can be seen for the low P_1 case in Fig. 3.28 (right side), although the effect is again hidden by the added ASE noise, which is non-central χ^2-distributed and has a high-pass characteristic. For higher P_1 the mirroring effect is smaller and the curvature of the transfer function redistributes the noise in the opposite direction compared to the pass-through case and the skewness at the output is positive. These noise redistributions are relevant to bit error rate, BER, estimations in a communication

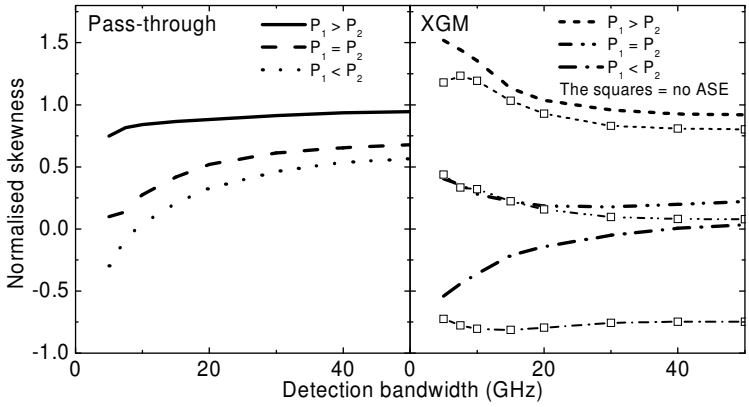

Figure 3.28: Skewness normalised with the input skewness for the pass-through and XGM case. The influence by the ASE is shown by also including calculations where the ASE has not been included (squares).

system since the BER is evaluated in the tails of the probability distributions where the redistribution due to non-linear transfer functions is large. In both the pass-through and XGM cases the redistribution skews the distribution in a direction that counteracts the improvement in SNR expected from the suppression of the standard deviation of the noise. How large an influence the change in standard deviation and skewness have on the BER will be investigated next.

3.6.4 Noise suppression and redistribution (σ v.s. γ_s)

We have just shown that the self and cross-gain modulation in an SOA can change both the width, i.e. standard deviation, and the overall shape, i.e. skewness, of the noise distribution as described by the PDF. The question to be answered in this section is how important these measures are for the BER.

In order to answer this question in a somewhat orderly manner a few assumptions has to be made. First of all, only the logical one-level is considered. This means that a fixed decision threshold has to be chosen since without a zero-level no optimum threshold can be defined. The second assumption is that this threshold is the same although the PDF changes. The final assumption is that a PDF with the shape of a non-central χ^2-distribution can be used, and in order to achieve negative skewness this PDF is simply mirrored at the mean value. All in all, this is not really a realistic situation but it should allow us to examine the influence of the skewness and standard deviation of a non-central χ^2-like distribution on the error probability.

The threshold is chosen to be a fixed distance from the mean value and the standard deviation is kept constant. Since the skewness is a function of both the standard deviation and the mean value, it is then changed by changing the mean

value. The error probability is calculated by integrating the PDF from a fixed distance very far from the mean to the threshold. The point where the integration starts is chosen such that the error rate does not noticeably change when the point is moved further away from the mean. Instead of directly integrating the PDF numerically one could also use the Marcum-Q function, which relates to the non-central χ^2 distribution in a similar way as the error function relates to the Gaussian distribution [6].

The results are shown in Fig. 3.29.

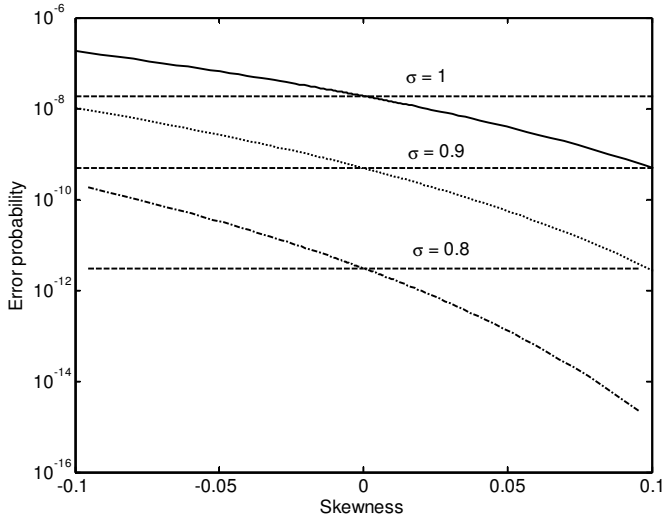

Figure 3.29: Error probability as a function of skewness for different standard deviations. A non-central χ^2-distribution is assumed and the error probability of Gaussian distributions ($\gamma_s = 0$), dashed lines, are plotted for comparison.

The figure show the error probability as a function of the skewness in an interval around zero, for different standard deviations. The dashed horizontal lines show the error probability for a Gaussian distribution with the same mean, standard deviation and threshold. When comparing Fig. 3.29 to the measured and simulated changes in standard deviation and skewness, Fig. 3.15 and Fig. 3.17, it is clearly seen that the largest impact on the BER from the noise redistribution in the SOA would be due to the suppression of the width of the distribution. The influence of the skewness, although much smaller, is large enough not to be disregarded. A change from $\gamma_s = 0.1$ to $\gamma_s = 0$, which is well withing what is possible in the SOA, changes the error rate by about one order of magnitude. It is also seen by the slopes of the curves that the influence of the skewness increases as the distribution gets more narrow.

The important conclusion from this is that when a non-linear redistribution of noise is considered, BER estimations using only the standard deviation, e.g. the use of the Q-factor, can give substantial under estimations of the BER.

3.7 Summary

In this chapter the noise redistribution in a saturated SOA was investigated. Direct measurements of the noise distributions show that the SOA changes both the width and skewness of the PDFs as compared to linear amplification. Due to the limited speed of the SOA, as dictated by the carrier life time, the static transfer function proved to not be an adequate description of the transformation. The measured PDFs ended up in between the limiting cases of transformation of the input PDF by the linear and nonlinear static transfer function.

Three different implementations of a model for the SOA including spontaneous emission noise was introduced for describing the noise redistribution. The small signal analysis to first order described the changes in noise variance, but could not describe the change in skewness. When the second order terms are included the model can describe also the change in PDF shape, and compares well with direct time domain simulations of the SOA. The strongest point of the small signal implementation was that the PDFs could be calculated far out in the tails of the distributions, which is relevant for BER estimations.

The models were used in order to in more detail investigate the noise redistribution in the SOA. The dependence on device speed for both pass-through and wavelength conversion operation was examined. It was shown that in both cases the change in skewness counter acted the potential gain in BER that the noise suppression, as expressed by a smaller standard deviation, indicates. This effect, although smaller than the improved signal-to-noise ratio, is large enough to be noticed at relevant levels of BER.

Chapter 4

Modeling of regeneration

Modeling of regeneration is not an easy task. First of all, regeneration is by definition a non-linear process. There is no linear process that can suppress some part of a signal and increase another, as discussed in Sec. 2.1.2. Secondly, the noise has to be considered in some detail, which can be quite challenging, as have been seen previously in this report. Finally, the devices and physical processes used for achieving the regeneration can be quite complex and difficult to model even under linear and deterministic circumstances. In this chapter one method, in two different 'flavors', of simplifying the problem to consideration of some central issues is presented.

4.1 Static transfer function models

The theory used to model regeneration in this section is based on the PDF and transfer function picture from Sec. 2.1.2. This picture reduces the regenerator to a memory less transformation of the input signal to the output. This transformation is represented by the static transfer function, which is just the time-averaged output power as a function of the input power. The PDF represents the time averaged signal, including noise, to be transformed. This way of modeling regeneration has been used for optoelectronic repeaters [9], all-optical regenerators [72, 73] and all-optical wavelength converters [74, 75]. The method presented here is a generalization of the model first presented in [73, 76, 77]. The method considers about 'one and a half' of the three issues stated as difficulties above, namely some of the nonlinearity and the noise. The non-linearity, calculated, measured or approximated is considered, but only in a static sense. As seen in Sec. 3.3.1, where the measured noise distribution was shown to lie in between the linear and static nonlinear case, this assumption will thus give a best case result, only valid for very large bandwidth regenerators or a small detection bandwidth. Limited considerations of dynamical effects in the form of patterning effects can be included [75], but this method still use the static transfer functions. The noise is considered in detail as far as the redistribution of the input intensity noise is considered, but any phase noise or time dependence are neglected, and the ASE added by the device is

somewhat troublesome, as will be seen later. No detailed consideration is made as to the exact physical implementation of the regenerator, but in the next chapter one possible all-optical approach will be presented.

One example of a non-linear transfer function that could, and in this report will, be used for regeneration, is shown in Fig. 4.1. It is described by the relations

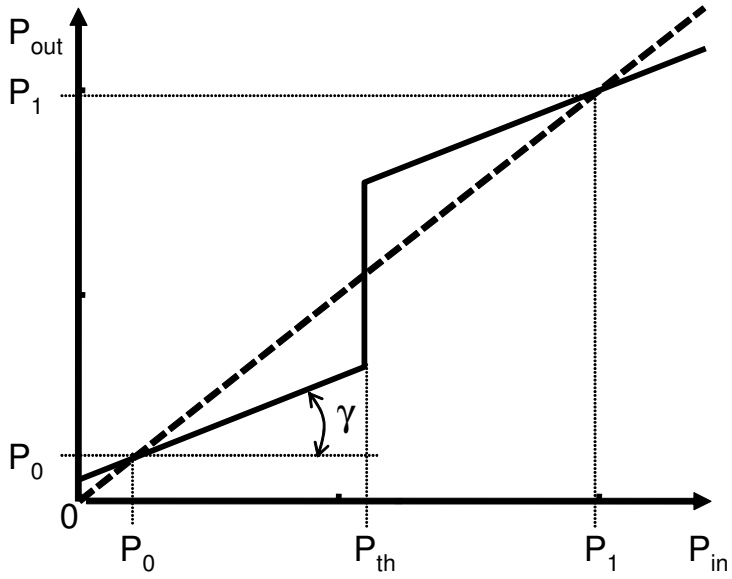

Figure 4.1: Piece-wise linear transfer function with finite extinction ratio. The stable points P_1 and P_0 as well as the threshold power P_{th} are shown.

$$\begin{aligned} P_{\text{out}} &= P_0 + \gamma(P_{\text{in}} - P_0);\ P_{\text{in}} < P_{\text{th}} \\ P_{\text{out}} &= P_1 + \gamma(P_{\text{in}} - P_1);\ P_{\text{in}} > P_{\text{th}} \end{aligned} \tag{4.1}$$

where γ is the slope of the curve at the zero and one level and P_{th} is the threshold value. By varying γ from zero to one, the transfer function can be changed from an ideal step function ($\gamma = 0$) to a linear function ($\gamma = 1$). In this section the strength of the nonlinearity will be expressed as $1 - \gamma$, so that a large value, close to one, represents a strong nonlinearity and a value close to zero a more or less linear case. The two points labeled P_0 and P_1, respectively, are the two stable points where the output power is equal to the input power. Stable points in this context refer to the situation that any input signal in the vicinity of the points will be even closer to the stable points at the output. The third point, where the output equals the input, is situated at the threshold. This point, however, is unstable, meaning that any signal close to it will be further away at the output. After the signal has passed a number of regenerators, cascaded after each other,

the one-level will thus be at P_1 and the zero-level at P_0, assuming they start at their respective sides of the threshold. The ratio between the two levels are called the extinction ratio of the regenerator

$$\mathrm{ER}_{\mathrm{reg}} = \frac{P_1}{P_0}. \tag{4.2}$$

This finite extinction ratio means that even for zero input power, the output power is non-zero. This is, for example, the case in a wavelength converter where the input signal modulates a clock- or cw-signal at another wavelength through a nonlinear gate. If this gate is not completely closed at the zero-level, a finite $\mathrm{ER}_{\mathrm{reg}}$ results. For a pass-through regenerator, the regenerator extinction ratio is infinite since the contribution of the ASE noise to the output power will be considered in other ways and is not part of the transfer function.

The regenerator described by the transfer function in Fig. 4.1 does not include any gain, and is hence not really a 2R-regenerator. Furthermore it does not add any noise to the signal but only redistributes the noise injected at the input. Any practical regenerator will add noise, either through an active gain component in the regenerator itself or by introducing additional losses, which have to be compensated by additional amplification. In order to include gain and noise a cascade of regenerators, as depicted in Fig. 4.2, is considered. In addition to the

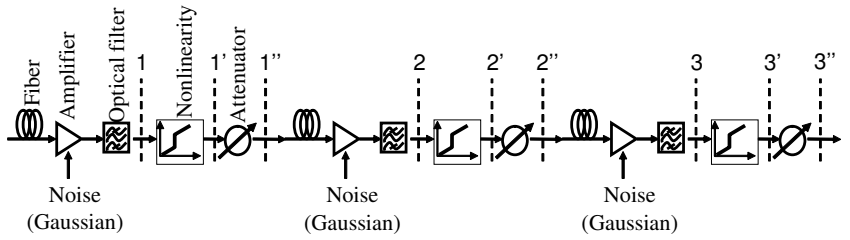

Figure 4.2: A cascade of regenerators modeled as linear amplifiers compensating for the link loss and adding noise, and non-linear re-shaping transfer functions.

non-linear elements the cascade consists of optical amplifiers, which are assumed to exactly compensate the loss of each link in Fig. 4.2. The amplifiers also add noise in the form of amplified spontaneous emission, which is assumed to be Gaussian distributed. The attenuator is added to the cascade in order to make sure that the input power to each new link is kept constant.

This picture obviously describes certain physical implementations of the regenerator better than others. In general it describes passive re-shaping elements with external amplifiers, for example fiber based non-linearities with external erbium doped fiber amplifiers, fairly well. Regenerators with an active amplifying medium inside the re-shaping device, such as SOA-based devices, are harder to conceptually separate in an amplifying and a reshaping part since both functions are performed by the same device. The picture does, however, include most of the

central parts of any regenerator, whether they are separated or not. It is a simple picture leading to a model capable of describing the interplay between different regenerator and signal properties, as will be shown in this section. The analysis emphasizes the general properties of regenerators, such as the interplay of noise and nonlinearity.

4.1.1 Numerical model

Using an approach similar to the one sketched above, Öhlén and Berglind have developed a numerical model for calculating the evolution of the PDFs for the one- and zero-level and hence the BER in a cascade of regenerators [9]. The model is not limited to a specific shape of the transfer function and any measured or calculated transfer function can be used. The model can thus be used for evaluating the regenerative properties of a device described by a detailed device model, as will be done in chapter 5.

The details of the model of reference [9] will not be presented here. The general principle of the model is to divide the transfer function into two staircase-like functions with constant values for each step. One of the functions lies above the proper function and the other one below. By increasing the numerical resolution the two functions approach the proper function. The probability for the signal to end up at a specific 'step' of the function, given a probability distribution at the input and added random noise, can then be calculated. The transformation of the input PDF, including the addition of Gaussian noise, can in this way be described in a transfer matrix formalism:

$$\mathrm{PDF}(n) = T^n \mathrm{PDF}(0) \tag{4.3}$$

where T is the probability transfer matrix and PDF(0) is the discrete PDF at the input of the cascade. Once the transfer matrix is known it is therefore easy and quick to calculate the PDFs and hence the BER for any number of cascaded regenerators. The transfer matrix, though, can be a bit cumbersome to calculate, especially for strong non-linearities where a fine numerical resolution needs to be used. Another drawback of the approach is that, being purely numerical, it is quite time consuming to draw more general conclusions regarding the importance of specific properties of the regenerator, such as non-linearity, extinction ratio and added noise. In the next section we will present an approximate approach using similar basic assumptions that allows us to make more detailed investigations of the interplay between different regenerator properties.

4.1.2 Approximate BER model

The basic assumption of this model, which leads to an expression for the BER in a cascade of regenerator, is that a piece-wise linear transfer function as described in Fig. 4.1 is used. This assumption, although it seems to limit the generality of the approach, is justified by the fact that different forms of transfer functions but with the same strength of the nonlinearity give very similar BERs [9]. The piece wise linear transfer functions can significantly simplify calculations and has,

in different flavors, been used for both pass-through regenerators [72] and wavelength converters [74]. The approach used here was first presented in [73] and is here expanded to include a finite extinction ratio of the transfer function, a finite extinction ratio of the signal entering the cascade as well as the contribution to the mean power from the added ASE noise.

The noise added by the amplifiers is considered to be Gaussian distributed with a mean value, $\bar{P}_{\text{ase}}$, and standard deviation, σ_{ase}. The addition of noise is mathematically described by a convolution of the input PDF with the PDF of the noise

$$PDF_{\text{out}} = PDF_{\text{in}} \otimes PDF_{\text{ase}}, \tag{4.4}$$

assuming that the ASE is independent of the input noise. The assumption of Gaussian noise is, as discussed before, only a good approximation for not too small signal levels, where signal-spontaneous beat noise dominates over for example spontaneous-spontaneous beat noise. In this investigation Gaussian noise will, however, be used for all signal levels. Furthermore the same amount of noise, calculated for the one-level, will be used for both the one- and zero-level. This overestimates the width of the PDF at the zero-level and hence the BER. The assumption of a Gaussian distribution, on the other hand, underestimates the BER since this distribution is symmetric as opposed to a more correct PDF for a low intensity spontaneous-spontaneous beat noise that has a longer high power tail. In order to keep the Gaussian approximation, and make the calculations as simple as possible, it therefore makes sense to calculate the width of the PDFs from the expressions for signal-spontaneous beat noise at the one-level. However, a next step in the development of this model could be to more accurately represent the noise at the zero-level. The convolution expressed, by Eq. (4.4), gives an output noise variance from the amplifier that is the sum of the input and noise variances,

$$\sigma^2_{\text{out,amp.}} = \sigma^2_{\text{in,amp.}} + \sigma^2_{\text{ase}}, \tag{4.5}$$

and a mean power that is

$$\bar{P}_{\text{out,amp.}} = \bar{P}_{\text{in,amp.}} G + \bar{P}_{\text{ase}}. \tag{4.6}$$

The linear transformation used in the regenerators changes the standard deviation by a factor equal to the slope, γ, and the attenuator just gives a linear change, $L_{\text{att.}}$,

$$\sigma_{\text{out}} = L_{\text{att.}} \gamma \sigma_{\text{in}}. \tag{4.7}$$

The evolution of the variance of the signal in the cascade can thus be described as

$$\begin{aligned}
\sigma_1^2 &= \sigma_{\text{ase}}^2 \\
\sigma_{1''}^2 &= (L_{\text{att.}}\gamma)^2\sigma_1^2 \\
\sigma_2^2 &= \sigma_{1'}^2 + \sigma_{\text{ase}}^2 = (L_{\text{att.}}\gamma)^2\sigma_1^2 + \sigma_{\text{ase}}^2 \\
\sigma_{2''}^2 &= (L_{\text{att.}}\gamma)^2\sigma_2^2 \\
\sigma_n^2 &= (L_{\text{att.}}\gamma)^2\sigma_{n-1}^2 + \sigma_{\text{ase}}^2 \\
&= (1 + (L_{\text{att.}}\gamma)^2 + (L_{\text{att.}}\gamma)^4 + ... + (L_{\text{att.}}\gamma)^{2(n-1)})\sigma_{\text{ase}}^2 \\
&= \frac{(L_{\text{att.}}\gamma)^{2n} - 1}{(L_{\text{att.}}\gamma)^2 - 1}\sigma_{\text{ase}}^2
\end{aligned} \tag{4.8}$$

where the numbering refers to Fig. 4.2, and a noiseless signal is assumed at the input of the cascade. As long as equal slope, γ, of the transfer function is assumed for both the one- and zero-level, Eq. (4.8) is valid for them both.

The ASE noise of the amplifiers thus enters the model in two ways; as a contribution to the mean power of the signal, $\bar{P}_{\text{ase}}$, and as a broadening of the signal PDF, σ_{ase}. Since the regenerator is modeled as the combination of a linear amplifier and a non-linear element, the ASE mean power is straight-forward to calculate using expressions for a linear amplifier from for example [46]. Assuming the noise figure to be $F_{\text{N}} = 2n_{\text{sp}}$ [5] the ASE power from the amplifier is

$$\bar{P}_{\text{ase}} = F_{\text{N}}(G-1)\hbar\omega_0 B_{\text{o}}, \tag{4.9}$$

where B_{o} is the bandwidth of the optical filter.

When considering the broadening of the PDF, i.e. σ_{ase}, the picture becomes somewhat more problematic. The amount of signal-spontaneous beat noise that is converted to intensity noise described by the PDF is determined by, among other things, the bandwidth within which the conversion takes place. In the simple example of an opto-electronic regenerator this is the electrical bandwidth of the photo detector [46], but for an all-optical device there is no detection and not such a clear cut physical limitation. It has been argued [72] that the use of an intensity transfer function, as in this case, does in fact correspond to a detection as far as conversion from signal-spontaneous beat noise to intensity noise is concerned. Following this argument, the maximum bandwidth in our picture is the bandwidth of the optical filter, since ideally there is no ASE outside this bandwidth. The non-linearity assumed in the model is a static transfer function and as such it corresponds to an infinitely fast device, i.e. the optical filter would limit the bandwidth. A real device, however, has a limited speed, as we have seen for the SOA in Sec. 3.6, and the limit would then be set by the physical limits of the device, for example the carrier dynamics in an SOA. In this work an effective limiting bandwidth of the device, B_{D}, different from the filter bandwidth will be used in order to examine the different influence of the signal-spontaneous beat noise and the mean ASE power on the BER accumulation in the cascade. In accordance with this discussion the broadening of the PDF in the regenerator is

described by [46]

$$\sigma_{\mathrm{ase}}^2 = 2F_{\mathrm{N}}\bar{P}_{1,\mathrm{s}}(G-1)\hbar\omega_0 B_{\mathrm{D}} \tag{4.10}$$

By using the piece-wise linear transfer function the transformation of the PDF can be divided into two parts, as seen in Fig. 4.3, which shows the concept of the transformation. The input-PDF is transferred to the output by a linear trans-

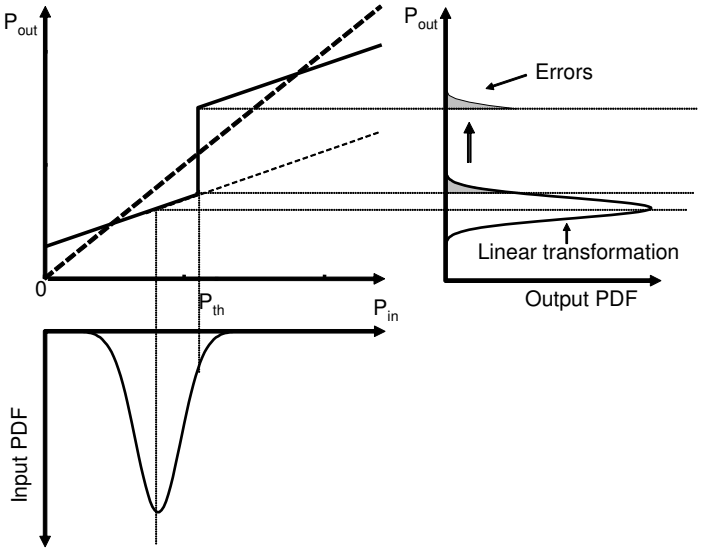

Figure 4.3: Principle of the nonlinear transformation of the PDF. The output PDF consists of the input PDF transfered by the linear part extended beyond the threshold, plus a part representing the unrecoverable errors.

formation, using the linear part of the transfer function extended beyond the threshold. By this extension the same transformation is used for the whole PDF. The second part of the PDF, the part above the threshold, is also included at the output as unrecoverable errors, and thus contributes to the accumulation of errors in the cascade. The output PDF can therefore be described as a linear transformation of the input PDF plus the part giving errors. This means that the part of the PDF above the threshold both contributes to the errors in this regenerator and is transmitted to the next regenerator and potentially contributes to the errors there as well. Thus this approach over-estimates the BER. The effect is largest for the linear case and zero for a step function.

The errors, $E(\sigma, \bar{P})$, for zeros and ones, respectively, after each amplifier can

be described, using the Gaussian assumption [5], as

$$E_0(\sigma_0, \bar{P}_0) = \frac{1}{2}\text{erfc}\left(\frac{P_{\text{th}} - \bar{P}_0}{\sqrt{2}\sigma_0}\right) \approx \frac{\sigma_0}{\sqrt{2\pi}(P_{\text{th}} - \bar{P}_0)}\exp\left(-\frac{(P_{\text{th}} - \bar{P}_0)^2}{2\sigma_0^2}\right) \quad (4.11)$$

$$E_1(\sigma_1, \bar{P}_1) = \frac{1}{2}\text{erfc}\left(\frac{\bar{P}_1 - P_{\text{th}}}{\sqrt{2}\sigma_1}\right) \approx \frac{\sigma_1}{\sqrt{2\pi}(\bar{P}_1 - P_{\text{th}})}\exp\left(-\frac{(\bar{P}_1 - P_{\text{th}})^2}{2\sigma_1^2}\right). \quad (4.12)$$

where erfc() is the complementary error function, $\bar{P}$ is the mean value of the signal and σ its standard deviation. The 1 and 0 refers to the one- and zero-level, respectively.

The evolution of the BER can be described by noticing that the non-linear elements do not add any errors, but just collects the errors added by the noise in the amplifier, and that the attenuator is just a linear loss, which does not change the BER. Furthermore we analyze the BER for the one- and zero-level separately so that

$$\text{BER} = \frac{1}{2}(\text{BER}_0 + \text{BER}_1) \quad (4.13)$$

where the one- and zero-bits are assumed to appear with equal probability. The result, which is the same for both ones and zeros, is

$$\begin{aligned}
&\text{BER}_1 = E(\sigma_1, \bar{P}_1)\\
&\text{BER}_{1''} = \text{BER}_1\\
&\text{BER}_2 = \text{BER}_1 + E(\sigma_2, \bar{P}_2)\\
&\text{BER}_{2''} = \text{BER}_2\\
&\text{BER}_n = \text{BER}_{n-1} + E(\sigma_n, \bar{P}_n)
\end{aligned} \quad (4.14)$$

where the numbering refers to Fig. 4.2. The BER is thus completely described by the evolution of the mean values and standard deviations for the one- and zero-level of the signal.

The mean value of the two signal levels will evolve in the cascade as:

$$\begin{aligned}
\bar{P}_{0,n} &= (L_{\text{att.}}\gamma)^{n-1}\bar{P}_{0,\text{s}} + \frac{(L_{\text{att.}}\gamma)^{n-1} - 1}{L_{\text{att.}}\gamma - 1}L_{\text{att.}}(1-\gamma)P_0\\
&\quad + \frac{(L_{\text{att.}}\gamma)^{n} - 1}{L_{\text{att.}}\gamma - 1}\bar{P}_{\text{ase}};\ \bar{P}_{0,\text{s}} < P_{\text{th}}\\
\bar{P}_{1,n} &= (L_{\text{att.}}\gamma)^{n-1}\bar{P}_{1,\text{s}} + \frac{(L_{\text{att.}}\gamma)^{n-1} - 1}{L_{\text{att.}}\gamma - 1}L_{\text{att.}}(1-\gamma)P_1\\
&\quad + \frac{(L_{\text{att.}}\gamma)^{n} - 1}{L_{\text{att.}}\gamma - 1}\bar{P}_{\text{ase}};\ \bar{P}_{1,\text{s}} > P_{\text{th}},
\end{aligned} \quad (4.15)$$

where $L_{\text{att.}}$ is the loss in the attenuator, $\bar{P}_{\text{ase}}$ is the contribution of the ASE to the mean power, P_0 and P_1 are given by Fig. 4.1 and $\bar{P}_{0,\text{s}}$ and $\bar{P}_{1,\text{s}}$ are the values at the start of the cascade. This means that signal levels below the threshold move toward P_0 and signal levels above the threshold move toward P_1.

Now, finally, the BER after N regenerators can be expressed by use of Eq. (4.14), Eq. (4.15) and Eq. (4.8) as

$$\mathrm{BER}_{0,N} = \frac{1}{\sqrt{2\pi}} \sum_{n=1}^{N} \frac{\sigma_n}{[P_{\mathrm{th}} - \bar{P}_{0,n}]} \exp\left(-\frac{[P_{\mathrm{th}} - \bar{P}_{0,n}]^2}{2\sigma_n^2} \right) \tag{4.16}$$

$$\mathrm{BER}_{1,N} = \frac{1}{\sqrt{2\pi}} \sum_{n=1}^{N} \frac{\sigma_n}{[\bar{P}_{1,n} - P_{\mathrm{th}}]} \exp\left(-\frac{[\bar{P}_{1,n} - P_{\mathrm{th}}]^2}{2\sigma_n^2} \right) \tag{4.17}$$

The sum in Eq. (4.16) and Eq. (4.17) cannot, as far as this author knows, be evaluated analytically. In [73] it was shown that for the special case of infinite extinction ratio, both for the transfer function and the input signal, and where the contribution to the mean power by the ASE is neglected, it was possible to get good analytical approximation to the sums. However, the inclusion of the arbitrary input ER makes the same approach difficult in this, more general, case. Although the lack of an analytical expression lessens the direct understanding given by the model, it is still much easier, and faster, to extract information about the cascaded regenerator system from Eq. (4.16) and Eq. (4.17) compared to the models in [9] and [72].

4.1.3 Numerical versus approximate model

How does the approximate BER expression in Eq. (4.16) and Eq. (4.17) compare to the numerical calculation in [9]? This is examined in Fig. 4.4, where the BER as a function of number of regenerators has been calculated using the two models. In the comparison the influence of the ASE mean power has been neglected since this is not included in the numerical model. The noise figure was 7 dB, the device bandwidth 20 GHz, the mean power at the input of the amplifier was -23 dBm, the amplifier gain was 20 dB, the input extinction ratio, $\mathrm{ER}_{\mathrm{in}}$, 10 dB and the regenerator had an $\mathrm{ER}_{\mathrm{reg}}$ of 40 dB. The parameter values have been chosen to give a BER around 10^{-9}, which is the normal definition of an error free signal. With the use of error correction techniques [3] a much higher BER can be accepted and it might also be interesting to investigate regeneration at larger error rates. This will, however, not be done here. As seen in the figure the two models give very similar results, except for the linear case. The reason for the obviously bad result of the approximate model (BER > 1), in this case, has already been touched upon when describing the model. It is due to the extra errors introduced by assuming that the PDF at the output consists of a linear transformation of the input PDF plus a part that represents the unrecoverable errors. In principle, this adds extra errors also for stronger non-linearities and only for the ideal step function does this approximation not give additional errors. However, as seen in the figure the approximation is a good one already for fairly modest non-linearities.

The strong point of the approximate expression is that it is extremely fast in computing the BER, which means that it can be used for numerically solving for different parameters in Eq. (4.16) and Eq. (4.17) assuming a certain BER and number of regenerators. This can be used to obtain a better understanding of the

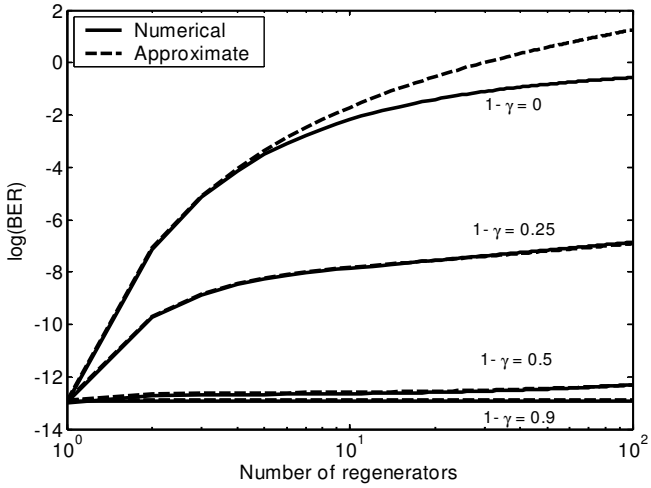

Figure 4.4: Comparison between numerical calculation of BER, according to [9], and the approximate expression from Eq. (4.16) and Eq. (4.17). The noise figure was 7 dB, the gain 20 dB, the device bandwidth 20 GHz, the mean input power into the cascade was -3 dBm, the input signal ER was 10 dB and the regenerator ER was 40 dB

regenerator cascade, in particular the influence of different parameters. This will be used in the following sections in order to investigate the different mechanisms of regeneration.

4.2 The mechanisms of regeneration

Which mechanisms are at play in a regenerator and how do they influence the BER evolution in a cascade of regenerators? The answers to this question will be investigated in this section using the approximate model. If nothing else is stated, the parameter values are: mean input power, $P_{in} = -3$ dBm, $B_D = 20$ GHz, $B_o = 125$ GHz, $F_N = 7$ dBm, $G = 20$ dB and the attenuator was used to keep the output power of the one-level at the same value as the input to the cascade.

4.2.1 Extinction ratio and threshold

The use of a regenerator to suppress the mean power in the zero-bits while leaving the one-bits unchanged, and hence increase the extinction ratio of the signal, is probably the most straight forward application of a regenerator. Apart from the input ER, that might be limited by for example the modulator, partly dropped channels and noise, the non-linearity of the regenerator has to counteract any noise power added by the regenerator itself. If the regenerator is of the wavelength conversion type where the incoming signal modulates the transmission of another

co-injected signal with a different wavelength, there might also be a limit as to how much it can increase the ER of the signal due to a finite $\mathrm{ER_{reg}}$ of the regenerator itself.

Let us start by looking at the influence of a finite input extinction ratio. In Fig. 4.5 the BER as a function of number of regenerators is plotted for an $\mathrm{ER_{reg}}$ of 40 dB and two different values for the input ER, 7 and 15 dB, in both cases $1-\gamma = 0.25$. To fully exploit the improvement in ER in the cascade of regenerators

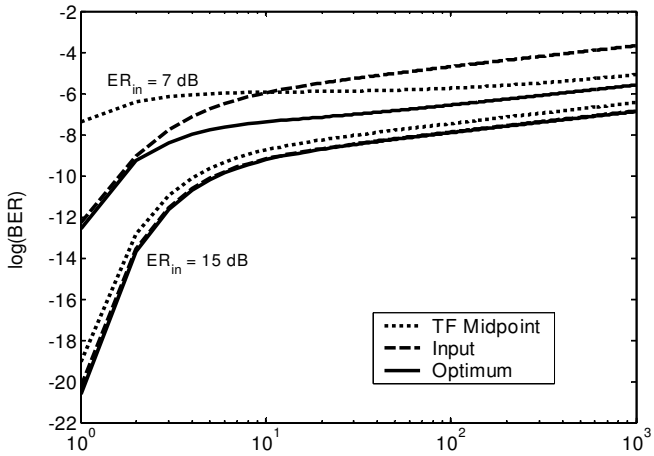

Figure 4.5: Comparison of different choices of threshold for two different values of input ER. The thresholds were either optimized for each regenerator, solid lines, or held constant at the best value for the input signal, dashed lines, or the best value for the regenerator, dotted lines. The upper set of lines is for $\mathrm{ER}_{in} = 7$ dB and the lower set is for $\mathrm{ER}_{in} = 15$ dB, in both cases $1 - \gamma = 0.25$.

it is crucial to use the correct decision threshold. This is shown in Fig. 4.5 by plotting the results for three different choices of threshold. The solid lines show the result when the threshold is adjusted for each regenerator to give as few errors as possible at that regenerator. For the dashed lines the threshold was kept constant for all regenerators at the optimum value for the first regenerator of the cascade. Finally, for the dotted lines the threshold was set midway between the one- and zero-levels of the transfer function, i.e. $P_{\mathrm{th}} = (P_1 + P_0)/2$.

Obviously the best result is always achieved when the threshold is optimized for each regenerator. If the optimization is not possible for practical reasons (the simultaneous optimization of several tens or even hundreds of regenerators seems like a daunting task) and one fixed threshold needs to be used, Fig. 4.5 gives some indication on which considerations that have to be made. For a large $\mathrm{ER_{in}}$, in this case 15 dB, at the input the improvement in the cascade is not that important and only a small difference is seen between the two choices. The best choice is to minimize the errors from the first regenerator by choosing the threshold according to the input. For a bad $\mathrm{ER_{in}}$, 7 dB in this case, the changes through the cascade can be substantial and the choice of threshold has to be made in relation to how

many regenerators are cascaded. For a few regenerators it is advantageous to consider the input signal, while for many regenerators where the signal has been much more influenced by the non-linear transfer functions, the choice should be made considering the properties of the regenerator. It should be noted that the choice of threshold is related to our assumptions. The choice of the midpoint between the one- and zero-level of the transfer function is due to our assumption of symmetric noise on the two levels. For another assumption the threshold would probably have another value. The conclusion that for many regenerators the choice should be made with regard to the properties of the regenerator rather than the input is, however, more general. Another note that could be made is that in a network environment it is hard, if not impossible, to define a specific cascade of regenerators. Depending on how the signals are switched, dropped and added, regenerators could in one situation be the first regenerator and in another it could be the last, or anything in between. From Fig. 4.5 this situation seems to be best handled by the choice of threshold according to the properties of the regenerator, since for this choice the BER depends less strongly on the number of regenerators, and hence it is less important what number in the cascade the regenerator is.

How much the regenerators influence the choice also depends on the strength of the non-linearity, which is shown in Fig. 4.6. Here a input ER of 10 dB is

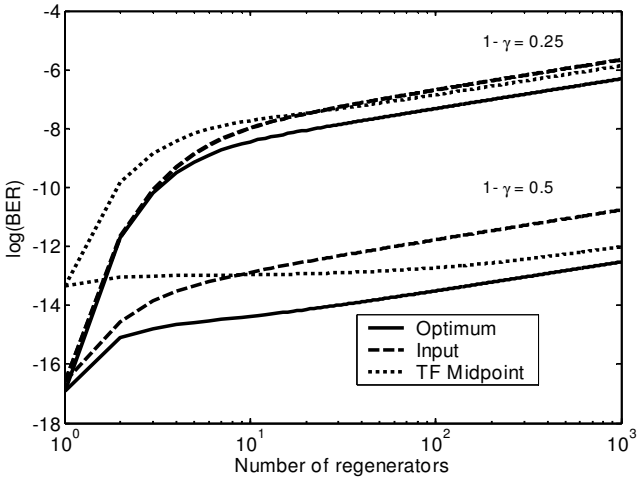

Figure 4.6: Comparison of different choices of threshold; optimized at each regenerator, solid lines, constant and optimized to the input ER, dashed lines, and constant and optimized to the transfer function ER, dotted lines. The input ER is 10 dB and the ER of the transfer function is 40 dB.

considered for two different non-linearities, 1-γ = 0.25 and 0.5. As seen, the stronger non-linearity give a larger influence on the ER evolution in the cascade and hence the choice of threshold becomes more important.

In the next figure, Fig. 4.7, where the influence of the ASE mean power on the BER is examined, the way of presenting the results have been somewhat altered.

Instead of explicitly showing the BER as a function of number of regenerators, the relationship between two regenerator parameters is investigated at a specific BER and a specific number of regenerators. The lines in the figure thus describe the relation between the two parameters that give a BER of 10^{-9}. The lines divide the parameter space into regions where the BER is larger or smaller than 10^{-9}. In this way it is possible to examine the interplay between these two parameters, for example the need of a stronger nonlinearity as the amount of ASE-power is increased. In Fig. 4.7 the ASE power is changed by changing the bandwidth of the

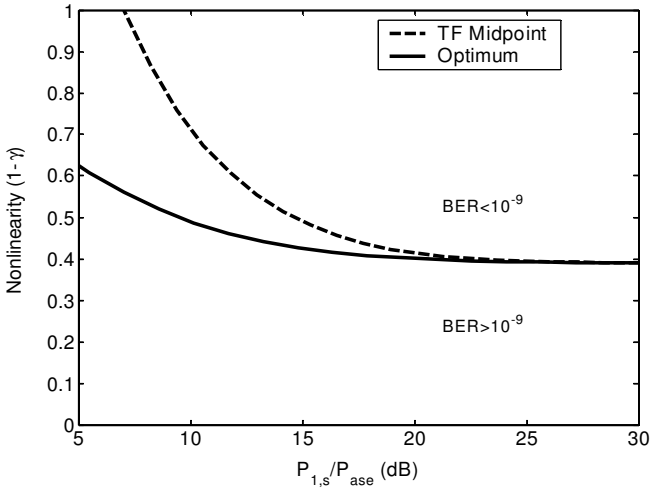

Figure 4.7: Influence of the ASE mean power on the BER, expressed as the nonlinearity required to get a BER of 10^{-9} after 100 regenerators. Both the input and transfer function ER are 10 dB.

optical filter. In this way all other parameters can be kept constant. The change of the optical signal-to-noise ratio (OSNR), here defined as $P_{1,s}/P_{\text{ase}}$, from 5 to 30 dB corresponds to a change in B_o from about 30 nm down to 0.1 nm. It shows that the reduction in extinction ratio due to the ASE power is fairly insignificant as long as the OSNR is large enough. As the ASE power increases the need for a stronger nonlinearity in order to keep a low BER indicates that the ASE has an influence on the extinction ratio. This means that the mean power from the ASE starts to influence the BER at a bandwidth of around 1 nm, which in the presented case corresponds to an OSNR of 20 dB. This influence is, as in the previous examples, less severe if the threshold can be optimized at each regenerator. In this case the input and transfer function extinction ratios are the same, 10 dB, in order to only investigate the influence from the ASE.

Finally the interplay between signal ER and nonlinearity will be investigated. In Fig. 4.8 the extinction ratio of the regenerators are kept at the same value as the input ER and the mean power of the ASE is neglected, so that the extinction ratio of the signal is constant through the cascade. The required nonlinearity for a BER=10^{-9} is plotted as a function of the ER. The figure show that an increase

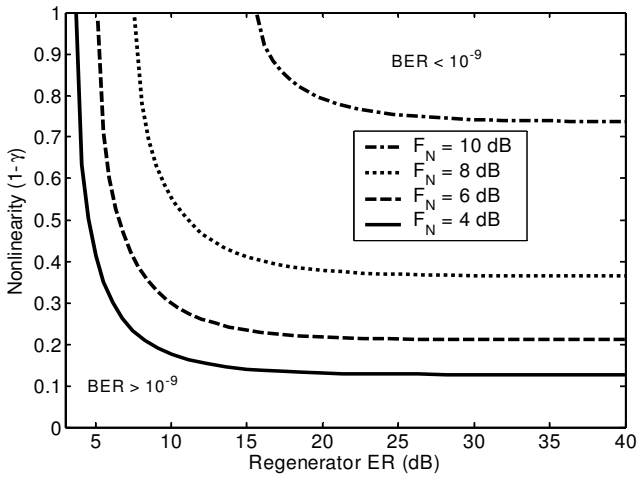

Figure 4.8: The interplay between ER and nonlinearity for a BER of 10^{-9} and 100 regenerators. The other parameters were: mean input power, $P_{in} = -3$ dBm, $B_D = 20$ GHz, $B_o = 125$ GHz, and $G = 20$ dB

in nonlinearity can compensate for a bad extinction ratio down to a certain limit, where even an ideal step function does not suffice. This limit is of course higher for a larger noise figure, as seen in the figure at the low ER end of the curves.

4.2.2 Noise redistribution

Improving the extinction ratio and keeping the noise power at the zero-level low are not the only ways to regenerate the signal, as we have seen before in this report. Another important effect is the redistribution of the noise at both the one- and zero-level, due to the low slope of the transfer function, which has the potential to make the noise variance smaller.

In this section the interplay between the nonlinearity, noise figure and input power will be investigated. In Fig. 4.9 the nonlinearity is plotted as a function of noise figure for different number of regenerators. Two different cases are plotted, one with -3 dBm mean input power into the cascade and one with 0 dBm. The input ER was 15 dB and $\mathrm{ER}_{\mathrm{reg}}$ was 40 dB. The ability of a stronger nonlinearity to compensate for an increase in noise figure can clearly be seen. For example a 3 dB increase in noise figure around a noise figure of 6 dB in the 0 dBm input power case can be compensated by a modest decrease of γ of about 10%. Put in another way this means that it might be beneficial to increase the nonlinearity at the expense of a higher noise figure, by for example the use of several regenerators after each other in the same node. The benefit of increasing the nonlinearity is also greater for a larger number of regenerators, as seen when comparing the curves for 10 and 100 regenerators. This kind of investigation can also be used to compare the cascading properties of different devices and regenerator types, with known

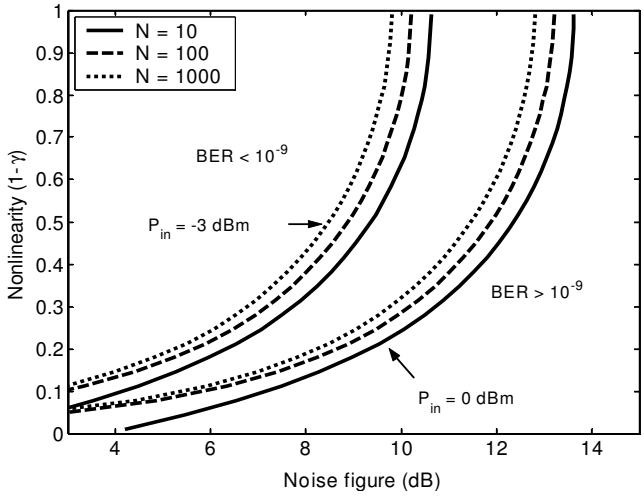

Figure 4.9: Non-linearity as function of noise figure for BER=10^{-9} and different number of regenerators at mean input power -3 dBm and 0 dBm. The input ER was 15 dB and the transfer function ER was 40 dB. The other parameters were: $B_D = 20$ GHz, $B_o = 125$ GHz, and $G = 20$ dB

nonlinearity and noise figure.

Looking at the other end of the curve, where the nonlinearity is close to an ideal step function, γ plays a smaller role, and increasing the nonlinearity above $1 - \gamma = 0.5$ seems to make little sense in this case.

In Fig. 4.10 the influence of the nonlinearity on the needed input power to the amplifier is investigated for different number of regenerators at a noise figure of 7 dB. The gain and the link loss was 20 dB, which means that the mean input power into the cascade is 20 dB higher than into the amplifier. Again it is seen that a small increase in nonlinearity can compensate for a signal degradation, especially for a large number of regenerators. In this case a stronger nonlinearity can increase the distance a signal can be transmitted between regenerators or decrease the transmission power needed in the system by improving the power budget.

4.3 Summary

2R regeneration as a static transfer of PDFs was investigated in this chapter. For this purpose a simple and efficient model for the BER in a cascade of regenerators was developed. The model takes the noise, the nonlinearity and the extinction ratio into consideration and makes it possible to investigate the interplay between these parameters.

The usefulness of the increase in extinction ratio in a cascade of regenerators was shown to be closely related to the choice of threshold value in the nonlinearity.

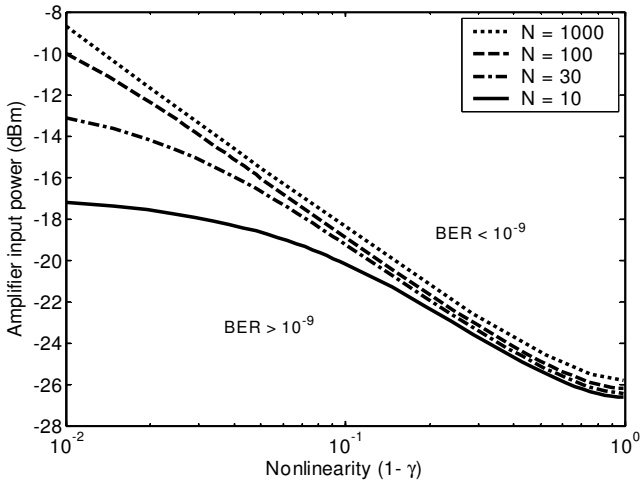

Figure 4.10: Amplifier input power as function of nonlinearity. The parameters were: $B_D = 20$ GHz, $B_o = 125$ GHz, $F_N = 7$ dBm, $G = 20$ dB, $\mathrm{ER}_{\mathrm{reg}} = 40$ dB and $\mathrm{ER}_{\mathrm{in}} = 15$ dB.

If the threshold cannot be optimized at each regenerator the best choice is to chose a threshold considering the properties of the regenerator itself, rather that the signal coming into the cascade. Finally the interplay between the amount of reshaping through the nonlinearity and the other regenerator parameters was investigated. It was shown that a fairly small increase in nonlinearity, in many cases, can compensate for a degradation of noise figure, extinction ratio or input power. These kind of investigation could be used to investigate how the cascading properties of different regenerators compare to each other and how to best optimize regenerators.

Chapter 5

SOA-EA regenerators

So far in this report basic noise properties of SOAs and regenerators have been presented, but not much have been written about real regenerator devices. This chapter will remedy this, and deal with one example of a simple device with regenerative properties.

As suggested in Sec. 2.4 there are quite a few different suggestions for implementing all-optical regenerators. However, many of the suggestions for all-optical regenerators are quite complex, using for example interferometers, optical delays and polarizers. The device described here on the other hand is quite simple, and the simplicity of the design is one of its main advantages. The concept was first suggested in [21, 39] and the ideas were further developed and the specific device of this investigation suggested by the author in [38, 40, 77, 78].

5.1 Description of the SOA-EA device

The device that will be presented and investigated is a combination of an SOA and a saturable absorber in the form of an electroabsorber (EA). Previous suggestions for similar devices have either used just a saturable absorber [19,37,79] or an SOA with an ion implanted absorber [21]. The single absorber, which can improve the ER of the signal needs bulky fiber amplifiers to compensate for the insertion loss, while the ion implanted absorber lacks the possibility to control the absorption and saturation characteristics in a simple manner. In our suggestion both components can be implemented as waveguide devices on the same semiconductor chip by dividing the waveguide into one section with forward and one with reverse electrical bias, which creates one amplifying and one absorbing section. The use of a single waveguide for implementing both the gain and the absorber sections, makes it straight-forward to add several concatenated sections. This gives the potential to increase the nonlinearity of the device and hence improve the regenerative properties. The direct electrical control through the electrodes also makes it easy to adjust and optimize both sections. This structure is very similar to that of a monolithic mode-locked laser and, as will be shown, the two devices have some similarities in their physical properties and functionality. A schematic picture of

the device is shown in Fig. 5.1.

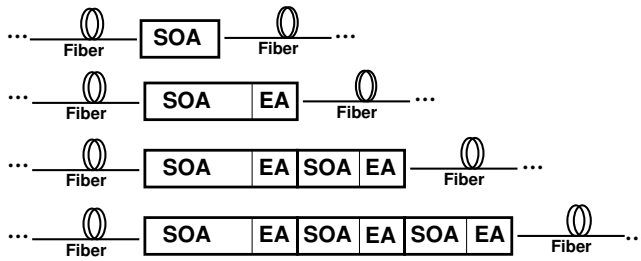

Figure 5.1: The simulated module consisting of concatenated SOAs and EAs. The module is considered as an in-line regenerator, the fiber span is considered as a constant loss.

First, a theoretical investigation of the device will be made, using the already presented models. Later in the section some experimental results and comparison between the experiments and models will be presented.

In the first pair of the simulated device the SOA is 800 μm long and the EA is 220 μm, in the following pairs the lengths are 500 and 295 μm respectively. We have investigated devices with one, two and three SOA-EA pairs in order to further improve the regenerative properties. The long first SOA has the effect that all net gain comes from this part of the device, the following pairs do not contribute to the net gain. This choice was made in order to have as much of the total gain as possible in the beginning of the device, since this will keep the noise figure lower, based on the experience from concatenation of linear amplifiers and absorbing elements [8]. All other parameter values used in the calculations are listed in Table 5.1. Typical parameter values are used, and these may in some cases differ from what is considered state of the art, which will limit the modulation bandwidth of the presented devices. However, all-optical signal processing at 40 GHz and above in both SOAs and EAs have been reported [80, 81], and the fabricated device that will be presented later in this section has been used for regeneration at 10 Gbit/s [20]. Here we emphasize the analysis and understanding of the nonlinear device properties, rather than the optimization of device performance.

Parameter	Value	
	SOA	**EA**
Time constant, τ_s [ps]	100	100
Saturation energy, E_{sat} [pJ]	2.17	0.54
Internal loss, α_{int} [m^{-1}]	2000	2000
Linewidth enhancement factor, α	5	5
Small signal gain, g_0 [m^{-1}]	11000	-19158
Differential gain, a [m^2]	$2{\cdot}10^{-20}$	$8{\cdot}10^{-20}$
Carrier density at transparency, N_0 [m^{-3}]	$1{\cdot}10^{24}$	$0.8{\cdot}10^{24}$

Table 5.1: Parameter values used in the calculations.

5.1.1 Principle of operation

The noise redistribution of the SOA has already been investigated thoroughly in chapter 3. It was shown that the gain saturation and self modulation of the gain by the signal can be used to reduce the noise at high input powers, representing the logical one-level. However, a single SOA is not a regenerator, mainly because it lacks two important features; noise suppression at the zero-level and extinction ratio improvement. The SOA actually makes the signal worse in both these ways. It adds noise to the zero level in the form of ASE and the same gain saturation that gives the noise suppression at the one-level also decreases the extinction ratio. The saturable absorber is added in order to remedy this.

The transfer function of the EA modeled in this section is shown in Fig. 5.2. The useful characteristic of this device is that the absorption is high at low input powers but bleaches, i.e. becomes lower, at high input powers. This means that the zero-level of a modulated signal experiences larger absorption loss than the one-level, and the extinction ratio is thus increased. When it comes to noise redistribution the picture is somewhat less straight-forward. For a single EA the slope of the transfer function at a specific input power is larger than the corresponding mean absorption, shown as the dashed line in Fig. 5.2. This results in that for a varying signal, for example a cw signal with intensity noise, the absorption in the EA is smaller for a power higher than the mean value, leading to even higher relative power at the output. For a signal lower than the mean the absorption is higher, leading to a even lower relative power at the output. The influence on the noise variance is thus opposite that of the SOA and the signal-to-noise ratio for a string of ones is decreased. For a string of zeros, however, the concept of signal-to-noise ratio is not relevant, since the mean power in the zeros should be as low as possible. The redistribution of the noise, as described by a reduction in signal variance, has to be viewed in relation to that of a linear amplifier with the same gain as the complete SOA-EA device. If the slope at the zero-level is lower than this mean gain the probability density function at the output will be smaller than for the corresponding linear amplifier.

The short story of the discussion above is that the SOA is good for the ones and the EA is good for the zeros. By combining the two an s-shaped nonlinear

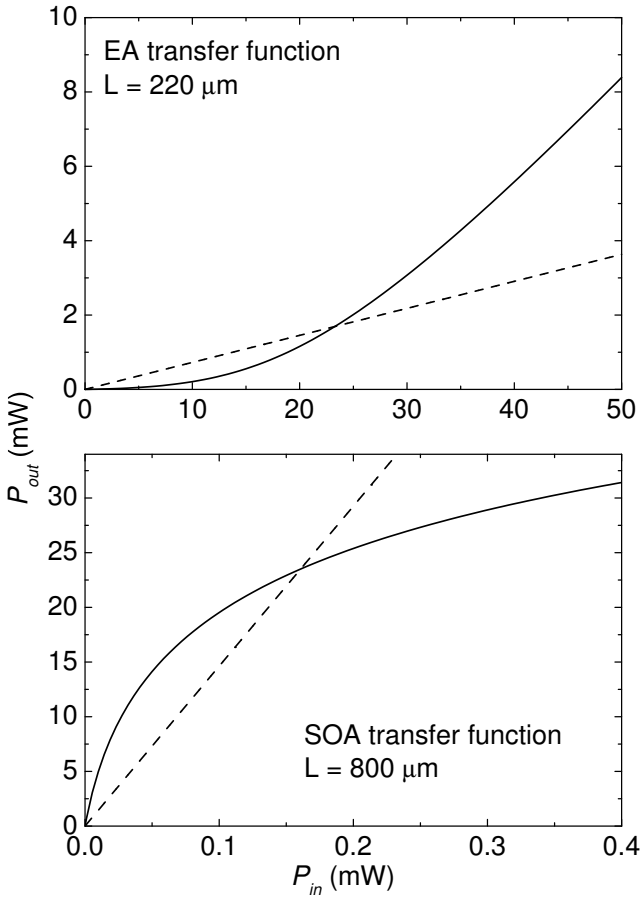

Figure 5.2: Transfer function of the modeled SOA and EA (solid line). The non-linear behavior, due to absorption bleaching and gain saturation, respectively, is clearly seen. The dashed lines show the transfer function of a linear device with the same absorption/gain as the devices at the chosen operating point.

transfer function is obtained, which should make all-optical regeneration possible. The transfer functions for a single SOA and concatenated SOA-EAs with one, two and three SOA-EA-pairs are shown in Figure 5.3. It should already here be noted that the component giving these transfer functions have not been optimized, and that it is possible to obtain much stronger non-linearities [20]. In the example shown a constant loss, representing for example fiber loss between regenerators, have been included in the transfer curve. A choice of one-level can be made, within the limits given by the gain of the device, by changing the amount of fiber loss in the link between the devices. The gain of the device at the one-level, which

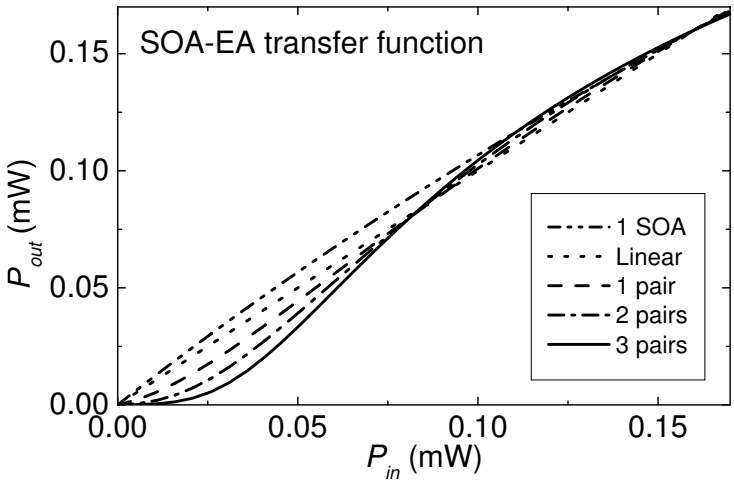

Figure 5.3: Static transfer functions of the SOA-EA device, including fiber loss, for one, two and three SOA-EA pairs. The functions are compared to a single SOA and a linear function, both with the same gain as the SOA-EA devices at the one-level.

exactly matches the loss of the fiber, is chosen to be around 10 dB for all the examined devices. This choice was made in order to set the decision threshold, i.e. the middle crossing point between the non-linear transfer function and the linear transfer function, approximately midway between the one- and zero-level.

Fig. 5.4 shows the same transfer curves as in Fig. 5.3 but plotted using dB-scale in order to show the extinction ratio improvement from the EAs. Although the extinction ratio increases, it is not obvious that the addition of a saturable absorbing element is advantageous with respect to regeneration. The induced loss has to be balanced by a larger gain, leading to additional noise. However, this is in principle not different from the inevitable insertion loss that has to be outweighed by the degree of reshaping in any regenerator, e.g. interferometric devices. Furthermore the investigations in chapter 4 indicate that increasing the nonlinearity might be beneficial even if the noise figure is increased.

5.1.2 Device properties

The properties of the SOA-EA device can be investigated by using the SOA models introduced in Sec. 3.4 and using the same equations for the EA, Eq. (3.7) and Eq. (3.8). In this case the characteristic time constant, τ_s, is an effective carrier sweep-out time describing the time it takes for the photo-generated carriers to be swept out of the active region by the applied electrical field. The absorption is described by a negative value of the gain (g). Both noise terms are assumed to be zero since there is no ASE in the EA and the carrier noise is assumed to be small

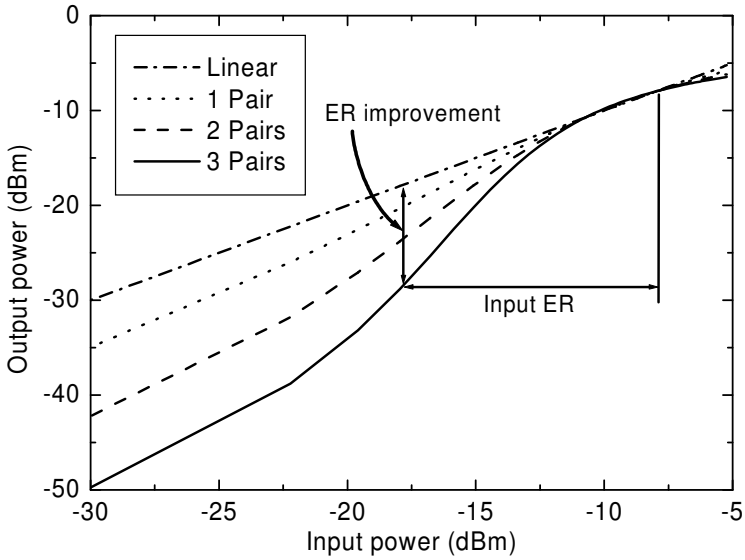

Figure 5.4: The transfer functions of the devices in dB scale, where the extinction ratio improvement is clearly shown, for one, two and three SOA-EA pairs.

compared to the ASE in the SOA for the SOA-EA combinations. A more detailed model for the EA dynamics could be used [79]. However, the present model incorporates the main feature of EA saturable absorption, and suffices for the present analysis of situations where ultrafast processes like spectral hole-burning and carrier heating [30] can be neglected.

Noise suppression

Figure 5.5 shows the RIN-spectrum at the one-level of a device with 1,2 and 3 SOA-EA pairs, using the simulations and the first order small-signal calculations. Figure 5.6 shows the SNR for the same situation and compares the SOA-EA devices to the linear transfer and the static transfer function of the three-pair case.

As seen from the close-up in the insert of Figure 5.5 and also in Figure 5.6 the noise is, as expected from the transfer function, reduced for low bandwidth and the reduction is larger for a larger number of SOA-EA pairs, although the redistribution is smaller than for the single SOA (not shown) due to the influence of the EA. The noise enhancement from the EA is also evident and limits the amount of noise redistribution for small bandwidth and leads to a noise enhancement for larger bandwidth. The bandwidth limit, where the noise is enhanced rather than suppressed, is easily seen in Figure 5.6, and is about 1.8 GHz. As mentioned before this rather low bandwidth is due to our conservative choice of device parameters and should not be considered to be a performance limit for this type of device in general.

From Fig. 5.4 and Fig. 5.5 it is seen that the main advantage of adding more

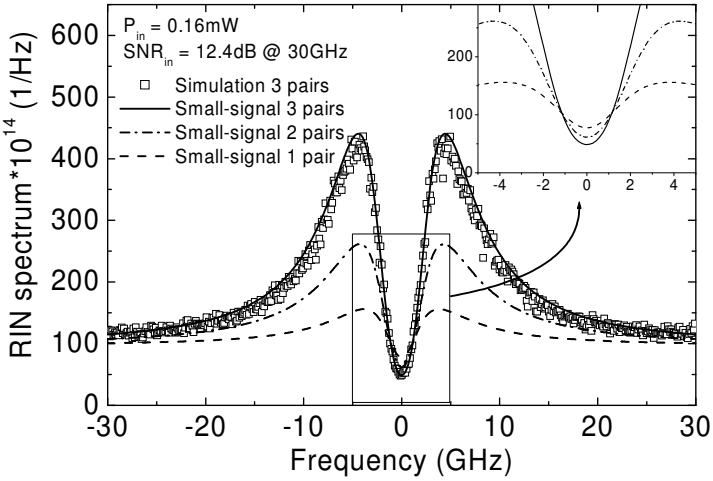

Figure 5.5: RIN-spectrum of three SOA-EA pairs for an input power of 0.16 mW, corresponding to the one-level. The solid, dash-dotted and dashed lines represents the small-signal analysis of three, two and one SOA-EA pairs, respectively. The squares show the simulated data for three pairs. The noise enhancement is due to the EAs and the noise suppression is due to the SOAs. The inset shows a close-up of the improvement in noise redistribution from more pairs, at low frequencies (without the simulation for clarity).

SOA-EA pairs comes from increasing the extinction ratio, while only a modest increase in redistribution at the one-level could be seen. The noise enhancement of the EA furthermore limits the bandwidth over which noise suppression can be achieved, compared to the single SOA case.

Pulse compression

The similarity of the structure of the proposed SOA-EA concatenation to a mode-locked laser has already been mentioned. In this section another similarity, pulse compression, will be briefly investigated. One example is shown in Fig. 5.7 where the output pulses after one, two and three SOA-EA pairs are compared to the input pulse. All pulses are normalized to the peak power of the input pulse. The pulse compression in the device is quite obvious and it is seen that the narrowing of the pulse is larger for more pairs. Another effect is a shift of the pulse in time.

The reason for the pulse compression is again the saturation of the gain and absorption in the different device sections. In the SOA the rising edge of the pulse experiences higher gain than the peak and especially more than the trailing edge since the gain has been saturated and has not yet recovered. This leads to a shift in time in the negative direction compared to the input pulse, and to

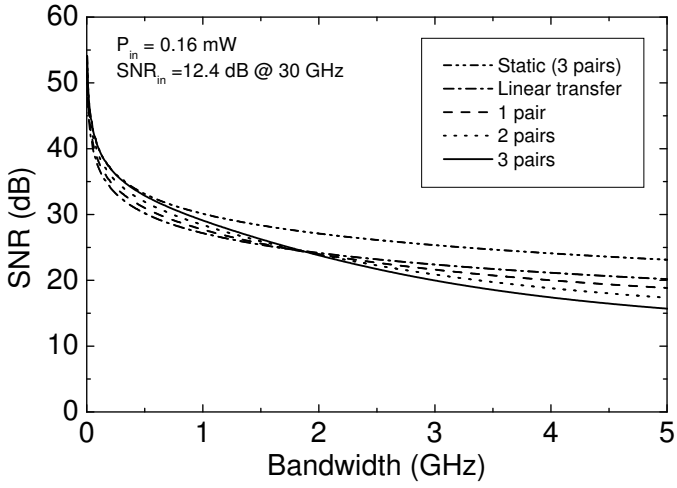

Figure 5.6: SNR as a function of detector bandwidth for one, two and three SOA-EA pairs compared to a linear transfer and the static transfer function of the three-pair device.

some degree a broadening of the pulse [60]. The EA again works in the opposite direction and absorbs more of the rising than the trailing edge and the peak, which sees the smallest absorption. If the recovery of the absorption is fast enough the trailing edge of the pulse will also experience higher absorption than the peak. The combined effects of the two components is that the peak is amplified and the tails are absorbed, which leads to a narrowing of the pulse. This effect is similar to the pulse compression in a passively mode-locked laser and the concatenation of several pairs might be seen as a few round trips in such a laser.

5.2 Noise and regeneration in an SOA-EA

5.2.1 Noise redistribution

We have previously seen that the non-linear noise redistribution in an SOA changed the shape of the PDFs. In this section the redistribution of noise in the SOA-EA device will be investigated using the simulated PDFs for both one- and zero-level.

An example of the non-linear redistribution of the PDF is shown in Figure 5.8, which depicts the simulated noise distribution after a device with three SOA-EA pairs in the form of a PDF. The Gaussian and non-central χ^2 distributions, with the same mean and standard deviation, are also plotted for comparison. The mean input power of the cw signal was 0.16 mW for the one-level and 0.03 mW for the zero-level, i.e. an extinction ratio of 7.3 dB. The input signal had a non-central χ^2 distribution.

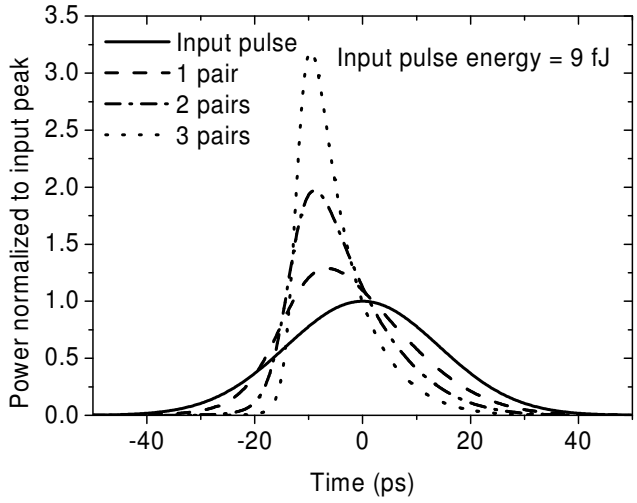

Figure 5.7: Pulse compression in an SOA-EA device with one, two and three SOA-EA pair/s.

Compared to the SOA this component show redistribution of both the one- and zero-level, and the stronger non-linearity for the zeros, as seen from the transfer functions, give a substantial difference between the simulation and the non-central χ^2-distribution in the tail. At the one-level, however the non-linearity is modest and the approximations fit fairly well with the simulations. Furthermore, the SOA-EA device is capable of improving the extinction ratio from 7.3 dB at the input to 11.2 dB at the output.

Due to the excessive computation time required, it is not feasible to simulate the distribution close to the decision threshold where the BER is evaluated. Instead, the non-linear redistribution can be approximately taken into account, when the BER is evaluated, by tail extrapolation [64]. In this method, the tails of the probability distribution functions are assumed to follow a generalized exponential distribution

$$f(x;\nu) = \frac{\nu}{2\sqrt{2}\sigma\Gamma(1/\nu)} \exp\left\{-\left|\frac{x-\mu}{\sqrt{2}\sigma}\right|^{\nu}\right\} \tag{5.1}$$

where $\Gamma()$ is the gamma function and μ is the mean value. The variance of the distribution is given by

$$Var = 2\sigma^2 \frac{\Gamma(3/\nu)}{\Gamma(1/\nu)}. \tag{5.2}$$

A normal (Gaussian) distribution is given by $\nu = 2$. By allowing the exponent ν in the tail to be different from the one in the central part of the distribution,

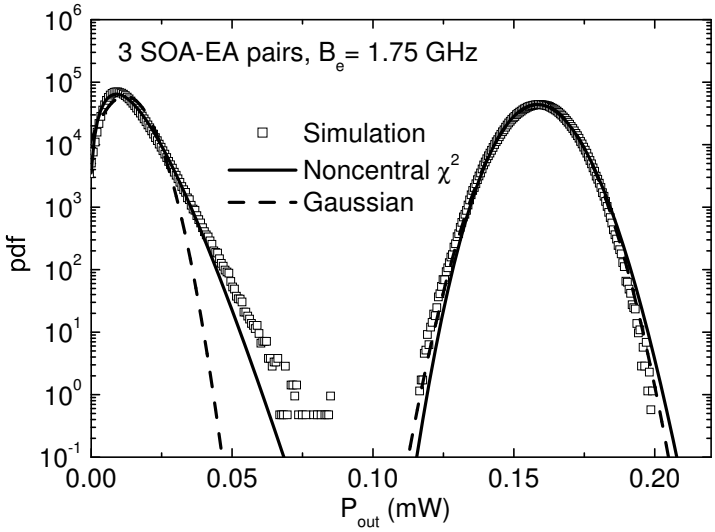

Figure 5.8: Noise distribution after three SOA-EA pairs for a bandwidth of 1.75 GHz. The squares show the result of the simulation and the lines show a non-central χ^2 distribution (solid line) and a Gaussian distribution (dashed line) with the same mean and variance.

non-linear behavior can be accounted for. The BER contribution from the '0'-level is, as usual defined as the integral of the distribution above a certain threshold

$$BER(t) = \int_{t+\mu}^{\infty} f(x,\nu)dx, \tag{5.3}$$

and the contribution from the one-level as the usual integral from zero to the threshold. By using the asymptotic expansion for the gamma function, calculating the BER at a few different pseudo-thresholds (t) in the tail, and fitting the exponent ν to a plot of the BER versus threshold value, an extrapolation can be made to the actual decision threshold where we want to estimate the BER. This fit can be seen as the insert in Figure 5.9 for the zero-level. The fitting is performed using transformed coordinates so that a linear interpolation using the least squares technique can be used, as seen in the insert. Figure 5.9 shows the BER as a function of the threshold power for the zero- and one-level. This gives a BER of approximately 10^{-8} for the simulated distribution, which should be compared to a BER of 10^{-12} for the non-central χ^2 distribution and 10^{-21} for the Gaussian approximation. It should be emphasized that the extrapolated results based on the simulations represents an approximation. However, the large differences in BER again show the importance of using the correct noise distribution when dealing with regenerators.

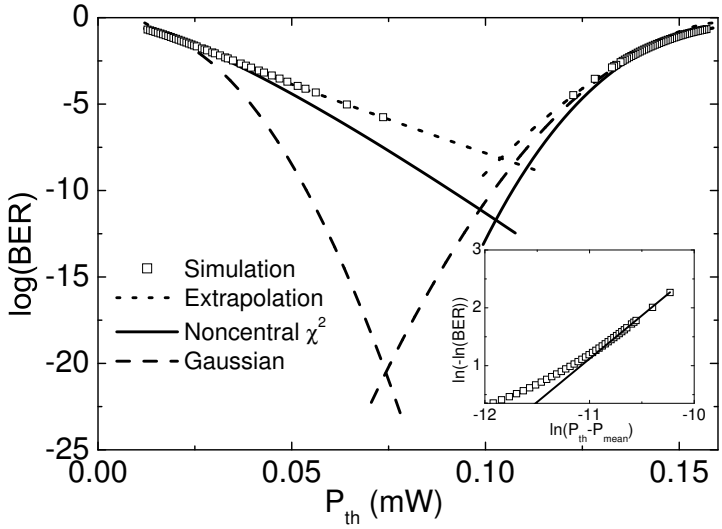

Figure 5.9: Tail extrapolation of the simulated noise distributions at the one- and zero-level. The squares are the simulated data. The lines are the extrapolation for the simulation (dotted), the Gaussian approximation (dashed) and the non-central χ^2 distribution (solid), respectively. The insert show the extrapolation technique with the zero-level of the simulation as an example.

5.2.2 Regeneration and cascadability

We have seen that additional SOA-EA pairs in the regenerator give an increase in non-linearity and better noise redistribution and extinction ratio improvement for small bandwidth, but the extra SOAs also add more ASE and the EAs increase the noise at higher bandwidth. In this section we want to examine how these two effects influence the cascadability of the devices by estimating the BER. We have used two different methods to estimate the regeneration capability of the SOA-EA cascades, the static transfer function and the first order small signal analysis. For the static case the model presented in [9, 75] and shortly described in Sec. 4.1.1 was used. The probability density functions for ones and zeros are assumed known initially and Gaussian noise, representing spontaneous emission for the SOAs, is then added for each link. The amount of noise added, i.e. the standard deviation, is calculated using the small-signal analysis and a choice of bandwidth. The bandwidth limitations will be discussed later.

In the small signal case, the cascadability is investigated by using the Q-factor, defined as

$$Q = \frac{P_1 - P_0}{\sigma_1 + \sigma_0} \tag{5.4}$$

where P_1, σ_1, P_0 and σ_0 are the mean power and standard deviation for the one- and zero-level respectively. The small-signal analysis gives us a possibility to examine how the bandwidth dependence of the regeneration influences the cascadability

of the devices.

The choices of bandwidth for these calculations require some further comments. In reality the use of optical filters between the cascaded regenerators are needed in order to limit the growth of ASE power that would otherwise saturate the regenerators and lead to a decrease in ER. Saturation from ASE is not taken into account in the two models used here, but the ASE power is kept low by the absorption in the EAs. Furthermore, since the static case only involves transfer of probability density functions, it is not possible to include the effect of optical band-pass filters in the cascade. Hence the important limiting bandwidth is the effective bandwidth of the regenerator, as discussed in Sec. 4.1.2. The standard deviation of the noise added in each regenerator is thus calculated using an effective bandwidth of 2 GHz in the static case. For the small signal case no filtering is assumed except for the final detection bandwidth, which is chosen to be 1 and 2 GHz in order to show the bandwidth dependence. The choice of such small bandwidth is made in order to be inside the modulation bandwidth of our devices, which is limited by the conservative choice of device parameters, as discussed before.

The result for an input signal with a signal to noise ratio for the one-level of 25.5 dB and the same noise variance at the zero-level is shown in Figure 5.10 and Figure 5.11 for the static and small-signal case, respectively. The BER (static case) and Q-factor (small-signal case) are plotted versus the number of cascaded regenerators for one, two and three SOA-EA pairs as well as for a single SOA with the same gain as the SOA-EA combinations. In the static case the obvious result

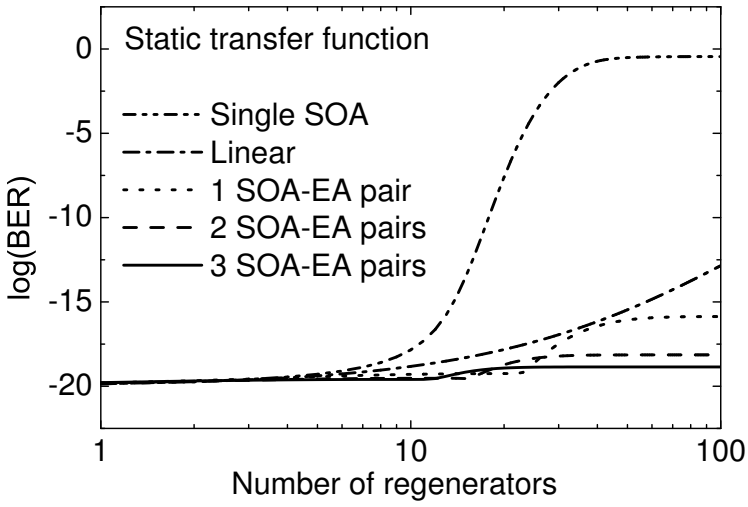

Figure 5.10: BER as a function of cascaded fiber links, including SOA-EA regenerators. The BER has been calculated using the static transfer function and ASE noise for 1, 2 and 3 SOA-EA pairs. The SNR for the one-level at the input was 25.5 dB and the noise variance at the zero-level was the same.

is the improvement in BER for the regenerators compared to the single SOA and linear transfer function due to the increase in extinction ratio by the EAs. For few regenerators the noise of the input signal dominates, but as more ASE accumulates from several regenerators the BER increases due to the added noise. The BER is evaluated at the optimum threshold value after each link, and due to the larger noise redistribution at the zero-level, compared to the one-level, the threshold value decreases during the first few links as the input noise is redistributed. The rapid increase in the BER, that occurs at about 10-20 regenerators comes about when the optimum threshold value cannot decrease further due to the added noise. If instead a fixed threshold is used this large noise suppression at the zero-level can not be properly utilised and the BER increases faster due to noise added at the one-level, as discussed in chapter 4 (not shown). A detection with fixed threshold should therefore be combined with a symmetric regenerator where the noise at the zero- and one-level is redistributed more equally. For a large number of regenerators the BER only increases slowly due to ASE added in each regenerator, similar to the linear BER degradation with number of regenerators that is obtained for an ideal step function. It is also seen that the sharper transfer functions do indeed improve the performance of the system for many regenerators even though the additional SOA-EA pairs gives additional noise.

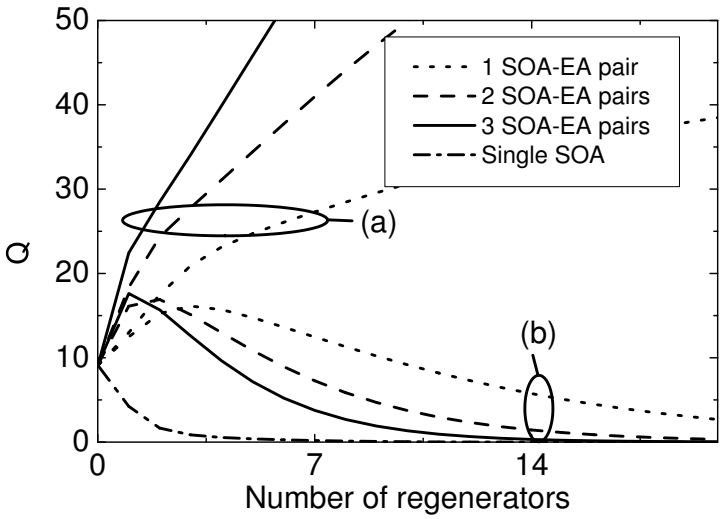

Figure 5.11: BER as a function of cascaded fiber links, including SOA-EA regenerators, calculated from the Q-factor from the small-signal analysis for a detection bandwidth of 1 GHz (a) and 2 GHz (b) .

The small signal analysis with B_e=2 GHz ((b) in Figure 5.11) shows a qualitative behavior somewhat different from the static case. For few regenerators, the redistribution of the noise at the '0'-level and the increase in extinction ratio keep the Q-factor high and more SOA-EA pairs give a better result. However, for

many regenerators the noise at the one-level decreases the Q-factor and the single SOA-EA device gives the best result, as opposed to the static case. For a smaller bandwidth (B_e=1 GHz, (a) in Figure 5.11) the stronger redistribution and smaller ASE make the Q-factor increase even for many regenerators. It is also seen that the sharper non-linear transfer function gives a higher Q for more SOA-EA pairs for the whole cascade at small bandwidth, although the additional pairs add more noise. Just as in the static case the lack of extinction ratio improvement in the single SOA gives worse performance. The reason for the large difference between a detection bandwidth of 1 and 2 GHz can be explained by Figure 5.6 where it is easy to see the upper bandwidth limit for noise suppression at the one-level.

It should be noted that an increase in Q-value does not imply an improvement in BER, only an increase in extinction ration and/or decrease of the noise variances at the one- and/or zero-level. To properly calculate the BER the complete non-linear transfer of the pdf has to be taken into account, like in the static calculations above.

The conclusion from this is that a sharper non-linear transfer function can improve the cascadability of the regenerator at small bandwidths, although the means to achieve this, i.e. additional SOA-EA pairs, also adds more noise, as also seen in chapter 4. Further we have seen a strong bandwidth dependence of the regenerative properties, hence demonstrating the limitations of the static nonlinear transfer function description, which is only valid for very low data rates. Due to the possibility of having a simple scheme to investigate the cascadability of all-optical regenerators and the possibility of evaluating non-linear transformation of the PDFs, it is nevertheless very attractive for BER estimations. However, measured and calculated static nonlinear transfer functions should be used with care when analyzing all-optical regenerators incorporating SOAs, EAs or, in general, devices with limited modulation bandwidth.

5.3 Optimization

In previous sections it was shown that the SOA-EA regenerator does indeed have regenerative properties and that these can be improved by concatenating several amplifier absorber pairs. In this section we want to look closer on the single pair and investigate how it can be improved by using different device parameters. To begin, we have chosen somewhat different base parameters in order to achieve a larger bandwidth over which noise redistribution takes place, as will be seen later. The new set of parameters are shown in table 5.2. The carrier life time of the SOA might seem somewhat short, and indeed it is. In order to reach such fast SOAs special techniques like the use of a holding beam is needed [82, 83].

There are, as we have seen, several ways of evaluating the regenerator performance. The ones we have looked at are the static non-linear transfer function, which we want as steep as possible, the intensity noise spectrum, where a noise suppression over a large frequency range is desirable, and finally the BER accumulation in a cascade of regenerators, which is the final and true test of a regenerator. Here we will find parameters that give a strong non-linearity in the transfer func-

Parameter	Value	
	SOA	EA
Carrier life time/sweep out time, τ_s [ps]	25	25
Saturation energy, E_{sat} [pJ]	3.47	varies
Internal loss, α_{int} [m^{-1}]	400	400
Linewidth enhancement factor, α	2	2
Small signal gain, g_0 [m^{-1}]	11000	-19158
Differential gain, a [m^2]	$0.75 \cdot 10^{-20}$	varies
Carrier density at transparency, N_0 [m^{-3}]	$1 \cdot 10^{24}$	$1 \cdot 10^{24}$

Table 5.2: Parameter values used in the calculations.

tion and then look at how the noise spectrum and BER is effected. The objective is to see to what degree a stronger non-linearity of the SOA-EA gives better BER-performance.

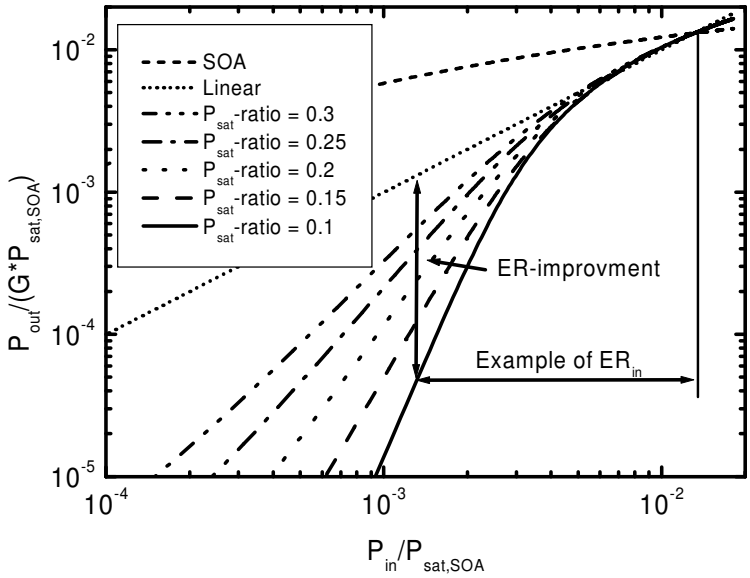

Figure 5.12: Transfer functions of the SOA-EA combination for different ratios between the saturation power for the EA and the SOA.

As shown in Sec. 5.1 the extinction ratio improvement in the EA is central to the regenerative performance of the device. In order to have a large extinction ratio improvement a large absorption is desired for small input powers, i.e. for the zero-level, and no or small absorption at the one-level. These considerations seems to imply that a large unbleached absorption, which is easily bleached at higher input powers, i.e. a long EA with low saturation power, is wanted. This is

also shown in Fig. 5.12

In this figure the transfer functions for a single SOA-EA pair is shown for different ratios between the saturation power of the SOA, $P_{sat,SOA}$, and the EA, $P_{sat,EA}$. The saturation power of the SOA is held constant, and the length of the EA is changed in order to keep the gain at the chosen one-level constant. This means that the EA is made longer when the saturation power is decreased, and the other way around. A lower saturation power in the EA, combined with a longer device, leads to stronger non-linearity and larger ER improvement. So far the case seems pretty clear, since a large non-linearity is wanted, but let us look at some other issues.

It is hard to see the threshold value on the logarithmic scale of Fig. 5.12, but as we change the transfer function to a steeper one, the threshold, i.e. the point between the one- and zero-level giving equal input and output power, also change. This is shown in Fig. 5.13, which shows the threshold compared to the one-level for the different saturation power ratios. The fact that the threshold does not vary

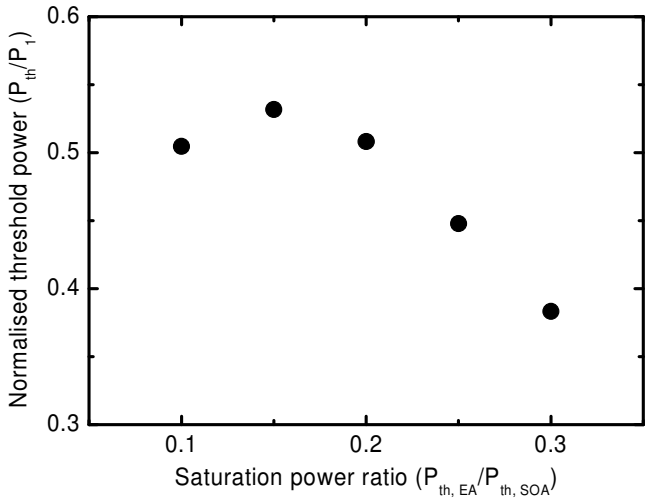

Figure 5.13: Normalized threshold power as function of saturation power ratio.

monotonically with the saturation power ratio will be seen to be important for the BER. More on this later.

The impact of the change of parameters compared to the previous sections becomes clear when looking at the relative intensity noise spectra in Fig. 5.14. The frequency range over which noise redistribution, though not necessarily noise compression, is seen is increased from about 10 GHz up toward 100 GHz. As before the EA is seen to increase the RIN at higher frequencies and limits the noise compression that is seen from the single SOA at low frequencies. Stronger saturation of the EA, i.e lower saturation power, leads to stronger noise enhancement at the one-level for higher frequencies. What is seen is basically that when the influence

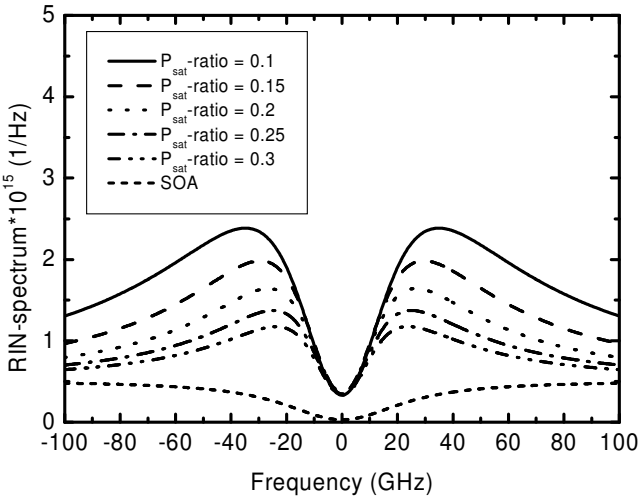

Figure 5.14: RIN spectra at the one-level, for different saturation power ratios. The RIN spectrum for the single SOA is plotted for comparison.

of the EA on the transfer function is made stronger, so is its effect on the noise spectrum.

Another way of looking at the effect seen in Fig. 5.14 is to consider the noise figure. Here we use a standard noise figure definition [8]

$$F_{\mathrm{N}} = \frac{\mathrm{SNR}_{\mathrm{in}}}{\mathrm{SNR}_{\mathrm{out}}}, \tag{5.5}$$

where the input signal-to-noise ratio is for a shot-noise limited signal, in order to plot the noise figure as a function of input power in Fig. 5.15. Due to the saturation behavior of the device as seen in the noise spectra, the output signal-to-noise ration, and hence the noise figure, becomes bandwidth-dependent. At a somewhat arbitrary choice of bandwidth of 40 GHz the noise enhancement of the EA is important, as seen in Fig. 5.14, and leads to higher NF for lower saturation power ratios.

In the comparison of BER below an ideal linear amplifier is included. It is assumed to have a constant noise figure of 4 dB, as shown in Fig. 5.15.

As before we will now look at how these changes in non-linearity and noise figure influence the accumulations of errors in a cascade of devices. In the BER-calculations shown in Fig. 5.16 and Fig. 5.17, a constant link loss equal to the gain of the device is assumed between the cascaded devices. Since a comparison is made to a single SOA that has the same parameters as the SOA in the SOA-EA

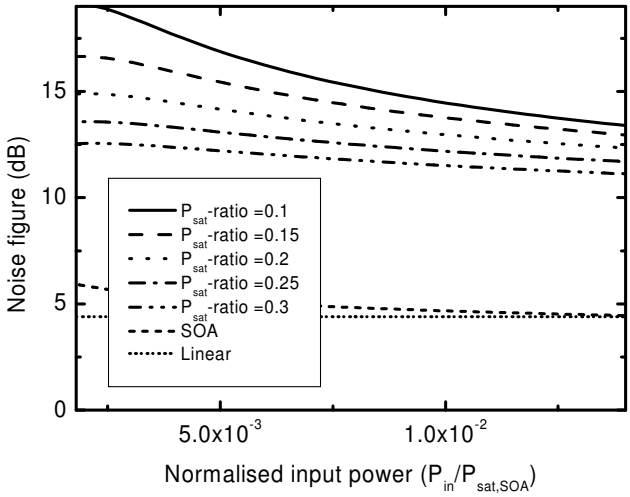

Figure 5.15: Noise figure for different saturation power ratios. The noise figure for the single SOA and a linear amplifier with constant noise figure is included for comparison.

device, and the gain decreases substantially when the EA is added, the BER is plotted versus total link loss rather than number of regenerators, in order to get a more fair comparison.

Remembering the change in threshold for the different cases, two different input extinction ratios, 10 and 13 dB, are considered in order to investigate the influence of the strength of the non-linearity compared to the influence of the threshold value. The noise of the input signal is chosen to give the same BER after one regenerator in both cases.

The figures show a few different interesting results. The decrease in ER after the single saturated SOA leads to bad performance even though the gain is higher than in the other devices. In general, a lower noise figure gives better performance for few regenerators where the noise redistribution has not yet had a large influence. This is especially clear when comparing to the low noise linear amplifier. A sufficiently large nonlinearity can, however, compensate for a high noise figure when many regenerators are cascaded and the BER only increases slowly, as opposed for the linear case. This is seen as a general trend when comparing the SOA-EA devices with different saturation power ratios. However, for the three cases with the strongest non-linearity the case is not that clear.

Comparing the cases with $P_{\mathrm{sat,EA}}/P_{\mathrm{sat,SOA}} = 0.1$, 0.15 and 0.2 in Fig. 5.16 and Fig. 5.17 one sees a discrepancy from the general trend, where stronger non-

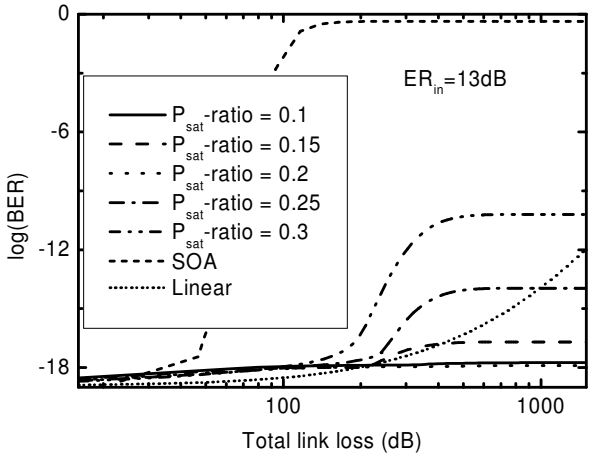

Figure 5.16: BER as function of cascaded regenerators for different saturation power ratios. The input extinction ratio is 13dB

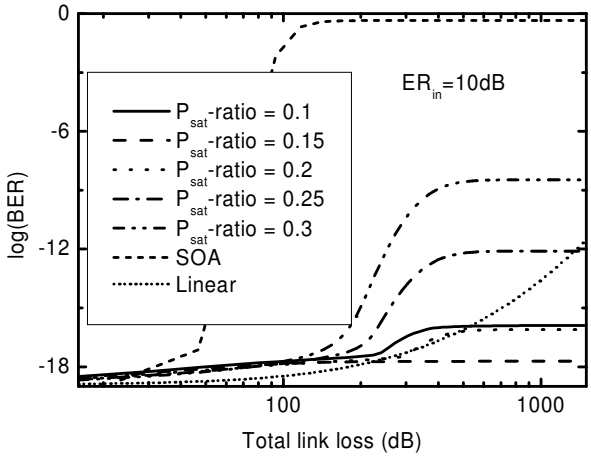

Figure 5.17: BER as function of cascaded regenerators for different saturation power ratios. The input extinction ratio is 10dB

linearity gives better BER performance. For the 10 dB case the best performance is not achieved for the regenerator with the strongest non-linearity, or the regenerator with the lower noise figure but, for the device with the highest threshold. This is a similar effect to the one studied in Fig. 4.5 and Fig. 4.6. For a larger input ER a lower threshold is beneficial while for a worse input ER it might be good to use a higher threshold. The best performance would of course be achieved if the threshold can be optimized for each regenerator, but if this is not possible a trade-off has to be made between accumulating many errors in the beginning or the end of the cascade, as seen in chapter 4.

A similar situation is shown in more general terms in Fig. 5.18 where the approximate BER model presented in Sec. 4.1.2 was used to calculate what non-linearity is needed to give a BER of 10^{-9} after 100 regenerators as a function of input extinction ratio for different thresholds. Since this calculation uses different non-linearity and noise properties than the SOA-EA they should not be compared directly, but rather in a qualitative way. In this figure, the limiting input extinc-

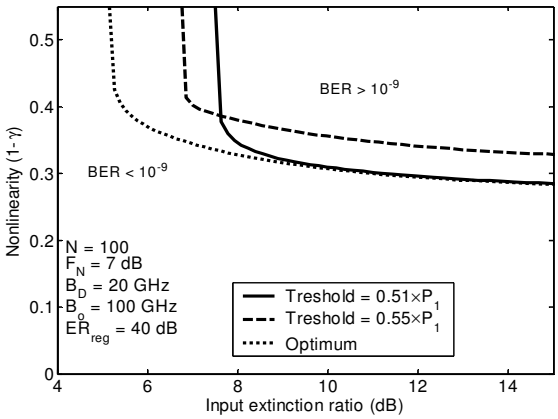

Figure 5.18: The influence of input extinction ratio for different values of threshold power.

tion ratio is seen to vary with the threshold as expected, and a high threshold is preferable. One can also see that for a higher input extinction ratio, where the ER improvement from the regenerator is less important, and the BER is dominated by the noise added by the amplifier at the one-level, much as the situation in the end of the cascade, the lower threshold is preferable. The two different fixed thresholds are compared to the case where the optimum threshold is used for each regenerator. This case obviously gives the best result.

5.4 Regeneration experiments

In order to experimentally show the potential of the concatenation of SOAs and EAs for regeneration integrated SOA-EA regenerators were fabricated and char-

acterized. All devices and measurements presented here were made by Lotte Jin Christiansen at Research Center COM [20]. One example of a two-pair device is shown in Fig. 5.19, but devices with one pair was also fabricated. The component

Figure 5.19: SOA-EA device fabricated at COM

has been designed to meet the requirements of a low saturation energy in the EA, compared to the SOA, and a large small signal absorption. The device is a ridge waveguide device and the SOAs are 545 μm long and the EAs are 120 μm. The ridge is angled by 7 degrees and the facets are anti reflection coated to reduce reflections. A regrowth MOVPE process has been used to implement an active material with a larger bandgap in the EA sections than in the SOA sections, so that the EAs are transparent at a wavelength where the SOAs have gain. By increasing the reverse bias on the EAs the absorption, at the signal wavelength, can then be controlled using the electro absorption effect. The SOA material consists of five 7.2 nm thick compressively strained InGaAsP quantum wells, and have a gain peak at 1535 nm. The EA material consists of fifteen compressively strained 10 nm thick wells, and have a photo-luminescence peak at 1480 nm.

As seen before, the transfer function of a regenerator is important and in Fig. 5.20 the measured static transfer functions of the two-pair device is shown for a bias voltage over the first EA section from 0 to -1 V, while the second EA section is completely unconnected. The total bias current to the SOAs is kept constant at 350 mA. The wavelength was 1500 nm. The transfer functions have for all bias points a strong nonlinearity with a very sharp threshold. It shows a potential output extinction ratio of 45 dB for an input extinction ratio of only 5 dB. The threshold is furthermore seen to be easily adjustable to different input power values by a simple change of reverse bias over one of the absorbing sections. The increase in reverse bias both increases the small-signal absorption and decreases the sweep-out time in the EA. The decreased sweep-out time increases the saturation power. The combined changes in absorption and saturation power results in the change in the threshold of the transfer function.

As discussed previously a strong nonlinearity is not enough to achieve a good regenerator, but also the dynamic properties are important. In Fig. 5.21 the measuring setup for measuring the regeneration of a modulated signal is shown. The cw signal from the laser is modulated with a 10 Gbit/s NRZ signal with a pseudo-random bit sequence, using a Mach-Zehnder modulator. The EDFA and attenuator ensures that the input power can be adjusted between -10 and 10 dBm. Polarization controllers are used at the input of the device since this first version

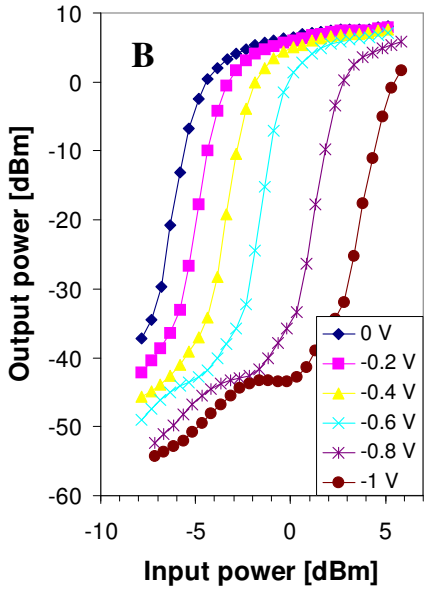

Figure 5.20: Measured transfer curves of a two-pair SOA-EA device for different bias voltage on the first EA, the second EA section is completely unconnected, the total bias current to the SOAs is kept constant at 350 mA.

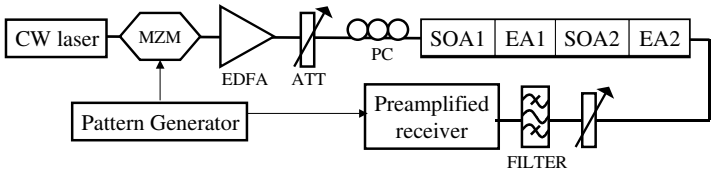

Figure 5.21: Experimental setup for measuring receiver sensitivity after regeneration with SOA-EA device

of the component is very polarization sensitive. The regenerated signal is then filtered and detected with a preamplified receiver.

In Fig. 5.22 the eye diagrams before and after the regenerator is shown. In this measurement the wavelength was 1545 nm, the input power was 3dBm and the bias levels of the four section were 13 mA, 0 V, 245 mA and 0 V, respectively. As seen an improvement of 5 dB from 2.2 to 7.2 dB is measured. Furthermore the

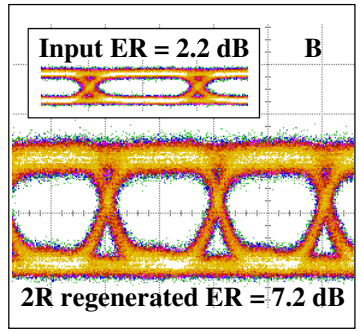

Figure 5.22: Measured eye diagram at the input and output of the two-pair SOA-EA regenerator

eyes are clear and there is almost no patterning effect. During the experiments the main improvement seemed to be achieved for the zero-level, while the noise at the one-level was not suppressed, indicating that the SOAs were not sufficiently saturated. Similar increases in ER were observed for input powers ranging from -8 dBm to 5 dBm by only adjusting the bias, which again show the possibility of adjusting the threshold in an easy manner.

The receiver sensitivity measurements, corresponding to the eye diagrams in Fig. 5.22, is shown in Fig. 5.23. A receiver sensitivity improvement of 8.5 dB was measured compared to the back-to-back measurement of the degraded signal.

5.5 Summary

In this chapter the SOA-EA 2R-regenerator was introduced and presented. The combination of gain saturation in the SOA and absorption bleaching in the EA gave a nonlinear transfer function. Although the addition of the EA, to some degree, lessened the effect of noise suppression at the one-level, it gave the possibility to increase the ER and redistribute the noise at the zero-level. Concatenation of several SOA-EA pairs resulted in sharper nonlinearity and better regenerating properties although the noise from the device increased.

The dependence of the nonlinearity on the saturation characteristics of the EA was investigated. By using a longer EA with lower saturation power a stronger nonlinearity and larger ER improvement was achieved for the same input power. The stronger saturation of the EA did, however, give a larger noise figure. Furthermore, it was shown that the largest nonlinearity did not necessarily give the

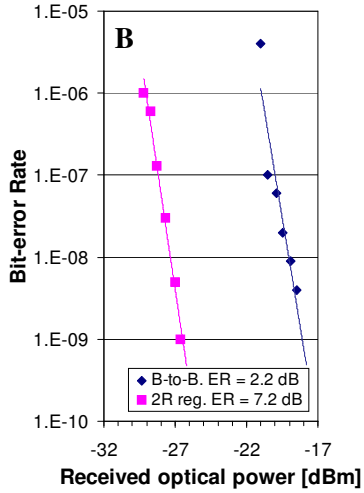

Figure 5.23: Measured receiver sensitivity after the SOA-EA regenerator compared to the back-to-back measurement of the degraded signal.

best cascading performance. It also proved important to adjust the threshold to fit the operating condition, which agree with the investigations in chapter 4.

Finally experimental results of regeneration in an SOA-EA device was presented. The experiments showed strong nonlinear transfer functions with an easily adjustable threshold, a large extinction ratio improvement and an improvement of the receiver sensitivity compared to the back-to-back measurement of a degraded signal.

Chapter 6

Conclusions and outlook

6.1 General conclusions

The main general conclusion of this work is that the details of the redistribution of the noise and the signal in a nonlinear device is central to 2R-regeneration. The main measure of signal quality is the BER, and the task of regeneration is to keep the rate of error accumulation in a communication link as low as possible. Regeneration cannot correct errors and improve the BER, but the best one can do is to collect the errors accumulated at the point of regeneration and to improve the signal in such a way that fewer errors are introduced at later stages of the link. This improvement can be achieved by a nonlinear redistribution of the signal, which increases the extinction ratio and decreases the width of the probability density functions, which describes the distribution of the signal and noise at the logical one- and zero-levels. However, the influence of the nonlinearity on the tails of these distributions has to be considered when regeneration is concerned, since it is the overlap of these tails that give errors, when intensity noise is considered. This means that any description of regeneration has to include, at least in an approximate way, the noise redistribution around the threshold value of the transfer function.

In more specific terms the details of noise redistribution in a saturated SOA was investigated. It was shown, from experiments and theoretical modeling, that this kind of redistribution not only changes the width of the distributions but also the overall shape. The same kind of redistributions was observed in simulations of a 2R-regenerator, showing pronounced changes in the tails of the distributions and hence the BER. Simpler models, and approximate BER estimations based only on the signal to noise ratio of the signal, does not consider these changes in noise statistics and can therefore underestimate the BER, and give a poor understanding of regeneration. The models were used to show that the redistribution depends not only on the strength of the nonlinearity of the regenerator transfer function, but also on the speed of the device and on the noise properties of the regenerator itself.

The noise added by the regenerator is, in addition to the nonlinearity, a very

important characteristic of the device. In general a regenerator transfer function can always be made sharper by optimizing the design or by cascading several regenerators at each node. This will, however, increase the amount of noise added as well. Furthermore, the threshold value of the regenerator, i.e. the value that separates the one- and zero-level, is important for the cascadability of the regenerator. The details of these kind of interplays were investigated using a model for the BER in a cascade of regenerators. Using simple assumptions of a piece-wise linear transfer function, Gaussian noise and a nonlinear collection of errors at the threshold, a quite general model was developed. The calculations show that an increase in nonlinearity can compensate for other signal impairments, such as an increase in noise figure or decreased power level. These kind of considerations can show how to best optimize 2R-regenerators or compare different regenerator types, when timing jitter is not included. Furthermore, the model showed that when cascading regenerators in a network environment the threshold value of the regenerator transfer function should be chosen with considerations to other regenerator properties, for example noise and extinction ratio, rather than to the properties of the input signal.

Finally a specific component for 2R-regeneration, consisting of a waveguide with alternating sections of saturable gain and absorption, was presented and examined. Both measurements and theory showed the potential for a sharp nonlinear transfer function by concatenation of several sections and device optimization. The very simple device showed both an increase in extinction ratio and improved receiver sensitivity in experiments. Theoretical modeling examined the noise properties and the cascadability of the device, and showed that several concatenated sections can improve the cascadability in a transmission link although the noise figure is increased. All-in-all the device show great promise as a simple 2R-regenerator.

6.2 Future work

One of the toughest tasks for 2R-regeneration is to combine the nonlinear transformation, device dynamics and noise in a model simple enough for investigating a cascade of several regenerators. Detailed device models, as the ones presented in this work, can properly describe the noise and dynamics of single components, but they are often too cumbersome to use when many devices are cascaded. On the other hand, simple and fast models using static transfer functions can easily calculate the PDFs after a large number of regenerators, but, as the investigations in this work show, these transfer functions can be a long way from the proper dynamical description of the noise transformation.

Another problem not properly covered in this work is that of patterning effects. All investigations in this work disregard the effects related to the data modulation of the signal, although patterning effects is one of the largest problems when considering all-optical signal processing in semiconductor components. The problem of properly including these effects is of course connected to the general problem of using static transfer functions or computationally heavy models. However, there

have also been suggestions on how to partially include patterning effects in an otherwise static description [75], that might be investigated further. From a technological point of view, a general solution to the problems of patterning effects would further strengthen the potential of all-optical signal processing in semiconductor components.

Another very important part omitted from this work is the third R, re-timing. To completely regenerate the signal the timing jitter also needs to be suppressed. If re-timing would be included in the modeling of regeneration in a simple way, it would greatly improve the usefulness of the theoretical investigations.

Finally, in order to properly compare the performance of regenerators it would be useful to define relevant and easily measurable figures of merit for a regenerator. As seen in this report, several properties of the regenerator influence the performance. In the literature one will find several different methods of characterizing regenerators. Although the most complete method is to study the regenerators in cascaded links or loop experiments, some measures of the performance can be tested through for example measuring the transfer function or studying extinction ratio improvement and receiver sensitivity after a single regenerator. There are however no well defined method of comparing regenerators to each other.

When, or if, all-optical regeneration will be employed in commercial communication systems is still an open question, which is not considered in this work. The theoretical investigation and fundamental understanding of the mechanisms of regeneration, however, is a very challenging and interesting field of research that needs further work.

Appendix A

The matrix of the second order model

The matrix $\tilde{O}$ used in Sec. 3.4.1 describes the second order contributions to the noise distribution. It is a $2M+2L_\omega \times 2M+2L_\omega$ matrix where M is the number of discrete steps in z, L_z, times the number of discrete steps in ω, L_ω, see Fig. A.1. It has an internal structure of sub-matrices where each sub-matrix describe the

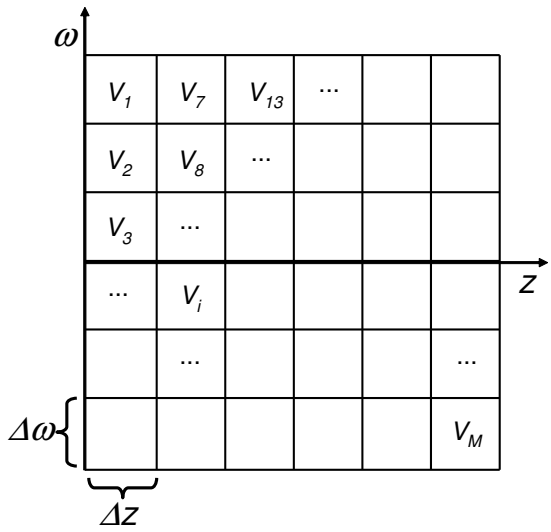

Figure A.1: The discretization of z and ω and definition of V_i.

contribution of one of all the combinations of ASE amplitude noise (N_ρ), ASE phase noise (N_ϕ), input amplitude noise ($N_{\rho 0} = \rho_1(z)\delta(z+)/\rho_\mathrm{s}(z)$) and input phase noise ($N_{\phi 0} = \phi_1(z)\delta(z+)/\rho_\mathrm{s}(z)$), as seen in Fig. A.2.

The matrix elements are given by the following:

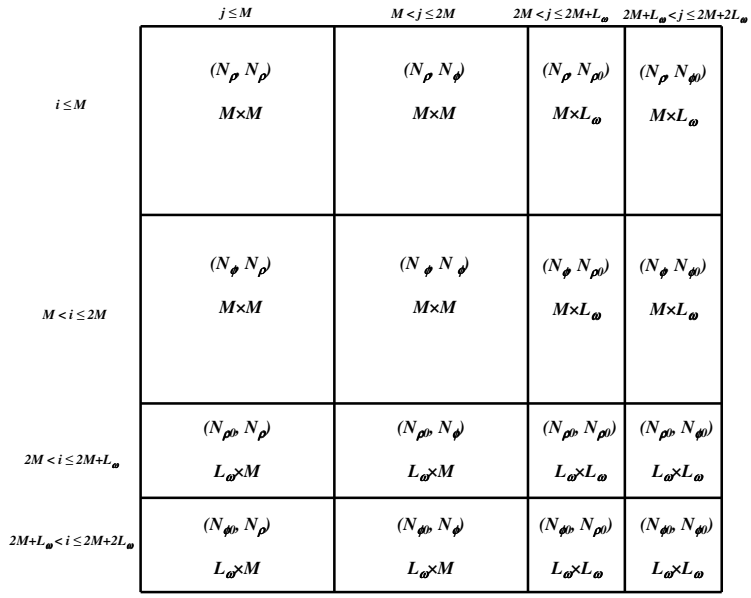

Figure A.2: The internal structure of the matrix $\tilde{O}$.

For $i \le M$ and $j \le M$, that is for (N_ρ, N_ρ):

$$\begin{aligned}\tilde{O}_{ij} &= F^*(\omega_1)H^*(z_1,\omega_1)F(\omega_2)H(z_2,\omega_2)\\ &+ F(\omega_2-\omega_1)\bar{M}_{\rho\rho}(z_1,\omega_1;z_2,\omega_2)\\ &+ (F^*(\omega_1)F(\omega_2) - F(\omega_2-\omega_1))\\ &\alpha^2\left(1-H^*(z_1,\omega_1)\right)\left(1-H(z_2,\omega_2)\right)\end{aligned} \tag{A.1}$$

where $(z_1,\omega_1) \in V_i$, $(z_2,\omega_2) \in V_j$ and

$$\begin{aligned}&\bar{M}_{\rho\rho}(z_1,\omega_1;z_2\omega_2) = \frac{1}{2}H(z_1,-\omega_1)H(z_2,\omega_2)\int_0^L \frac{H(z,\omega_2-\omega_1)}{H(z,-\omega_1)H(z,\omega_2)}\\ &\times\left[C(-\omega_1)+C(\omega_2)+C(\omega_2-\omega_1)+\frac{1}{g_{\rm s}(z)}C(\omega_2-\omega_1)\left(C(-\omega_1)+C(\omega_2)\right)\right]\\ &\times\theta(z-z_1)\theta(z-z_2)dz.\end{aligned} \tag{A.2}$$

Here θ is the Heaviside step function and

$$C(z,\omega) = -\frac{2g_{\rm s}\rho_{\rm s}^2}{1+\rho_{\rm s}^2+i\omega\tau_{\rm s}} \tag{A.3}$$

For $M < i \leq 2M$ and $j \leq M$, that is for (N_ϕ, N_ρ)

$$\begin{aligned}\tilde{O}_{ij} &= F(\omega_2 - \omega_1)\bar{M}_{\phi\rho}(z_1, \omega_1; z_2, \omega_2) \\ &\quad + \left(F^*(\omega_1)F(\omega_2) - F(\omega_2 - \omega_1)\right)\alpha\left(1 - H(z_2, \omega_2)\right)\end{aligned} \tag{A.4}$$

where $(z_1, \omega_1) \in V_{i-M}$, $(z_2, \omega_2) \in V_j$ and

$$\bar{M}_{\phi\rho}(z_1, \omega_1; z_2\omega_2) = \alpha\left(1 - \frac{H(z_2, \omega_2)}{H(z_1, \omega_2)}\right)\theta(z_1 - z_2)H(z_1, \omega_2 - \omega_1) \tag{A.5}$$

For $2M < i \leq 2M + L_\omega$, $j \leq M$, that is for (N_{ρ_0}, N_ρ)

$$\begin{aligned}\tilde{O}_{ij} &= F^*(\omega_1)H(0, \omega_1)^* F(\omega_2)H(z_2, \omega_2) \\ &\quad + F(\omega_2 - \omega_1)\bar{M}_{\rho_0\rho}(z_1, \omega_1; z_2, \omega_2) \\ &\quad + \left(F^*(\omega_1)F(\omega_2) - F(\omega_2 - \omega_1)\right) \\ &\quad \alpha^2\left(1 - H(0, \omega_1)^*\right)\left(1 - H(z_2, \omega_2)\right)\end{aligned} \tag{A.6}$$

where $(z_1, \omega_1) \in V_{i-2M}$, $(z_2, \omega_2) \in V_j$ and

$$\begin{aligned}\bar{M}_{\rho_0\rho}(z_1, \omega_1; z_2\omega_2) &= \frac{1}{2}H(0, -\omega_1)H(z_2\omega_2)\int_0^L \frac{H(z, \omega_2 - \omega_1)}{H(z, -\omega_1)H(z, \omega_2)} \\ &\times \left[C(-\omega_1) + C(\omega_2) + C(\omega_2 - \omega_1) + \frac{1}{g_{\mathrm{s}}(z)}C(\omega_2 - \omega_1)\left(C(-\omega_1) + C(\omega_2)\right)\right] \\ &\times \theta(z - z_2)dz\end{aligned} \tag{A.7}$$

For $2M + L_\omega < i \leq 2M + 2L_\omega$, $j \leq M$, that is for (N_{ϕ_0}, N_ρ)

$$\tilde{O}_{ij} = \left(F^*(\omega_1)F(\omega_2) - F(\omega_2 - \omega_1)\right)\alpha\left(1 - H(z_2, \omega_2)\right) \tag{A.8}$$

where $(z_1, \omega_1) \in V_{i-2M-L_\omega}$ and $(z_2, \omega_2) \in V_j$

For $M < i \leq 2M$, $M < j \leq 2M$, that is for (N_ϕ, N_ϕ)

$$\begin{aligned}\tilde{O}_{ij} &= F(\omega_2 - \omega_1)\bar{M}_{\phi\phi}(z_1, \omega_1; z_2, \omega_2) \\ &\quad + \left(F^*(\omega_1)F(\omega_2) - F(\omega_2 - \omega_1)\right)\end{aligned} \tag{A.9}$$

where $(z_1, \omega_1) \in V_{i-M}$, $(z_2, \omega_2) \in V_{j-M}$ and

$$\begin{aligned}&\bar{M}_{\phi\phi}(z_1, \omega_1; z_2\omega_2) = \\ &\theta(z_2 - z_1)H(z_2, \omega_2 - \omega_1) + \theta(z_1 - z_2)H(z_1, \omega_2 - \omega_1)\end{aligned} \tag{A.10}$$

For $2M < i \leq 2M + L_\omega$, $M < j \leq 2M$, that is for (N_{ρ_0}, N_ϕ)

$$\begin{aligned}\tilde{O}_{ij} &= F(\omega_2 - \omega_1)H(z_2, \omega_2 - \omega_1) \\ &\quad \times \alpha \left(1 - \frac{H(0, -\omega_1)}{H(z_2, -\omega_1)}\right) \\ &\quad + (F^*(\omega_1)F(\omega_2) - F(\omega_2 - \omega_1))\,\alpha\,(1 - H^*(0, \omega_1))\end{aligned} \tag{A.11}$$

where $(z_1, \omega_1) \in V_{i-2M-L_\omega}$ and $(z_2, \omega_2) \in V_{j-M}$.

For $2M + L_\omega < i \leq 2M + 2L_\omega$, $M < j \leq 2M$, that is for (N_{ϕ_0}, N_ϕ)

$$\begin{aligned}\tilde{O}_{ij} &= F(\omega_2 - \omega_1)H(z_2, \omega_2 - \omega_1) \\ &\quad + (F^*(\omega_1)F(\omega_2) - F(\omega_2 - \omega_1))\end{aligned} \tag{A.12}$$

where $(z_1, \omega_1) \in V_{i-2M-L_\omega}$ and $(z_2, \omega_2) \in V_{j-M}$

For $2M < i \leq 2M + L_\omega$, $2M < j \leq 2M + L_\omega$, that is for (N_{ρ_0}, N_{ρ_0})

$$\begin{aligned}\tilde{O}_{ij} &= F^*(\omega_1)H^*(0, \omega_1)F(\omega_2)H(0, \omega_2) \\ &\quad + F(\omega_2 - \omega_1)\bar{M}_{\rho\rho}(0, \omega_1; 0, \omega_2) \\ &\quad + (F^*(\omega_1)F(\omega_2) - F(\omega_2 - \omega_1)) \\ &\quad \alpha^2\,(1 - H^*(0, \omega_1))\,(1 - H(0, \omega_2))\end{aligned} \tag{A.13}$$

where $(z_1, \omega_1) \in V_{i-2M}$, $(z_2, \omega_2) \in V_{j-2M}$.

For $2M + L_\omega < i \leq 2M + 2L_\omega$, $2M < j \leq 2M + L_\omega$, that is for (N_{ϕ_0}, N_{ρ_0})

$$\tilde{O}_{ij} = (F^*(\omega_1)F(\omega_2) - F(\omega_2 - \omega_1))\,\alpha\,(1 - H(0, \omega_2)) \tag{A.14}$$

where $(z_1, \omega_1) \in V_{i-2M-L_\omega}$ and $(z_2, \omega_2) \in V_{j-2M}$

For $2M + L_\omega < i \leq 2M + 2L_\omega$, $2M + L_\omega < j \leq 2M + 2L_\omega$, that is for (N_{ϕ_0}, N_{ϕ_0})

$$\tilde{O}_{ij} = F^*(\omega_1)F(\omega_2) - F(\omega_2 - \omega_1) + F(\omega_2 - \omega_1)H(0, \omega_2 - \omega_1) \tag{A.15}$$

where $(z_1, \omega_1) \in V_{i-2M-L_\omega}$ and $(z_2, \omega_2) \in V_{j-2M-L_\omega}$

For all other elements

$$\tilde{O}_{ij} = \tilde{O}^*_{ji} \tag{A.16}$$

Finally, the detection and electrical filtering changes all matrix elements by: $\tilde{O}_{ij} \to F_e(\omega_2 - \omega_1)\tilde{O}_{ij}$.

Appendix B

List of abbreviation

Abbreviation	**Complete name**
1R	Re-amplification
2R	Re-amplification and Re-shaping
3R	Re-amplification, Re-shaping and Re-timing
ASE	Amplified Spontaneous Emission
BER	Bit Error Rate
BERT	Bit Error Rate Test-set
CGF	Cumulant-Generating Function
CW	Continuous Wave
DISC	Delayed-Interferometer Signal-wavelength Converter
EA	Electroabsorber
EAM	Electro-Absorption Modulator
EDFA	Erbium Doped Fiber Amplifier
ER	Extinction Ratio
InGaAsP	Indium-Gallium-Arsenide-Phosphide
InP	Indium-Phosphide
LD	Laser Diode
MGF	Moment-Generating Function
MMI	Multi Mode Interferometer
MOVPE	Metal Organic Vapor Phase Epitaxy
MZI	Mach-Zehnder Interferometer
MZM	Mach-Zehnder Modulator
NRZ	Non-Return to Zero
OEO	Opto-Electronic
OOK	On-Off Keying
OSNR	Optical Signal to Noise Ratio
PDF	Probability Density Function
PT	Pass-Through
RIN	Relative Intensity Noise
RZ	Return to Zero

Abbreviation	**Complete name**
SNR	Signal to Noise Ratio
SOA	Semiconductor Optical Amplifier
TE	Transverse Electric
TF	Transfer Function
TM	Transverse Magnetic
WDM	Wavelength Division Multiplexing
XGM	Cross Gain Modulation

Appendix C

List of symbols

Symbol	Description	Unit
α	Linewidth enhancement factor	
α_{int}	Waveguide loss	m^{-1}
a	Differential modal gain	m^2
A	Effective cross-section area	m^2
B_e	Detection bandwidth	Hz
B_o	Optical bandwidth	Hz
B_D	Effective device bandwidth	Hz
$1-\gamma$	Transfer function nonlinearity	
γ	Transfer function slope	
γ_s	Skewness	
D	Diffusion matrix	
$\tilde{E}$	Envelope of electrical field amplitude	$\sqrt{\mathrm{W}}$
E	Normalized $\tilde{E}$	
E_s	Steady state of E	
E_p	Perturbation of E_s	
$ER_\mathrm{reg.}$	Extinction ratio of regenerator	
ϕ	Phase of E	
ϕ_s	Steady state phase of E	
ϕ_i	Perturbation of ϕ_s of order i	
$\tilde{f}_N$	Langevin force, carriers	$\mathrm{m}^{-3}\mathrm{s}^{-1}$
f_N	Normalized Langevin force, carriers	
$\tilde{f}_E$	Langevin force, electric field	$\sqrt{\mathrm{W}}\mathrm{m}^{-1}$
f_E	Normalized Langevin force, electric field	
F	Filter function of optical filter	
F_e	Filter function of electrical filter	
F_N	Noise figure	
g	Gain coefficient	m^{-1}
g_0	Small signal gain coefficient	m^{-1}
g_s	Steady state gain coefficient	m^{-1}
g_i	Perturbation to g_s of order i	m^{-1}
G	Gain	

Symbol	Description	Unit
h	Integrated gain coefficient	
h_0	Integrated small signal gain coefficient	
$\hbar$	Plancks constant (h/2π)	Js
I	Current	A
k_n	Cumulant of order n	
λ	Wavelength	m
L	Device length	m
$L_{z,t,\omega}$	Number of discrete points in z, t and ω	
$L_{\text{att.}}$	Attenuator loss	
m_n	Central moment of order n	
μ	Mean value	
n_{sp}	Spontaneous emission factor	
N	Carrier density	m^{-3}
N_0	Carrier density at transparency	m^{-3}
N_ρ	Real part of f_E/E_s	
N_ϕ	Imaginary part of f_E/E_s	
P	Power	W
$\bar{P}_{1/0}$	Mean power of logical one/zero-level	W
P_{sat}	Saturation power	W
P_{th}	Threshold power	W
$\bar{P}_{\text{ase}}$	Mean ASE power	W
$\bar{P}_{1/0,s}$	Mean power of input signal at one/zero-level	W
$P_{1/0}$	Power of one/zero-level of transfer function	W
q	Elementary charge	C
Q	Signal quality factor	
ρ	Amplitude of E	
ρ_s	Steady state amplitude of E	
ρ_i	Perturbation of ρ_s of order i	
$R(\tau)$	Correlation of spontaneous emission noise	s^-1
$\sigma^2_{1/0}$	Variance of signal power at one/zero-level	W^2
σ^2_{ase}	Variance of ASE power	W^2
τ_s	Carrier life time/Sweep out time	s
t	Shifted time coordinate	s
Δt	Sampling interval	s
v_g	Group velocity	m/s
V	Active volume	m^3
V_{th}	Threshold voltage	V
ω_0	Angular frequency of optical carrier wave	Hz

Appendix D

List of Ph.D. publications

F. Öhman, S. Bischoff, B. Tromborg, and J. Mørk. Noise and regeneration in semiconductor waveguides with saturable gain and absorption. *IEEE J. Quantum Electron.*, 40:245 – 255, 2004.

F. Öhman, S. Bischoff, B. Tromborg, and J. Mørk. Noise properties and cascadability of SOA-EA regenerators. In *Proceedings of LEOS 2002*, page 895, 2002.

F. Öhman, B. Tromborg, J. Mørk, A. Aurelius, A. Djupsjöbacka, and A. Berntson. Measurements of non-linear noise re-distribution in an SOA. In *Proceedings of CLEO 2004*, page CtuP5, 2004.

F. Öhman, B. Tromborg, J. Mørk, A. Aurelius, A. Djupsjöbacka, and A. Berntson. Measurements and simulations of non-linear noise re-distribution in an SOA. *IEEE J. Photon. Technol. Lett.*, accepted for publication, 2004.

F. Öhman, S. Bischoff, B. Tromborg, and J. Mørk. Noise properties of semiconductor waveguides with alternating sections of saturable gain and absorption. In *Proceedings of CLEO/Europe 2003*, page CC7T, 2003.

L. J. Christiansen, L. Xu, K. Yvind, F. Öhman, L. Oxenløwe, and J. Mørk. 2R Regeneration in Concatenated Semiconductor Optical Amplifiers and Electroabsorbers. In *Proceedings of ECOC 2004*, 2004.

J. Mørk, F. Öhman, and S. Bischoff. Analytical expression for the bit error rate of cascaded all-optical regenerators. *IEEE J. Photon. Technol. Lett.*, 15(10):1479–1481, 2003.

J. Mørk, F. Romstad, S. Hojfeldt, L. Oxenløwe, K. Yvind, L. Xu, F. Öhman, L.J. Christiansen, A. Tersigni, K. Hoppe, M. Lobel, and J. Hanberg. Optical signal processing using electro-absorption modulators. *11th European Conference on Integrated Optics. Proceedings*, pages 45–54 vol.2, 2003.

F. Öhman, S. Bischoff, B. Tromborg, and J. Mørk. Semiconductor devices for all-optical regeneration. *Transparent Optical Networks, 2003. Proceedings of 2003 5th International Conference on*, 2:41–46 vol.2, 2003.

J. Mørk, F. Öhman, and Svend Bischoff. Analytical BER-expression for cascaded regenerators and analysis of non-linearity versus noise. In *Proceedings of LEOS 2002*, 2002.

F. Öhman, B. Tromborg, J. Mørk, A. Aurelius, A. Djupsjöbacka, and A. Berntson. Measurements of non-linear noise re-distribution in an SOA. In *Proceedings of CLEO 2004*, page CtuP5, 2004.

F. Öhman, B. Tromborg, J. Mørk, A. Aurelius, A. Djupsjöbacka, and A. Berntson. Measurements and simulations of non-linear noise re-distribution in an SOA. In *OAA 2004 Conference Digest*, page OTuD5, 2004.

J. Mørk, F. Öhman, and B. Tromborg. All optical regeneration using semiconductor devices. In *Frontiers in Optics/Laser Science XIX (87th OSA Annual Meeting)*, paper WY4, 2004.

F. Romstad, F. Öhman,J. Mørk, K. Yvind, J.M. Hvam and J. Hanberg. Short pulse absorption dynamics in a p-i-n InGaAsP MQW waveguide saturable absorber. In *In Proceedings of ECOC 2002)*, paper P2.25, 2002.

J. Mørk, S. Bischoff, T.W. Berg, M.L. Nielsen and F. Öhman. Modeling of semiconductor optical amplifiers. In *OSA 2002 Annual Meeting*, paper WT2, 2002.

Jesper Mørk, Kresten Yvind, Leif Oxenløwe, Peter M.W. Skovgaard, Francis Romstad, Svend Bischoff, Sune Højfeldt, Andrea Tersigni, Lotte Christiansen, Abbas Nik, Filip Öhman, Jørn M. Hvam, Jesper Hanberg, Karsten Hoppe, and Martin Løbel. SCOOP – Semiconductor COmponents for Optical signal Processing. *DOPS-NYT*, vol.16 pages 25-30 2001.

F. Öhman, S. Bischoff, L. Christiansen, and J. Mørk. Improvement of noise reduction by employing an SOA-EA cascade. *Proc. International Workshop on Optical Signal Processing*, pages 68-70, 2001.

Bibliography

[1] S Ferber, R Ludwig, C Boerner, A Wietfeld, B Schmauss, J Berger, C Schubert, G Unterboersch, and H G Weber. Optical communication - comparison of dpsk and ook modulation format in 160 gbit/s transmission system. *Electronics Letters*, 39(20):1458, 2003.

[2] A.J. Price and N. Le Mercier. Reduced bandwidth optical digital intensity modulation with improved chromatic dispersion tolerance. *Electronics Letters*, 31(1):58 –59, 1995.

[3] O. Ait Sab and H. Bissessur. Signal formats and error correction in optical transmission. *Comptes Rendus Physique*, 4(1):95–104, 2003.

[4] F. Ouellette, J.-F. Cliche, and S. Gagnon. All-fiber devices for chromatic dispersion compensation based on chirped distributed resonant coupling. *Lightwave Technology, Journal of*, 12(10):1728 –1738, 1994.

[5] G. P. Agrawal. *Fiber-Optic Communication Systems*. Wiley-interscience, New York, 2 edition, 1997.

[6] G. H. Einarsson. *Principles of lightwave communication*. John Wiley and Sons, 1 edition, 1996.

[7] O. Leclerc, B. Lavigne, E. Balmefrezol, P. Brindel, L. Pierre, D. Rouvillain, and F. Seguineau. Optical regeneration at 40 gb/s and beyond. *Lightwave Technology, Journal of*, 21(11):2779–2790, 2003.

[8] D. M. Baney, P. Gallion, and R. S. Tucker. Theory and Measurement Techniques for the Noise Figure of Optical Amplifiers. *Opt. Fiber Tech.*, 6(2):122 – 154, 2000.

[9] P. Öhlen and E. Berglind. Noise accumulation and BER estimates in concatenated nonlinear optoelectronic repeaters. *IEEE J. Photon. Technol. Lett.*, 9(7):1011 –1013, 1997.

[10] M.L. Nielsen. *Experimental and Theoretical investigation of Semiconductor Optical Amplifier (SOA) based All-Optical Switches*. PhD thesis, Lyngby, 2004.

[11] B.K. Mathason and P.J. Delfyett. Pulsed injection locking dynamics of passively mode-locked external-cavity semiconductor laser systems for all-optical clock recovery. *Lightwave Technology, Journal of*, 18(8):1111 –1120, 2000.

[12] R. Schreieck, M. Kwakernaak, and H. Jackel. All-optical clock extraction at 160 gbit/s with monolithic mode-locked laser diodes. *IEICE Transactions on Electronics*, E84-C(6):841–844, 2001.

[13] C. Bornholdt, J. Slovak, and B. Sartorius. Semiconductor-based all-optical 3R regenerator demonstrated at 40 Gbit/s. *Electron. Lett.*, 40(3):192 – 193, 2004.

[14] B. Sartorius. All-optical clock recovery for 3r optical regeneration. *Optical Fiber Communication Conference and Exhibit, 2001. OFC 2001*, 1:MG7–1, 2001.

[15] O. Leclerc. Optical vs. Electronic in-line Signal Processing in Optical Communication Systems: An exciting challenge for Optical Devices. In *Tech. Dig. ECIO'03*, pages 55–67, 2003.

[16] L. A. Coldren and S. W. Corzine. *Diode lasers and photonic integrated circuits*. John Wiley & Sons, New York, 1 edition, 1995.

[17] S. Bigo, O. Leclerc, and E. Desurvire. All-optical fiber signal processing and regeneration for soliton communications. *Selected Topics in Quantum Electronics, IEEE Journal on*, 3(5):1208 –1223, 1997.

[18] M. Matsumoto. Analysis of optical regeneration utilizing self-phase modulation in a highly nonlinear fiber. *IEEE Photonics Technology Letters*, 14(3):319–321, 2002.

[19] M. Tsurusawa, M. Usami, and Y. Matsushima. Demonstration of Optical Noise Reduction Using Nonlinear Absorption in a Semiconductor Laser Amplifier. *IEEE J. Sel. Top. Quantum Electron.*, 5:861–865, 1999.

[20] L. J. Christiansen, L. Xu, K. Yvind, F. Öhman, L. Oxenløwe, and J. Mørk. 2R Regeneration in Concatenated Semiconductor Optical Amplifiers and Electroabsorbers. In *Proceedings of ECOC 2004*, 2004.

[21] Z. Bakonyi, G. Onishchukov, C. Knoll, M. Golles, F. Lederer, and R. Ludwig. In-Line Saturable Absorber in Transmission Systems with Cascaded Semiconductor Optical Amplifiers. *IEEE J. Photon. Technol. Lett.*, 12(5):570 –572, 2000.

[22] D. Wolfson, T. Fjelde, A. Kloch, C. Janz, A. Coquelin, I. Guillemot, F. Gaborit, F. Poingt, and M. Renaud. Experimental investigation at 10 Gb/s of the noise suppression capabilities in a pass-through configuration in SOA-based interferometric structures. *IEEE J. Photon. Technol. Lett.*, 12(7):837 –839, 2000.

[23] D. Wolfson, A. Kloch, T. Fjelde, C. Janz, B. Dagens, and M. Renaud. 40-Gb/s all-optical wavelength conversion, regeneration, and demultiplexing in an SOA-based all-active Mach-Zehnder interferometer. *IEEE J. Photon. Technol. Lett.*, 12(3):332 –334, 2000.

[24] M. Zhao, G. Morthier, and R. Baets. Demonstration of Extinction Ratio Improvement from 2 to 9 dB and Intensity Noise Reduction with the MZI-GCSOA All-Optical 2R regenerator. *IEEE J. Photon. Technol. Lett.*, 14:992–994, 2002.

[25] M. Zhao, J. De Merlier, G. Morthier, and R. Baets. Experimental demonstration of all-optical 2R regeneration based on non-linear birefringence in a LOA. In *Proceedings of ECOC 2002*, 2002.

[26] J. De Merlier, G. Morthier, S. Verstuyft, T. Van Caenegem, I. Moerman, P. Van Daele, and R. Baets. Experimental demonstration of all-optical regeneration using an MMI-SOA. *IEEE J. Photon. Technol. Lett.*, 14(5):660–662, 2002.

[27] B. Mikkelsen, S.L. Danielsen, C. Joergensen, R.J.S. Pedersen, H.N. Poulsen, and K.E. Stubkjaer. All-optical noise reduction capability of interferometric wavelength converters. *Electronics Letters*, 32(6):566 –567, 1996.

[28] J. Leuthold and M. Kauer. Power equalisation and signal regeneration with delay interferometer all-optical wavelength converters. *Electronics Letters*, 38(24):1567–1569, 2002.

[29] A. Labrousse, B. Dagens, R. Brenot, B. Lavigne, S. Squedin, B. Martin, S. Fabre, M.L. Nielsen, and M. Renaud. Standard mode 40 gbit/s performance analysis of evanescent coupling 'active-passive' mach-zehnder interferometers for all-optical regeneration. *Electronics Letters*, 39(16):1201–1202, 2003.

[30] J. Mørk and A. Mecozzi. Theory of the ultrafast optical response of active semiconductor waveguides. *J. Opt. Soc. Am. B*, 13(8):2437–2452, 1996.

[31] Jesper Mørk, Tommy W. Berg, Mads L. Nielsen, and Alexander V. Uskov. The role of fast carrier dynamics in soa based devices. *IEICE Transactions on Electronics*, E87-C(7):1126–1133, 2004.

[32] S. Bischoff, M.L. Nielsen, and J. Mørk. Improving the all-optical response of soas using a modulated holding signal. *Journal of Lightwave Technology*, 22(5):1303–8, 2004.

[33] T. Durhuus, B. Mikkelsen, C. Jørgensen, S. Lykke Danielsen, and K. E. Stubkjær. All-optical wavelength conversion by semiconductor optical amplifiers. *IEEE J. Lightwave Technol.*, 14(6):942–954, 1996.

[34] J. Mørk, F. Romstad, S. Hojfeldt, L. Oxenlowe, K. Yvind, L. Xu, F. Öhman, L.J. Christiansen, A. Tersigni, K. Hoppe, M. Lobel, and J. Hanberg. Optical signal processing using electro-absorption modulators. *11th European Conference on Integrated Optics. Proceedings*, pages 45–54 vol.2, 2003.

[35] S. Højfeldt, S. Bischoff, and J. Mørk. All-optical wavelength conversion and signal regeneration using an electroabsorption modulator. In *Tech. Dig. LEOS'99*, 1999.

[36] J. Mangeney, S. Barre, G. Aubin, J.-L. Oudar, and O. Leclerc. System application of 1.5 /spl mu/m ultrafast saturable absorber in 10 gbit/s long-haul transmission. *Electronics Letters*, 36(20):1725 –1727, 2000.

[37] H. Yokoyama, Y. Hashimoto, and H. Kurita. Noise reduction in optical pulses and bit-error-rate improvement with a semiconductor-waveguide saturable absorber. In *Tech. Dig. CLEO'98*, volume 6 of *1998 Technical Digest Series*, pages 502–503, 1998.

[38] F. Öhman, S. Bischoff, B. Tromborg, and J. Mørk. Noise and regeneration in semiconductor waveguides with saturable gain and absorption. *IEEE J. Quantum Electron.*, 40:245 – 255, 2004.

[39] C. Knoll, M. Golles, Z. Bakonyi, G. Onishchukov, and F. Lederer. Optimization of signal transmission by an in-line semiconductor optical amplifier-saturable absorber module. *Optics Communications*, 187(1):141–153, 2001.

[40] F. Öhman, S. Bischoff, B. Tromborg, and J. Mørk. Noise properties and cascadability of SOA-EA regenerators. In *Proceedings of LEOS 2002*, page 895, 2002.

[41] M. Matsumoto and O. Leclerc. Analysis of 2R optical regenerator utilizing self-phase modulation in highly nonlinear fibre. *Electron. Lett.*, 38:576 –577, 2002.

[42] J. Leuthold. Signal Regeneration and All-optical Wavelength Conversion. In *Proceedings of LEOS 2002*, page 107, 2002.

[43] Y. Ueno, S. Nakamura, K. Tajima, and S. Kitamura. 3.8-THz wavelength conversion of picosecond pulses using a semiconductor delayed-interference signal-wavelength converter (DISC). *IEEE J. Photon. Technol. Lett.*, 10:346–348, 1998.

[44] M. Shtaif, B. Tromborg, and G. Eisenstein. Noise spectra of semiconductor optical amplifiers: relation between semiclassical and quantum descriptions. *IEEE J. Quantum Electron.*, 34(5):869 –878, 1998.

[45] H. Olesen, B. Tromborg, X. Pan, and H.E. Lassen. Stability and dynamic properties of multi-electrode laser diodes using a green's function approach. *Quantum Electronics, IEEE Journal of*, 29(8):2282 –2301, 1993.

[46] N.A. Olsson. Lightwave systems with optical amplifiers. *J. Lightwave Technol.*, 7(7):1071 –1082, 1989.

[47] Y. Yamamoto and K. Inoue. Noise in amplifiers. *Lightwave Technology, Journal of*, 21(11):2895–2915, 2003.

[48] M. Shtaif and G. Eisenstein. Experimental Study of the Statistical Properties of Nonlinearly Amplified Signals in Semiconductor Optical Amplifiers. *IEEE J. Photon. Technol. Lett.*, 9(7):904 –906, 1997.

[49] M. Shtaif and G. Eisenstein. Noise properties of nonlinear semiconductor optical amplifiers. *Optics Letters*, 21(22):1851–3, 1996.

[50] M. Shtaif and G. Eisenstein. Calculation of bit error rates in all-optical signal processing applications exploiting nondegenerate few-wave mixing in semiconductor optical amplifiers. *Lightwave Technology, Journal of*, 14(9):2069 –2077, 1996.

[51] K. Obermann, I. Koltchanov, K. Petermann, S. Diez, R. Ludwig, and H.G. Weber. Noise analysis of frequency converters utilizing semiconductor-laser amplifiers. *Quantum Electronics, IEEE Journal of*, 33(1):81 –88, 1997.

[52] K. Obermann, S. Kindt, D. Breuer, K. Petermann, C. Schmidt, S. Diez, and H.G. Weber. Noise Characteristics of Semiconductor-Optical Amplifiers Used for Wavelength Conversion Via Cross-Gain and Cross-Phase Modulation. *IEEE J. Photon. Technol. Lett.*, 9(3):312 –314, 1997.

[53] A. Bilenca and G. Eisenstein. On the noise properties of linear and nonlinear quantum-dot semiconductor optical amplifiers: The impact of inhomogeneously broadened gain and fast carrier dynamics. *Quantum Electronics, IEEE Journal of*, 40(6):690–702, 2004.

[54] O.L. Jørsboe. *Sandsynlighedsregning*. Matematiske institut, DTU, Lyngby, 1991.

[55] F. Öhman, B. Tromborg, J. Mørk, A. Aurelius, A. Djupsjöbacka, and A. Berntson. Measurements of non-linear noise re-distribution in an SOA. In *Proceedings of CLEO 2004*, page CtuP5, 2004.

[56] F. Öhman, B. Tromborg, J. Mørk, A. Aurelius, A. Djupsjöbacka, and A. Berntson. Measurements and simulationsof non-linear noise re-distribution in an SOA. In *OAA 2004 Conference Digest*, page OTuD5, 2004.

[57] F. Öhman, B. Tromborg, J. Mørk, A. Aurelius, A. Djupsjöbacka, and A. Berntson. Measurements and simulations of non-linear noise re-distribution in an SOA. *IEEE J. Photon. Technol. Lett.*, accepted for publication, 2004.

[58] B. Chan and J. Conradi. On the Non-Gaussian Noise in Erbium-Doped Fiber Amplifiers. *J. Lightwave Technol.*, 15:680–687, 1997.

[59] B. Saleh. *Photoelectron Statistics*. Springer-Verlag, New York, 1978.

[60] G.P. Agrawal and N.A. Olsson. Self-Phase Modulation and Spectral Broadening of Optical Pulses in Semiconductor Laser Amplifiers. *IEEE J. Quantum Electron.*, 25(11):2297 –2306, 1989.

[61] D. Cassioli, S. Scotti, and A. Mecozzi. A time-domain computer simulator of the nonlinear response of semiconductor optical amplifiers. *IEEE J. Quantum Electron.*, 36(9):1072 –1080, 2000.

[62] C.W. Gardiner. *Handbook of stochastic methods*. Springer-Verlag.

[63] E. Bedrosian and S. O. Rice. The Output Properties of Volterra Systems (Nonlinear Systems with Memory) Driven by Harmonic and Gaussian Inputs. *Proc. IEEE*, 59:1688–1707, 1971.

[64] M. C. Jeruchim, P. Balaban, and K. S. Shanmugan. *Simulation of communication systems, Modeling, Methodology and techniques*. Kluwer academic/plenum publishers, New York, 2 edition, 2000.

[65] M. Zhao, G. Morthier, and R. Baets. Analysis and optimization of intensity noise reduction in spectrum-sliced WDM systems using a saturated semiconductor optical amplifier. *IEEE J. Photon. Technol. Lett.*, 14(3):390–392, 2002.

[66] Sun-Jong Kim, Jung-Hee Han, Jae-Seung Lee, and Chang-Soo Park. Intensity noise suppression in spectrum-sliced incoherent light communication systems using a gain-saturated semiconductor optical amplifier. *IEEE Photonics Technology Letters*, 11(8):1042 –1044, 1999.

[67] A.D. McCoy, L.B. Fu, M. Ibsen, B.C. Thomsen, and D.J. Richardson. Intensity noise suppression in fibre DFB laser using gain saturated SOA. *Electronics Letters*, 40(2):107–109, 2004.

[68] F. Öhman, B. Tromborg, and J. Mørk. Comparison of noise redistribution in an SOA in pass-through and wavelength conversion mode. In *Proceedings of LEOS 2004*, pages 394–395, 2004.

[69] D. Marcenac and A Mecozzi. Switches and Frequency Converters Based on Cross-Gain Modulation in Semiconductor Optical Amplifiers. *IEEE J. Photon. Technol. Lett.*, 9:749–751, 1997.

[70] S. Wu, X. Sun, and M. Zhang. Small-signal Analysis Method of Noise Transfer of All-optical Wavelength Converters. *J. Opt. Commun.*, 23:91–94, 2002.

[71] K. Inoue. Noise Transfer Characteristics in Wavelength Conversion Based on Cross-Gain Saturation in a Semiconductor Optical Amplifier. *IEEE J. Photon. Technol. Lett.*, 8:888–890, 1996.

[72] R. Hainberger, T. Hoshida, S. Watanabe, and H. Onaka. Ber estimation in optical fiber transmission systems employing all-optical 2r regenerators. *Lightwave Technology, Journal of*, 22(3):746–754, 2004.

[73] J. Mørk, F. Öhman, and S. Bischoff. Analytical expression for the bit error rate of cascaded all-optical regenerators. *IEEE J. Photon. Technol. Lett.*, 15(10):1479–1481, 2003.

[74] K. Obermann and K. Petermann. Estimation of BER performance and cascadability of wavelength converters based on cross-gain modulation in semiconductor optical amplifiers. *Optoelectronics, IEE Proceedings-*, 147(2):133 –137, 2000.

[75] S. Bischoff, B. Lading, and J. Mørk. BER estimation for all-optical regenerators influenced by pattern effects. *IEEE J. Photon. Technol. Lett.*, 14(1):33–35, 2002.

[76] J. Mørk, F. Öhman, and Svend Bischoff. Analytical BER-expression for cascaded regenerators and analysis of non-linearity versus noise. In *Proceedings of LEOS 2002*, 2002.

[77] F. Öhman, S. Bischoff, B. Tromborg, and J. Mørk. Semiconductor devices for all-optical regeneration. *Transparent Optical Networks, 2003. Proceedings of 2003 5th International Conference on*, 2:41–46 vol.2, 2003.

[78] F. Öhman, S. Bischoff, B. Tromborg, and J. Mørk. Noise properties of semiconductor waveguides with alternating sections of saturable gain and absorption. In *Proceedings of CLEO/Europe 2003*, page CC7T, 2003.

[79] S. Hojfeldt, S. Bischoff, and J. Mørk. All-Optical Wavelength Conversion and Signal Regeneration Using an Electroabsorption Modulator. *J. Lightwave Technol.*, 18(8):1121–7, 2000.

[80] A. D. Ellis, A. E. Kelly, D. Nesset, D. Pitcher, and D. G. Moodie. Error free 100 Gbit/s wavelength conversion using grating assisted cross-gain modulation in 2 mm long semiconductor amplifier. *Electron. Lett.*, 34(20), 1998.

[81] H. Tanaka, M. Hayashi, T. Otani, K. Ohara, and M. Suz. 60 Gbit/s WDM-OTDM transmultiplexing using an electro-absorption modulator. *Optical Fiber Communication Conference and Exhibit, 2001. OFC 2001*, 1:ME4/1, 2001.

[82] T.P. Hessler, M.-A. Dupertuis, B. Deveaud, J.-Y. Emery, and B. Dagens. Experimental demonstration of optical speed-up at transparency in semiconductor optical amplifiers. *All-Optical Networking: Existing and Emerging Architecture and Applications/Dynamic Enablers of Next-Generation Optical Communications Systems/Fast Optical Processing in Optical Transmission/VCSEL and Microcavity Lasers. 2002 IEEE/LEOS Summer Topical Meeting*, pages TuK2–23, 2002.

[83] H. Wei, H. Dexiu, S. Junqiang, and L. Deming. Numerical simulation of recovery enhancement by a cw pump light in semiconductor optical amplifiers. *Optics Communications*, 214(1-6):335–341, 2002.